

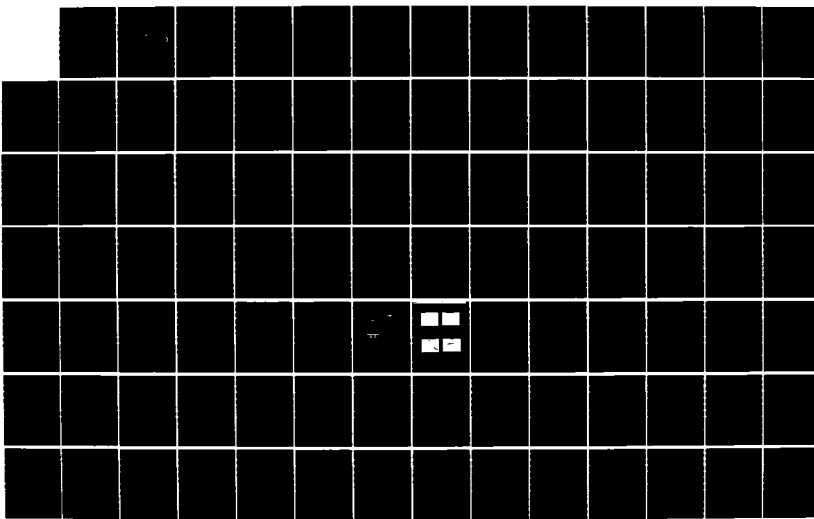
AD-A164 413

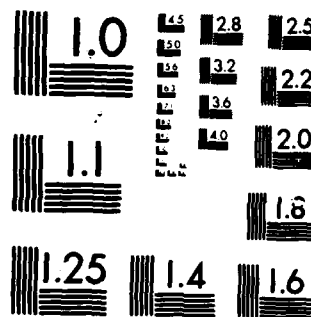
INP:FE AND GaAs:CR PICOSECOND PHOTOCONDUCTIVE RADIATION 1/2
DETECTORS(U) NAVAL POSTGRADUATE SCHOOL MONTEREY CA
P J KEPPEL DEC 85

UNCLASSIFIED

F/G 18/4

NL





MICROCOPY RESOLUTION TEST CHART
NATIONAL BUREAU OF STANDARDS 1963-A

(2)

NAVAL POSTGRADUATE SCHOOL

Monterey, California

AD-A164 413



DTIC
ELECTED
FEB 24 1986
S B D

THESIS

InP:Fe AND GaAs:Cr PICOSECOND
PHOTOCONDUCTIVE RADIATION DETECTORS

by

Phillip J. Keipper

December 1985

Thesis Advisor:

F.R. Buskirk

Approved for public release; distribution is unlimited

6 2 14

DTIC FILE COPY

REPORT DOCUMENTATION PAGE

1a. REPORT SECURITY CLASSIFICATION		1b. RESTRICTIVE MARKINGS	
1a. SECURITY CLASSIFICATION AUTHORITY		3. DISTRIBUTION/AVAILABILITY OF REPORT Approved for public release; distribution is unlimited	
1c. DECLASSIFICATION/DOWNGRADING SCHEDULE			
3. PERFORMING ORGANIZATION REPORT NUMBER(S)		5. MONITORING ORGANIZATION REPORT NUMBER(S)	
6a. NAME OF PERFORMING ORGANIZATION Naval Postgraduate School	6b. OFFICE SYMBOL (If applicable) Code 61	7a. NAME OF MONITORING ORGANIZATION Naval Postgraduate School	
6c. ADDRESS (City, State, and ZIP Code) Monterey, California 93943-5100		7b. ADDRESS (City, State, and ZIP Code) Monterey, California 93943-5100	
8a. NAME OF FUNDING/SPONSORING ORGANIZATION	8b. OFFICE SYMBOL (If applicable)	9. PROCUREMENT INSTRUMENT IDENTIFICATION NUMBER	
8c. ADDRESS (City, State, and ZIP Code)		10. SOURCE OF FUNDING NUMBERS	
		PROGRAM ELEMENT NO.	PROJECT NO
		TASK NO	WORK UNIT ACCESSION NO
11. TITLE (Include Security Classification) InP:Fe AND GaAs:Cr PICOSECOND PHOTOCONDUCTIVE RADIATION DETECTORS			
12. PERSONAL AUTHOR(S) Keipper, Phillip J.			
13a. TYPE OF REPORT Master's Thesis	13b. TIME COVERED FROM _____ TO _____	14. DATE OF REPORT (Year, Month, Day) 1985, December	15. PAGE COUNT 123
16. SUPPLEMENTARY NOTATION			
17. COSATI CODES		18. SUBJECT TERMS (Continue on reverse if necessary and identify by block number) InP:Fe; GaAs:Cr; Picosecond; Detectors	
FIELD	GROUP	19. ABSTRACT (Continue on reverse if necessary and identify by block number) The dark current, impulse and square-pulse response measurements of photoconductive devices fabricated from two different types of materials, Gallium Arsenide with Chromium dopant (GaAs:Cr) and Indium Phosphide with Iron dopant (InP:Fe) are reported. These devices have been subjected to irradiation from the Naval Postgraduate School S-band Electron Linear Accelerator (LINAC) with an energy of 100 MeV at room temperature. Fluence ranged between 10^{13} and 10^{16} electrons/cm ² . Dark current decreases with increasing fluence for the GaAs:Cr devices whereas InP:Fe shows an increase in the dark current. Both types of materials exhibit extremely fast impulse response after the irradiation. Electron mobility, drift velocity and response speed decrease with increasing fluence. Response speeds of < 100-ps are achieved by fast carrier relaxation in the semiconductor	SUB-GROUP
20. DISTRIBUTION/AVAILABILITY OF ABSTRACT <input checked="" type="checkbox"/> UNCLASSIFIED/UNLIMITED <input type="checkbox"/> SAME AS RPT. <input type="checkbox"/> DTIC USERS		21. ABSTRACT SECURITY CLASSIFICATION Unclassified	
22a. NAME OF RESPONSIBLE INDIVIDUAL Prof. Fred R. Buskirk		22b. TELEPHONE (Include Area Code) (408) 646-2765	22c. OFFICE SYMBOL Code 61Bs

UNCLASSIFIED

SECURITY CLASSIFICATION OF THIS PAGE (When Data Entered)

#19 - ABSTRACT - (CONTINUED)

due to the introduction of trapping and recombination centers resulting from the irradiation damage. The GaAs:Cr, unlike the InP:Fe, more closely follows the longer square-pulse exhibiting no nonlinearity. All results are consistent with previously investigated neutron irradiated devices. (Tas-s)

Authorization For	
ME	SI
DT	<input type="checkbox"/>
U	<input type="checkbox"/>
J	<input type="checkbox"/>
PER CALL TO	
By	
Dist	Now
Avail	Line Codes
	11/08
Dist	1
A-1	

Approved for public release; distribution is unlimited.

InP:Fe and GaAs:Cr Picosecond Photoconductive
Radiation Detectors

by

Phillip J. Keipper
Lieutenant, United States Navy
B.S., Ohio State University, 1975

Submitted in partial fulfillment of the
requirements for the degree of

MASTER OF SCIENCE IN PHYSICS

from the

NAVAL POSTGRADUATE SCHOOL
December 1985

Author:

Phillip J. Keipper

Approved by:

Fred R. Buskirk

F.R. Buskirk, Thesis Advisor

John R. Neighbours

J.R. Neighbours, Second Reader

G.E. Schacher

G.E. Schacher, Chairman,
Department of Physics

J.W. Dyer

J.W. Dyer,
Dean of Science and Engineering

ABSTRACT

The dark current, impulse and square-pulse response measurements of photoconductive devices fabricated from two different types of materials, Gallium Arsenide with Chromium dopant (GaAs:Cr) and Indium Phosphide with Iron dopant (InP:Fe) are reported. These devices have been subjected to irradiation from the Naval Postgraduate School S-band Electron Linear Accelerator (LINAC) with an energy of 100 MeV at room temperature. Fluence ranged between 10^{13} and 10^{16} electrons/cm². Dark current decreases with increasing fluence for the GaAs:Cr devices whereas InP:Fe shows an increase in the dark current. Both types of materials exhibit extremely fast impulse response after the irradiation. Electron mobility, drift velocity and response speed decrease with increasing fluence. Response speeds < 100-ps are achieved by fast carrier relaxation in the semiconductor due to the introduction of trapping and recombination centers resulting from the irradiation damage. The GaAs:Cr, unlike the InP:Fe, more closely follows the longer square-pulse exhibiting no nonlinearity. All results are consistent with previously investigated neutron irradiated devices.

TABLE OF CONTENTS

I.	INTRODUCTION -----	11
II.	THEORY -----	14
	A. RADIATION -----	14
	1. Interaction of Electrons with Matter -----	14
	a. Electron Mass Collision Stopping Power -----	15
	b. Electron Mass Radiative Stopping Power -----	17
	c. Energy Deposition--Dose Measurements -----	18
	2. Lattice Defects -----	19
	a. Atom Displacement Cross Section -----	20
	b. Number of Displaced Atoms -----	25
	c. Replacement Collisions -----	26
	d. Radiation Effects -----	27
	B. PHOTCONDUCTORS -----	28
	1. Photoconductivity -----	28
	2. Recombination Centers and Carrier Relaxation Time -----	31
	3. Impulse Response -----	38
	4. Square-Pulse Response -----	39
	5. Photoconductive Gain -----	40
III.	EXPERIMENTAL PROCEDURE -----	42
	A. RADIATION FACILITY -----	42
	B. SAMPLE FABRICATION -----	43

C. MEASUREMENT TECHNIQUES AND INSTRUMENTATION -----	44
1. Pre-Irradiation -----	44
2. Post-Irradiation -----	47
IV. EXPERIMENTAL RESULTS -----	70
A. DARK CURRENT -----	70
B. IMPULSE RESPONSE -----	71
C. SQUARE-PULSE RESPONSE -----	72
D. COMPUTER SIMULATION -----	73
E. DISPLACEMENTS -----	81
F. COMPARISON WITH NEUTRON DAMAGED DEVICES --	81
V. CONCLUSIONS -----	83
APPENDIX A: IMPULSE RESPONSE EQUIPMENT LIST -----	85
APPENDIX B: SQUARE-PULSE RESPONSE EQUIPMENT LIST -----	86
APPENDIX C: INPUT PROGRAM FOR ELECTRON/PHOTON TRANSPORT ACCEPT CODE -----	88
LIST OF REFERENCES -----	120
INITIAL DISTRIBUTION LIST -----	122

LIST OF TABLES

TABLE

1.	THRESHOLD DISPLACEMENT ENERGIES -----	22
2.	INP AND GaAs ENERGY LEVELS -----	28
3.	IMPULSE RESPONSE MEASUREMENTS -----	54
4.	SQUARE-PULSE RESPONSE MEASUREMENTS -----	62
5.	DISPLACEMENTS -----	82

LIST OF FIGURES

FIGURE

1.	Kinchin and Pease assumptions for calculating the average number of displacements -----	24
2.	Kinchin and Pease assumptions for calculating the average number of replacements -----	24
3.	Picosecond Photoconductive Radiation Detector -----	29
4.	Method of Operation -----	29
5.	Semiconductor Fermi levels and demarcation levels -----	33
6.	Recombination processes -----	35
7.	Relative positions between Fermi level, recombination center level, center of band gap and demarcation level in a semiconductor -----	35
8.	Mounted photoconductive detector in the double-ended configuration -----	45
9.	Dark Current--InP:Fe Ingot number: CCIPS-3148B -----	49
10.	Dark Current--InP:Fe Ingot number: CCIPS-2223 -----	50
11.	Dark Current--InP:Fe Ingot number: CCIPS-3148T -----	51
12.	Dark Current--GaAs:Cr Ingot number: Cambridge-A852/R -----	52
13.	Dark Current--GaAs:Cr Ingot number: Cambridge-A852/R -----	53
14.	Impulse response measurement for InP:Fe Drift velocity -----	56

FIGURE

15.	Impulse response measurement for GaAs:Cr Drift velocity -----	57
16.	Impulse response measurement for InP:Fe Full-width at half maximum (response speed) -	58
17.	Impulse response measurement for GaAs:Cr Full-width at half maximum (response speed) -	59
18.	Comparison of InP:Fe Impulse and Square-pulse laser response before and after electron irradiation for a representative sample -----	60
19.	Comparison of GaAs:Cr Impulse and Square-pulse laser response before and after electron irradiation for a representative sample -----	61
20.	Square-pulse response measurement for InP:Fe Peak current vs Risetime (10%-90%) -----	64
21.	Square-pulse response measurement for GaAs:Cr Peak current vs Risetime (10%-90%) -----	65
22.	Square-pulse response measurement for InP:Fe Peak current vs Fluence -----	66
23.	Square-pulse response measurement for GaAs:Cr Peak current vs Fluence -----	67
24.	Square-pulse response measurement for InP:Fe Risetime (10%-90%) vs Fluence -----	68
25.	Square-pulse response measurement for GaAs:Cr Risetime (10%-90%) vs Fluence -----	69
26.	Angular Distribution (Electrons) -----	75
27.	Angular Distribution (Photons) -----	76
28.	Energy Spectra (Electrons) -----	77
29.	Energy Spectra (Photons) -----	78
30.	Electron Flux Distribution -----	79
31.	Photon Flux Distribution -----	80

ACKNOWLEDGEMENT

I would like to thank Dr. Robert B. Hammond, Ronald S. Wagner and Jeffery M. Bradley of the Los Alamos National Laboratory Group E-11. I sincerely appreciate their help in supplying and evaluating the photoconductive samples along with their insight in interpreting the results of this experiment. This project would not have been possible without their assistance.

I would also like to thank Joseph M. Mack and Edward Pogue of the Los Alamos National Laboratory M-4 Division. Their time, patience and facilities allowed me to successfully complete the Coupled Electron/Photon Transport Accept Code thereby giving a profile of the electron beam through the photoconductive samples.

Finally, I would like to extend my appreciation to Don Snyder of the Naval Postgraduate School for his expertise in operating the Electron Linear Accelerator.

I. INTRODUCTION

There has been recent interest in the development of bulk-semiconductor photoconductors with picosecond carrier relaxation time to be used as radiation detectors. Data on the response of semiconductor devices to radiation damage is required for design and development of their use in a radiation environment. These environments include space applications, accelerators, nuclear reactors and nuclear explosions, each of which involve specific irradiating particles. Compact radiation detectors with a high degree of sensitivity to photons, x-rays, soft x-rays, gamma rays, electrons, protons and neutrons are being developed by the Los Alamos National Laboratory Electronics Division. The current response of these devices is proportional to the incident-radiation intensity [Ref. 1].

Particles passing through devices deposit part of their energy into ionization and the remainder into displacement. The interaction with matter depends on properties of both the particle (mass, charge, kinetic energy) and the target (mass, charge, density). Bulk device characteristics are degraded by displacement damage which can decrease carrier mobility, carrier concentration and carrier recombination lifetime.

In the development of these bulk-semiconductor radiation detectors, irradiating particles are being utilized to

damage the device thereby creating trapping and recombination centers. The desired characteristic, specifically, a decrease in carrier relaxation time resulting in response time < 100 -ps is obtained while maintaining the sensitivity of the device. In particular, this development entails the use of neutrons with a thermal neutron flux of 9.0×10^{13} (neutrons/cm²-sec) for periods ranging from 2000-4000 seconds. Neutron transmutation doping in the bulk-semiconductor device is impeded by the filtration of low-energy neutrons [Ref. 1]. This source is provided by the OMEGA WEST REACTOR located at the Los Alamos National Laboratory.

In this thesis, discussion is presented on the radiation effects of high energy electrons on two different types of materials. Before irradiation, measurements of dark current, impulse response (source response shorter than detector carrier relaxation time) and square-pulse response (source response longer than detector carrier relaxation time) were made. The same measurements were made after the irradiation to determine changes in carrier relaxation time giving an indication of the resulting damage. These measurements were carried out utilizing the processes of photoconductivity.

The purpose of the experiment reported here is to determine the effect of 100 Mev electron irradiation on these bulk-semiconductor radiation detectors and the degree to which the displacement effects can be compared with those

of neutron irradiated devices. It is desirable to obtain similar results with the charged particle source (100 MeV electrons) as has been demonstrated with the neutron source.

II. THEORY

A. IRRADIATION

1. Interaction of Electrons with Matter

Electrons incident on a semiconductor interact with the atoms primarily through the process of Coulomb scattering. The electron path may be deflected through large angles and ranges may vary widely even for electrons of the same energy. The electron energy loss per collision may be very high.

At an energy of 100 MeV, the electrons lose energy partly due to ionization of the atoms and partly due to Bremsstrahlung (radiation loss). Stopping power is defined as the amount of energy lost by a particle per unit length of path through the stopping material. For electrons, the total stopping power is divided into two components: 1) collision stopping power--the average energy loss per unit pathlength due to inelastic Coulomb collisions with bound atomic electrons of the medium resulting in ionization and excitation, and 2) radiative stopping power--the average energy loss per unit pathlength due to the emission of bremsstrahlung in the electric field of the atomic nucleus and of the atomic electrons [Ref. 2]. As the electron traverses its path, energy going into ionization and excitation is absorbed by the target relatively close to the path. Energy lost through bremsstrahlung travels farther from the path before being absorbed.

a. Electron Mass Collision Stopping Power

The electron mass collision stopping power is calculated according to Bethe's stopping power theory using the formulation of Rohrlich and Carlson [Ref. 3].

$$\frac{1}{e} \left[\frac{\partial E}{\partial X} \right]_{\text{collision}} = \frac{2\pi N_a r_e^2 m c^2 z}{3^2 A} \left\{ \ln \left(\frac{T}{I} \right)^2 + \ln \left(1 + \frac{\tau}{2} \right) + F^-(\tau) - \beta \right\} \quad (1)$$

where:

$$F^-(\tau) = (1 - \beta^2) \left[1 + \frac{\tau^2}{8} \right] - [2\tau + 1] \ln 2$$

The collision stopping power of a compound can be approximated by the weighted sum of stopping powers of the atomic constituents of the compound. In formula 1, the following replacements are applicable.

$$Z/A \text{ by } \langle Z/A \rangle = \sum_j w_j (Z_j/A_j)$$

$$\ln I \text{ by } \ln I = \left[\sum_j w_j (Z_j/A_j) \ln I_j \right] / \langle Z/A \rangle \quad (2)$$

$$\beta \text{ by } \beta = \left[\sum_j w_j (Z_j/A_j) \beta_j \right] / \langle Z/A \rangle$$

where:

1) w_j is the fraction by weight of the j 'th atomic constituent

2) Z_j , A_j , I_j and β_j pertain to the j 'th atomic constituent

Properties of the medium are:

Z = atomic number

A = atomic weight

ρ = density (gm/cm^3)

I = mean excitation energy (eV)

β = density effect correction

Properties of the electron are:

γ = T/mc^2 - kinetic energy in units of rest mass

β = $v/c \approx 1$

Other parameters are:

$$2\pi N_a r_e^2 mc^2 = .153536 \left(\frac{\text{MeV cm}^2}{\text{mole}} \right)$$

Listed under the properties of the medium are the mean excitation energy and the density effect correction. The mean excitation energy is the logarithmic average of the excitation energies of the medium weighted by the corresponding oscillation strengths. One assumption used in determining the mean excitation energy is the use of the I -values of the elemental substances for the I -values of the atomic constituents of the compound. This neglects the molecular binding energies. The density effect correction takes into account the polarization of the medium which screens the electric field acting on the relativistic particle. The effect is a reduction of collision stopping power. [Ref. 2]

b. Electron Mass Radiative Stopping Power

The electron mass radiative stopping power can be expressed using the following formula [Ref. 2].

$$\frac{1}{\nu} \left[\frac{\partial E}{\partial X} \right]_{\text{radiative}} = \frac{N_a \alpha r_e^2 E Z^2}{A} \phi^{\text{e}(\tau)}_{\text{rad}} \phi^{\text{n}(\tau)}_{\text{rad}} \left[1 + \frac{1}{Z} \frac{\phi^{\text{e}(\tau)}_{\text{rad}}}{\phi^{\text{n}(\tau)}_{\text{rad}}} \right] \quad (3)$$

Properties of the medium (compound) are:

$$A = w_j A_1 + w_j A_2$$

$$Z = w_j Z_1 + w_j Z_2$$

where:

- 1) w_j is the fraction by weight of the j 'th atomic constituent
- 2) A_1 = atomic weight of element 1
- 3) A_2 = atomic weight of element 2

Properties of the electron are:

$$E = T + mc^2 = 100.511 \text{ MeV}$$

Other parameters are:

$\phi^{\text{e}(\tau)}_{\text{rad}}$ and $\phi^{\text{n}(\tau)}_{\text{rad}}$ are dimensionless, scaled, radiative energy loss cross sections

$$N_a = 6.022045 \times 10^{23} / \text{mole}$$

$$r_e^2 = 7.940775 \times 10^{-26} \text{ cm}^2$$

$$\alpha = Z/137$$

Implicit in the formulation of the electron mass radiative stopping power is electron-nucleus bremsstrahlung (emission of a photon due to the interaction of the electron with the screened Coulomb field of the atomic nucleus) and the electron-electron bremsstrahlung (Coulomb interaction with one of the atomic electrons). The ratio of the scaled, radiative energy-loss cross sections ($\sigma^e(\tau)_{\text{rad}}/\sigma^n(\tau)_{\text{rad}}$) is assumed to be one and values for ($\sigma^n(\tau)_{\text{rad}}$) are approximated from least-squares curves fitted from theoretical points based on Davies, Bethe and Maximon (1954) and Olsen (1955). [Ref. 2]

c. Energy Deposition--Dose Measurements

The range of the electron is defined as the average path length the electron travels until it is stopped by the medium as a result of energy loss. The electrons are assumed to lose energy continuously. If the range is divided by the density of the material, the distance an electron will travel can be determined.

Dose represents the total amount of energy deposited to the medium. It is given in rads (100 ergs/gram) and must be specified for the particular material. The front surface dose (thin sample) is expressed by the following formula [Ref. 4].

$$R = 1.6 \times 10^{-8} \phi \left[\frac{1}{\rho} \left[\frac{\partial E}{\partial X} \right]_{\text{collision}} \right]^{\text{RADS}} \quad (4)$$

where:

ϕ = electron fluence (electrons/cm^2) is determined from formula (24)

2. Lattice Defects

The type of lattice structure inherent in the study of these devices is the zinc-blende structure. In the diamond lattice structure, each atom lies in the center of a tetrahedron formed by the four nearest neighbors. This structure is restricted to elements. The zinc-blende structure is similar to the diamond lattice with the exception that the two nearest neighbors are occupied by different elements.

There are various types of lattice defects that can occur from 100 MeV electron irradiation. Considering only point defects, the lattice defects are broken up into two main categories which include isolated defects and cluster defects. Within isolated defects, the simplest type of defect assumed is the Frenkel defect. This is an empty lattice site (vacancy) and an atom occupying an interstitial position. The Frenkel defect requires an amount of energy given to the atom needed to displace it to the metastable interstitial site. The displacement process depends on the energy of the recoil and its direction with respect to other lattice atoms [Ref. 5]. Other isolated defects include divacancies which result when a high energy recoil atom imparts sufficient energy to displace a secondary atom along with the primary atom. The more complicated cluster defects involve regions containing large numbers of isolated defects.

For binary compounds (zinc-blende structure), the number of possible lattice defects is considerably higher than for elements. The displacement or replacement of atoms may result

in eight types of point defects: two types of vacancies, four types of interstitial atoms (surrounded by similar or dissimilar atoms) and two types of substitution defects [Ref. 6].

In the following sections, the irradiation induced processes of atomic displacements will be considered on a microscopic level. Both single atom and multiple atom displacements are discussed along with the assumptions made in determining the total number of displaced atoms. A complete review of damage theory is found in Seitz and Koehler [Ref. 7].

a. Atomic Displacement Cross Sections

For 100 MeV incident electrons (relativistic), enough energy is transferred to the lattice atoms to knock them from their normal lattice position into an interstitial site. These primary knock-on atoms may in turn depart some of their energy to form secondary displaced atoms. Radiation damage theories concentrate on these few elastic collisions.

In the relativistic range, McKinley and Feshbach [Ref. 8] formulated an expression for lower Z elements using the Rutherford differential cross section.

$$d\sigma_{mf} = R_{mf} d\sigma_{ruth} \quad (5)$$

where

$$R_{mf} = (1-\beta^2) [1-\beta^2 \frac{T}{T_m} + \pi \alpha \beta \left(\frac{T}{T_m} \right)^{1/2} - \frac{T}{T_m} \cdot]$$

The differential cross section of the atom must be integrated over all transferred energies. Additionally, the assumption

is made that recoil energies below the threshold displacement energy (T_d) have a probability of zero for displacing an atom whereas those recoil energies above the threshold displacement energy (T_d) have a probability of one. For thin samples, the energy loss is approximately constant over the sample thickness. The displacement cross section is dominated by small angle scattering at 100 MeV energies and is given by

$$\sigma_{mf} = 2.495 \times 10^{-25} \text{ cm}^2 \frac{z^2}{\beta \gamma^2} \left[\left(\frac{T_m}{T_d} - 1 \right) - \beta^2 \ln \frac{T_m}{T_d} \right. \\ \left. + \pi \alpha \beta \left\{ 2 \left[\left(\frac{T_m}{T_d} \right)^{1/2} - 1 \right] - \ln \frac{T_m}{T_d} \right\} \right] \quad (6)$$

Parameters are:

$$T_m = \text{maximum recoil energy} = \frac{2(E+2mc^2)E}{M^2c^2} \text{ (eV)}$$

$$E = \text{energy of the incident electron} = 100 \text{ MeV}$$

$$m = \text{rest mass of the electron}$$

$$M = \text{mass of the target atom}$$

$$T_d = \text{threshold displacement energy (values given in Table 1)}$$

$$\alpha = Z/137$$

If the primary atom has sufficient energy, additional displaced atoms are produced forming a displacement cascade. In order to determine the effective cross section for both primary and secondary displacements, $\nu(T)$, the average number of displacements per primary recoil of energy T , must be determined. A number of assumptions are made. [Refs. 5,9,10]

TABLE 1
THRESHOLD DISPLACEMENT ENERGIES [REF. 9]

Substance	GaAs		InP	
Displaced Atom	Ga	As	In	P
Threshold Electron Energy E_b (keV)	228	273	270	110
Threshold Displacement Energy T_d (eV)	8.8	10.1	6.6	8.8
Self-Diffusion Energy (eV)	5.6	10.2	3.85	5.65

1. A step junction threshold is assumed.
2. Atom-atom collisions are treated as hard-sphere elastic interactions.
3. The ordered arrangement of atoms in the lattice structure is not considered.
4. Damage is considered homogeneous.
5. Annealing is not considered.
6. Glancing collisions are not considered even though energy loss may be incurred.
7. The number of replacements per primary are not considered. The moving atom will replace the struck atom if the latter receives energies greater than T_d and the former retains energy less than T_d .
8. Lattice atoms are considered at rest.
9. Long range effects from other atoms are not considered.
10. There is no account for ionization losses.

Kinchin and Pease [Ref. 11] consider the threshold energy by postulating that both the striking and struck atoms

require an energy T_d or greater after the collision. This accounts for replacements but does not account for the energy loss of the primary atom in climbing out of its potential well. Figure 1 displays the assumptions made by Kinchin and Pease in calculating the average number of displacements. The Snyder and Neufeld model [Ref. 12] does not account for replacement but does account for the potential binding energy. In this model, the secondary atom loses energy T_d before making subsequent displacements. The average number of displacements per primary recoil of energy T_d is given by

$$\begin{aligned} v(T) &= 1 \quad T_d \leq T \leq 2T_d \\ &= \frac{BT}{T_d} \quad 2T_d < T < T_i \end{aligned} \quad (7)$$

Parameters are:

$$T = \text{average energy transferred} = T_d (\ln T_m/T_d - 1 + \dots)$$

$$T_i = \text{Ionization Energy} = M_E G / 8m_e$$

$$B = .5 \text{ (Kinchin and Pease); } .56 \text{ (Snyder and Neufeld)}$$

For compounds, the ratio of the atomic masses influences the transferred energy. The maximum energy transferred is λ times the energy of the striking atom where [Ref. 9]:

$$\lambda = \frac{4M_1 M_2}{(M_1 + M_2)^2} \quad (8)$$

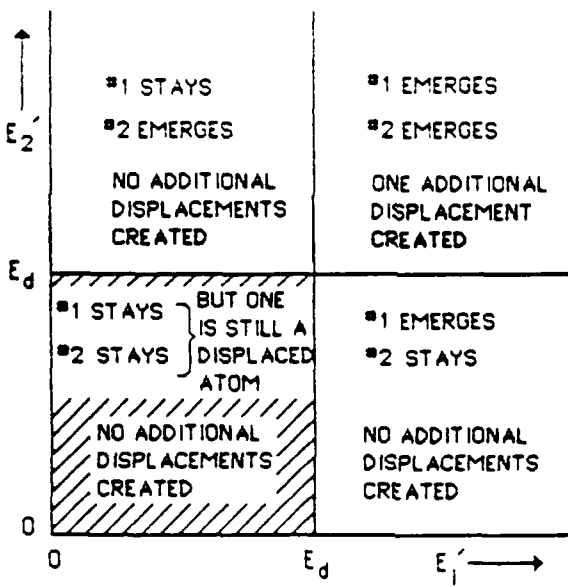


Figure 1. Kinchin and Pease assumptions for calculating the average number of displacements [Ref. 10]

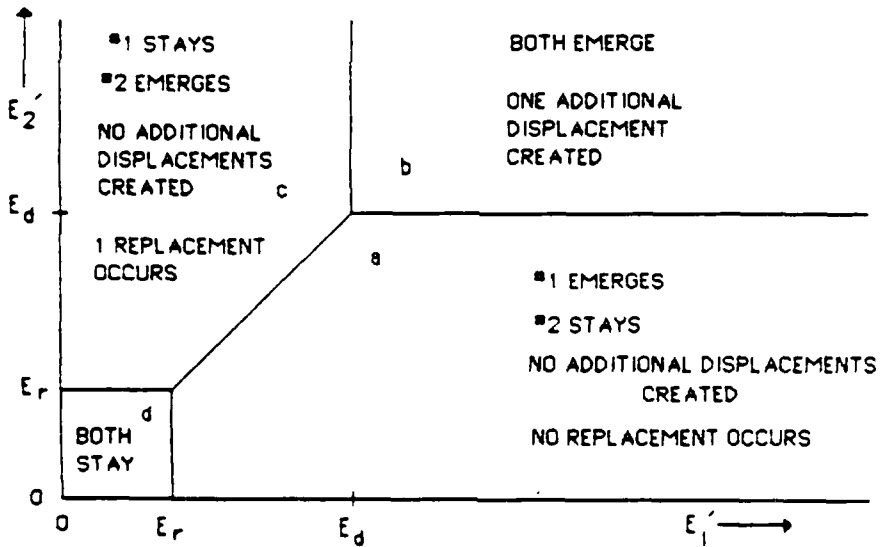


Figure 2. Kinchin and Pease assumptions for calculating the average number of replacements [Ref. 10]

The Kinchin and Pease model holds for compounds provided there is equal probability of collision for the secondary atoms. Replacement collisions involving unlike atoms are called misplacements and account for a substantial portion of the damage.

The effective cross section for primary and secondary displaced atoms in compounds is determined by multiplying (6), (7) and (8).

$$\sigma_d = \sigma_{mf} \nu(T) \lambda \quad (9)$$

b. Number of Displaced Atoms

In the previous section, the total cross section for both primary and secondary displacements was determined. From this, the density of Frenkel defects (for thin samples) produced per cm^3 can be determined given the incident electron energy and fluence. [Ref. 13]

$$N_F = f_e \sigma_d N_O \quad (10)$$

Parameters are:

N_F = number of Frenkel defects per cm^3

σ_d = total displacement cross section

f_e = electron fluence

N_O = number of lattice atoms per cm^3 = $\frac{N_a \text{ atoms}}{A}$

where:

ρ = density (gm/cm³)

N_a = Avogadro's number = 6.02×10^{23} (atoms/mole)

A = atomic number of the target molecule

The number of Frenkel defects determined experimentally from various sources is always less than the number predicted by theory. This is a function of the assumptions made in formulating the various models.

c. Replacement Collisions

Replacement collisions occur when there is an exchange of roles between the primary and secondary knock-on atoms. For binary compounds, the exchange can be between similar or dissimilar atoms and will occur when the moving atom imparts sufficient energy to the stationary atom to cause displacement but does not retain sufficient energy to escape the potential well of the vacancy, thereby replacing the displaced atom.

Dienes and Vineyard [Ref. 10] have determined the number of replacements per primary atom of energy T to be

$$u(T) = \frac{T}{2T_d} [1.614 \ln(\frac{T_d}{T_r}) + 1] \quad T \geq 2T_d \quad (11)$$

The replacement threshold T_r has not been determined experimentally, however, Kinchin and Pease have suggested a ratio of $T_d/T_r = 10$. A summary of the Kinchin and Pease assumptions for

determining the average number of replacements is found in Figure 2.

d. Radiation Effects

The macroscopic electrical properties of semiconductors are affected by the microscopic defects resulting from electron irradiation. The specific type of damage is a function of many different variables including temperature during irradiation, energy spectra, impurity and dopant concentrations, rate and history of the irradiation and minority carrier injection ratio. The introduction of energy levels within the forbidden gap due to point defects will be considered.

Point defects primarily affect the electrical properties by their ability to either produce or remove charge carriers, change carrier mobility or both. Several models have been proposed to explain the behavior of Frenkel pairs in semiconductors, especially in silicon and germanium. James and Lark-Horovitz [Ref. 14] have suggested that interstitials act as donors below the conduction band with two donor levels assigned whereas empty acceptor states above the valence band are produced by vacancies. The relative location in the forbidden gap will ultimately determine the net effect of these localized states with electrons redistributing themselves to fill the low energy states. Blount [Ref. 15] based his arguments on atomic and molecular orbitals stating that each defect can act as either donor or acceptor, depending on the position of the Fermi level. As the concentration of irradiation defects increase to a level

which is considerably greater than the concentration of impurities, the Fermi level approaches saturation and is determined by the distribution of defect levels in the forbidden gap. Table 2 lists energy levels that have been experimentally determined for InP and GaAs [Refs. 9,16].

TABLE 2
InP AND GaAs ENERGY LEVELS

<u>Band Gap E_G, opt (300°K)</u>		Forbidden Gap Energy Levels in eV at 300°K with Electron or Gamma Irradiation			
InP	GaAs	Below Conduction Band		Above Valence Band	
		InP	GaAs	InP	GaAs
1.260	1.430	0.285	0.13		0.35
			0.38		
			0.52		

The effect on the processes of photoconductivity due to the introduction of energy levels in the forbidden gap during electron irradiation will be discussed in the following sections.

B. PHOTOCODUCTORS

1. Photoconductivity

A photoconductor consists of a bulk-semiconductor material with ohmic contacts (Figure 3). The electrical conductivity is equal to the product of the number of charge carriers, their charge and their mobility. The steady-state

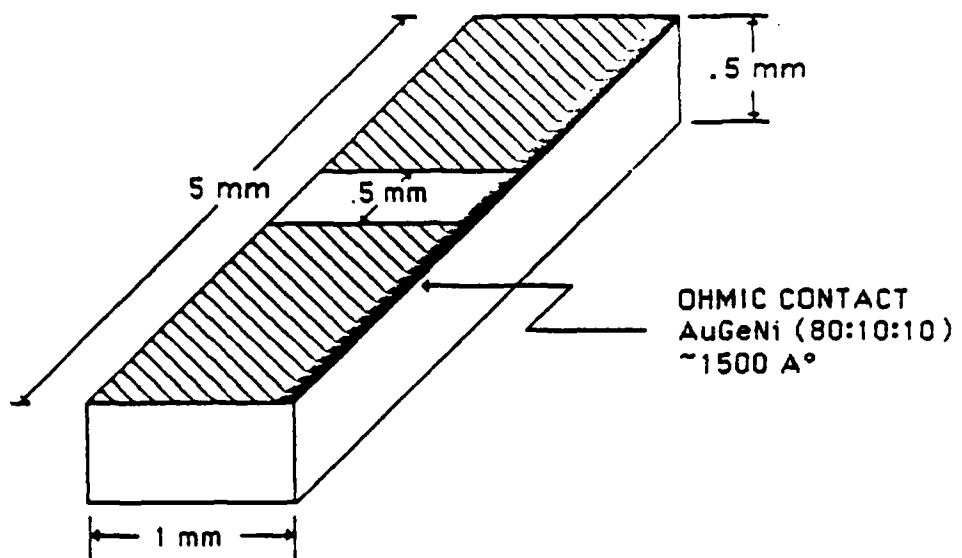


Figure 3. Picosecond Photoconductive Radiation Detector

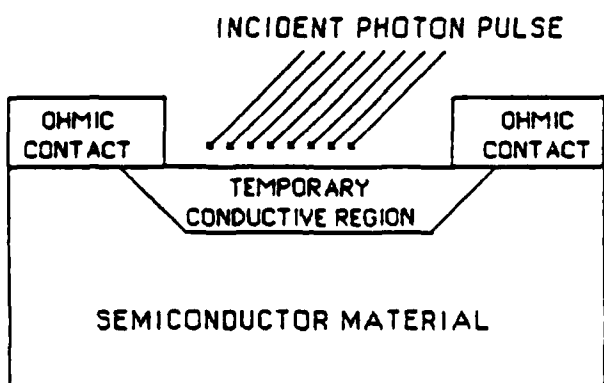


Figure 4. Method of Operation. The region between the ohmic contacts is illuminated with the photon source. The photons are absorbed creating free charged carriers (electrons and holes) which produce a temporary conductive path between the contacts. The full-width at half maximum (FWHM) impulse response measurement is a measure of the photoconductor response speed. It is a function of the carrier recombination lifetime in the active region. [Ref. 22]

contribution to the electrical conductivity resulting from photon irradiation is defined as the photoconductivity. In nonhomogenous semiconductors, the ideal of an "effective mobility" is used to describe low conductivity barriers which limit the flow of current through the material [Ref. 6]. Steady-state photoconductivity is expressed as

$$\Delta\sigma = q(n\Delta\mu_n^* + p\Delta\mu_p^*) \quad (12)$$

When excited by an external photon source, charged carriers are generated by either band-to-band transitions (intrinsic) or by transitions involving forbidden gap energy levels (extrinsic). It is the extrinsic transitions which will be of interest in this experiment. Photoconductivity takes place by the absorption of photons of energy equal to or greater than the energy separation between the forbidden gap levels and the conductance or valence band levels. The conductance of these devices is proportional to the intensity of the incident photon source and takes place via a temporary conductive region between the ohmic contacts (Figure 4) resulting from the creation of free electrons and holes. This nearly intrinsic region consists of a high concentration of forbidden gap energy levels acting as recombination centers. For transient photoconductivity, the picosecond response time depends on the carrier relaxation time and not on the spacing between contacts. This allows for a large bias across the device thereby increasing

the sensitivity. Quasi-neutrality and ideal ohmic contacts are assumed. [Ref. 17]

Desirable material properties for radiation detector applications include short carrier recombination lifetime, high carrier drift velocity, high resistivity (low dark current) and high carrier mobility [Ref. 18]. The efficiency of the photoconductor is measured in terms of its photoconductive gain, response time and sensitivity. It has been concluded that the transient recombination is a bulk controlled process for InP:Fe [Ref. 18].

2. Recombination Centers and Carrier Relaxation Time

The time that a charged carrier is available to contribute to the conductivity is defined as the free lifetime. For excited electrons, it is the time spent in the conduction band. For excited holes, it is the time spent in the valence band. Both minority and majority carriers contribute. The free lifetime is limited by three different processes: 1) extraction of the carriers from the photoconductor without replacement as a result of a voltage bias, 2) absorption into a trapping center, 3) recombination with a carrier of opposite sign at a recombination center. The distinction between a trapping center and a recombination center is statistical in nature and is delineated as follows: in a trapping center, a captured carrier has a greater probability of thermal re-excitation to a free state whereas a recombination center provides the captured carrier with a greater probability of recombining with a carrier of the opposite

sign. A demarcation line represents that level which gives equal probability for either event to occur. Figure 5 displays the relative position between the Fermi level and the demarcation level. Area I represents those levels (electron traps) in which the occupation depends on the thermal equilibrium between the conduction band and the level. The occupation of the levels in Area IV (hole traps) depends on the thermal equilibrium between the valence band and the level. Due to the high density of occupied levels in Area II, recombination is taking place even though the conduction band is still in thermal equilibrium with these levels. [Ref. 19]

Recombination takes place via bound states in the forbidden gap. These bound states are comprised of impurities, crystal defects, vacant lattice sites and interstitial atoms [Ref. 20]. Before irradiation, the energy levels in the forbidden gap are due to the chemical doping of the sample and determine the number of charge carriers. Irradiation produces defects resulting from atomic displacements and introduces energy levels into the forbidden gap of semiconductors. These energy levels are often deeper in the gap than those dominating conductivity and serve as recombination centers for electrons and holes. The process of recombination at the local centers is influenced by the carrier population of the centers. The capture of the minority carrier is generally the limiting step in the recombination process. There are four processes through which free carriers interact at these recombination centers: 1) electron

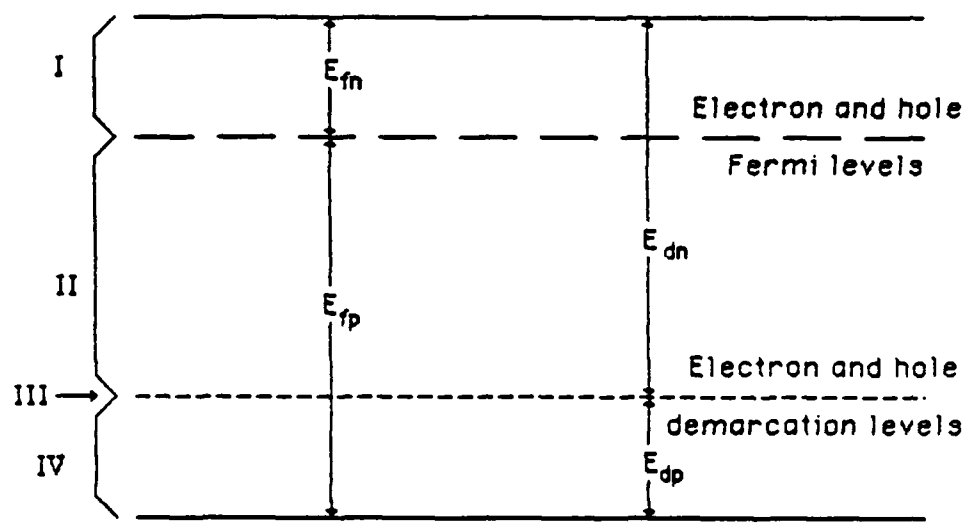


Figure 5. Semiconductor Fermi levels and demarcation levels [Ref. 19]

capture--the process in which an electron falls from the conduction band into an neutral localized state, 2) electron emission--the emission of an electron from the negatively charged localized state into the conduction band, 3) hole capture--the falling of an electron from the negatively charged localized state into the valence band, 4) hole emission--the excitation of an electron from the valence band into the neutral localized state. These processes are illustrated in Figure 6. The net rate of recombination is defined by the following equation:

$$\begin{aligned}
 U &= \frac{N_t v_{th} \sigma_n \sigma_p (pn - n_i^2)}{\sigma_p \left[p + n_i \exp \left(\frac{E_i - E_t}{kT} \right) \right] + \sigma_n \left[n + n_i \exp \left(\frac{E_t - E_i}{kT} \right) \right]} \\
 &= \frac{(pn - n_i^2)}{\tau_{no} \left[p + n_i \exp \left(\frac{E_i - E_t}{kT} \right) \right] + \tau_{po} \left[n + n_i \exp \left(\frac{E_t - E_i}{kT} \right) \right]} \quad (13)
 \end{aligned}$$

where σ_n and σ_p are the electron and hole capture cross sections, v_{th} is the carrier thermal velocity, N_t is the recombination center density, E_t is the recombination energy level and E_i is the intrinsic Fermi level.

Figure 7 displays the relative position of the Fermi level (E_f), the recombination center (E_t), center of the band gap (E_i) and the demarcation level (E_d). The minority lifetime of a free carrier varies depending on the relative positions of these levels. All six cases assume the density of the recombination centers to be greater than the density of the

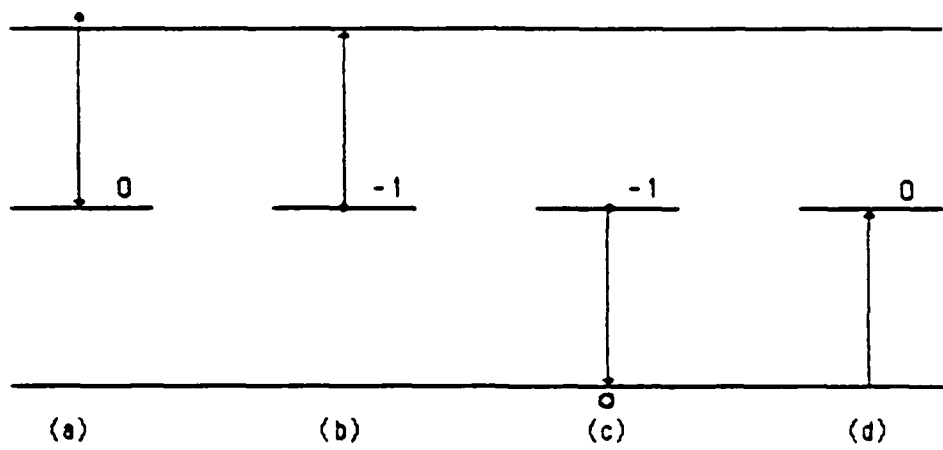


Figure 6. Recombination processes [Ref. 19]

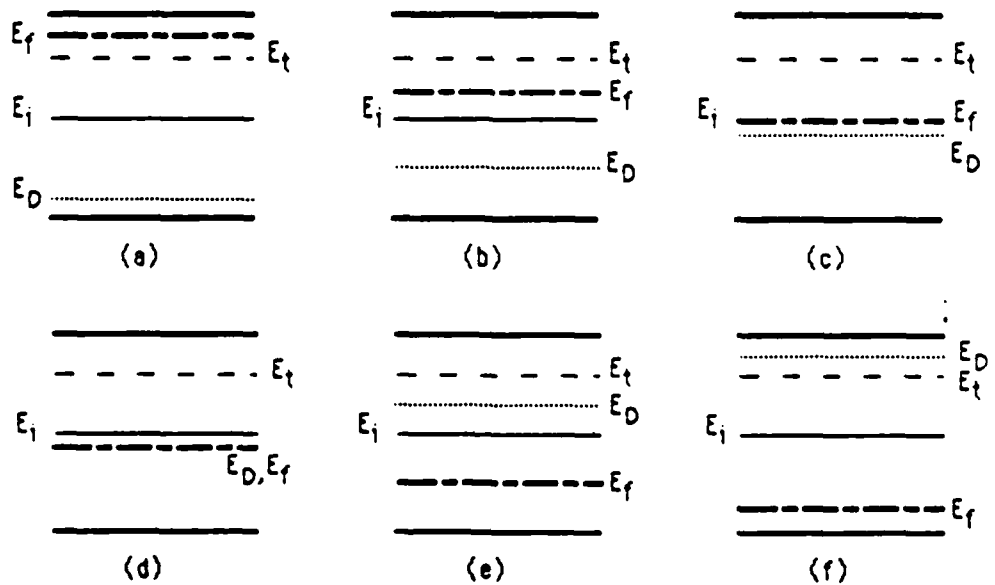


Figure 7. Relative positions between Fermi level, recombination center level, center of band gap and demarcation level in a semiconductor [Ref. 19]

free carriers. Additionally, the recombination processes apply to all levels lying between the Fermi level and the demarcation level, with an exponential decrease in the contribution to centers outside the bounds of these levels. The Fermi level and demarcation level move in opposite directions but at an equal rate.

The carrier relaxation time is due to the trapping and recombination of the free carriers in the conductive region. A mechanism for electron and hole capture in the InP:Fe samples suggests that an acceptor state .61 eV below the conduction band results from the Fe dopant. This acceptor state can exist in either of two charged configurations. Electrons are captured via the neutral state. The negatively charged state acts as a recombination center with the capture of holes. The relaxation time is characterized by the following equations. [Ref. 1]

$$\frac{dn(t)}{dt} = f(t) - r_{CT} \quad (14)$$

$$\frac{dp(t)}{dt} = f(t) - r_{TV} \quad (15)$$

$$\frac{dn_{T-}(t)}{dt} = r_{CT} - r_{TV} \quad (16)$$

$$r_{CT} \equiv v_e \sigma_e n_{TO}(t) n(t) \quad (17)$$

$$r_{TV} \equiv v_h \sigma_h n_{T-}(t) p(t) \quad (18)$$

where $n(t)$ and $p(t)$ represent the electron and hole concentrations, $n_{T-}(t)$ and $n_{T_0}(t)$ are the concentration of charged and neutral acceptor states, $\dot{e}(t)$ is the generation rate, r_{eT} is the capture rate of electrons by the neutral acceptor states, r_{TV} is the capture rate of free holes by the negatively charged acceptor state, v_e and v_h are the thermal velocities of electrons and holes, and σ_e and σ_h are the capture cross section for electrons and holes at the neutral and negatively charged acceptor state.

Transient photoconductivity involves the assignment of two characteristic times to the forbidden gap energy levels to describe the recombination process. The transient time constants for small excess carrier densities in a nondegenerate semiconductor near thermal equilibrium are described by the following formulas. [Ref. 17]

$$n(t) = A_n \exp(-t/\tau_{RA}) + B_n \exp(-t/\tau_{MR}) \quad (19)$$

and

$$p(t) = A_p \exp(-t/\tau_{RA}) + B_p \exp(-t/\tau_{MR}) \quad (20)$$

where the initial conditions determine the coefficients A_n , B_n , A_p and B_p . The equal capture rate for electrons and holes by a recombination center requires a readjustment of charges. The time needed for this readjustment is denoted by τ_{RA} and is identical for both electrons and holes. For the condition

when $N_{TT} \ll n_i$, τ_{MR} (the main recombination lifetime) does not equal the steady-state lifetime. [Ref. 17]

3. Impulse Response

Impulse response occurs when the source response is shorter than the detector carrier relaxation time. The conductance of the device is the result of photon absorption and increases linearly with the energy of the radiation pulse. This absorption produces free electrons and holes that provides a conductive path between the metallic contacts (as illustrated in Fig. 4). The response time is a property of the material and depends inversely on the uncharged recombination centers. The 100 MeV electron irradiation damages the device in such a way as to create trapping and recombination centers which produce faster response times and increased sensitivity.

Desirable properties for detector application includes a peak current response which is proportional to the light intensity and a response speed which is independent of light intensity [Ref. 21]. The peak current response is indicated by the following formula. [Ref. 22]

$$I = \frac{(1-R_r) q v_d E}{S w} \quad (21)$$

Parameters are:

I = observed peak current

q = electronic charge = $(1.6 \cdot 10^{-19} \text{ C})$

v_d = electron drift velocity = $\sim V_{appl}/S$

E = Energy deposited into detector by incident radiation = $(580 \pm 20\% \text{ pJ})$

S = contact spacing = (.05 cm)

W = Energy to create an electron-hole pair = (5 eV)

R_r = Reflectivity = (30 percent)

The assumptions implicit in this formula are an incident radiation pulse which is much shorter than the carrier relaxation time of the device, the impedance of the device is always much greater than that of the 50 ohm load and current resulting from the free holes is ignored because of the much lower drift velocity.

The electron mobility in the radiation detector may be approximated by using the measured peak current.

$$u = \frac{I S^2 W}{(1-R_r) q V_{appl} E} \quad (22)$$

where:

V_{appl} = applied voltage

4. Square-Pulse Response

Square-pulse response occurs when the source response is longer than the detector carrier relaxation time. It is a measure of the relative change in the electron and hole populations. The transient response for InP:Fe is controlled by the trap-assisted recombination of electrons and holes [Ref. 1].

For square-pulses (long radiation pulse), the uncharged acceptor states become negatively charged due to electron trapping. This is a very fast process which leads to saturation

by the negatively charged acceptor states. At the same time, hole trapping by the negatively charged acceptor states is occurring but at a slower rate due to a substantially lower hole mobility. At a certain point, the hole population exceeds the electron population and thus makes the dominant contribution to the current. When both electron and hole trapping rates equal the hole-electron generation rate, steady-state is achieved. [Ref. 1] This is entirely dependent on the intensity of the incident square-pulse. The peak current response is measured by the following formula.

$$I = \frac{(1-R_r) q v_d p \tau}{S W} \quad (23)$$

Parameters are:

p = optical power

τ = recombination lifetime

5. Photoconductive Gain

Photoconductive gain is defined as the ratio of the recombination lifetime of the charged carriers to the transit time across the active area between electrodes. The bulk picosecond photoconductor decouples the dependency of the carrier recombination lifetime with the transit time. The response speed is a function of the carrier relaxation time within the active region and is thus independent of electrode spacing and bias. A necessary condition for photoconductive gain to be greater than unity is provided by the injection of electrons

into the device by the metallic contacts. This replenishes those electrons leaving the exit electrode. For each non-reflected incident photon, more than one electron is delivered to the external circuit. Photoconductive gains as high as 5 have been demonstrated in InP:Fe photocnductors with AuGe and AuSn contacts annealed at 450 C [Ref. 22].

III. EXPERIMENTAL PROCEDURES

A. RADIATION FACILITY

Irradiations were performed using the Electron Linear Accelerator (LINAC) at the U.S. Naval Postgraduate School. The LINAC is a travel-wave accelerator consisting of a disk-loaded circular waveguide thirty feet long divided into three ten-foot sections. A series of three klystron amplifiers are used to feed RF power into each ten-foot section. Electrons are initially produced by an electron gun and are injected into one end of the sections where those in proper phase relation will be accelerated. A magnetic quadrupole doublet located downstream from the deflection magnets serves to focus the beam on the target.

The LINAC operates with an electron beam pulse length of 1.0 micro-second at a repetition rate of 60 pulses per second. Electrons are focused on a target positioned in a target chamber with a vacuum of 10^{-6} Torr maintained by a diffusion pump. In this experiment, electrons leave the accelerator at an energy of 100 MeV and an average electron current of 1 micro-ampere.

Electron fluence is measured by secondary emission monitors (SEM). Two SEM's were used during the experiment. A smaller SEM was placed inside the vacuum chamber in front of the target. A larger SEM was placed outside of the vacuum chamber in the beam line after the target. Prior to irradiation of the target, the SEM's were calibrated. The larger SEM was previously calibrated

against a Faraday cup and was determined to have a 6% efficiency [Ref. 23]. The smaller SEM was calibrated against the larger SEM. As the electrons impact the SEM's, secondary electrons charge a capacitor. A voltage integrator measures a voltage developed across the capacitor which is proportional to the charge. The ratio of voltages between SEM's is 2.33 which equates to a 2.6% efficiency for the smaller SEM. The electron fluence is determined by the formula

$$\Phi = \frac{C V}{(.026) q A} \quad (24)$$

where Φ is the electron fluence in electrons/cm², C is the capacitance in Farads, V is the integrated voltage in Volts, q is the charge of an electron, A is the area of the beam in cm² and .026 the SEM efficiency correction factor. A more extensive description of the LINAC and its operating parameters may be found in Reference 24.

B. SAMPLE FABRICATION

Devices are fabricated from two different types of materials: Indium Phosphide with Iron dopant (InP:Fe) and Gallium Arsenide with Chromium dopant (GaAs:Cr). The procedure was developed and performed by the Los Alamos National Laboratory (LANL) Group E-11. The single crystal materials are obtained commercially, the InP:Fe from CrystaComm Inc. and the GaAs:Cr from Cambridge Instruments LTD. The InP:Fe samples are claimed by the manufacturer to have a resistivity of 2×10^7 ohm-cm and an electron mobility of 2200 cm²/V-sec.

The crystal is cut with a diamond saw to a specified size (5 mmL \times 1 mmH \times .5 mmD). The surface is polished and bromine etched to remove any damage. The samples are then rinsed with methanol and de-ionized water to remove the bromine solution. Positive resist photolithographic liftoff is applied while spinning @ 1000 rpm/5 sec and then baked for 30 minutes at 60°C. The samples are then rinsed with methanol while spinning, baked again and placed in a masked aligner where they are exposed to ultra-violet light for 25 seconds. Metallic contacts are applied to the device by a multi-step vacuum evaporation of Au, Ge, Ni compound (80% 10% 10%). Acetone is used to dissolve the .5 mm masked gap exposing the material. The samples are then annealed at 450°C for 2 min. The sample is supported by a 5 cm \times 5 cm alumina substrate with 50 ohm microstrip transmission lines and SMA coaxial connectors. A section of the transmission line is removed and the sample is mounted with conductive silver epoxy which makes electrical contact. During all tests, one end of the sample connection was biased and the opposite end (current-signal measurement) was connected into the sampling oscilloscope (25-ps risetime). The mounted sample is illustrated in Figure 8.

C. MEASUREMENT TECHNIQUES AND INSTRUMENTATION

1. Pre-irradiation

Before irradiation, all samples were evaluated to determine current vs voltage characteristics (dark current), impulse response and square-pulse response measurements. A total of

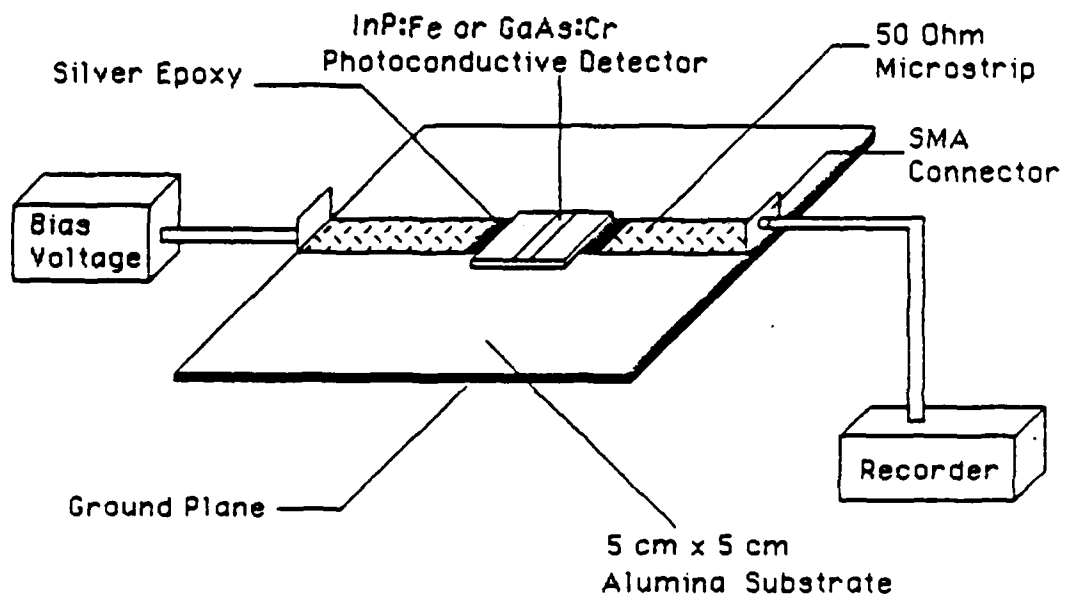


Figure 8. Mounted photoconductive detector in the double-ended configuration

eight InP:Fe and four GaAs:Cr samples were prepared. Ingot numbers are listed in Table 3. All measurements were performed at LANL.

Dark current curves were determined using an Ortec Detector Control Unit (Model 210). The InP:Fe samples were biased up to 500 volts in 100 volt increments. The GaAs:Cr samples were biased up to 125 volts in 25 volt increments. Figures 9 through 13 display the reference plots.

Impulse response measurements were evaluated using the equipment listed in Appendix A. The coaxial, double-ended mounted samples (with separate bias and signal cable connections) were pulsed with the Hamamatsu Picosecond Light Pulser (90-ps FWHM optical pulses) at a frequency of 10 KHz and a wavelength of 820 nm. During the procedure, a bias of 200 volts was maintained on the InP:Fe samples and 100 volts on the GaAs:Cr samples. The signal was evaluated using the Tektronix TDR/Sampler, Processor, Acquisition Unit and Oscilloscope. The determination of amplitude, full-width at half maximum and baseline tail was made and photographs taken. Results are listed in Table 3.

Square-pulse response measurements were evaluated using the equipment listed in Appendix B. The samples were pulsed with the Tektronix PG 501 Pulse Generator which produces an optical source with fast risetime and falltime (150-ps), constant power (3 mW) and continuously-variable-duration optical pulses at a wavelength of 830 nm [Ref. 1]. As in the impulse response measurements, the InP:Fe samples were biased at 200

volts and the GaAs:Cr samples were biased at 100 volts. The signal was processed using the Tektronix 7104 Oscilloscope (with listed supplemental units) and was sent through the Princeton Applied Research Signal Averager before being recorded on the Hewlett Packard 7044A X-Y Recorder. Both photographs of the oscilloscope signal and the final X-Y graphs were used to determine the rise time constants of the square-pulse response. The results are listed in Table 4.

2. Post-Irradiation

After the above characterization was made, the samples were irradiated. Two coaxial, double-ended mounted samples plus a phosphor target plate were mounted on an aluminum ladder and placed in the vacuum chamber of the LINAC for irradiation. A vacuum of approximately 10^{-6} Torr was maintained. The samples were connected to coaxial cables to allow for a bias voltage and current measurement (dark current) during the irradiation. The beam was focused on the phosphor target plate and the area was adjusted. A video camera monitored the samples to allow for proper positioning of the beam. The smaller SEM was used along with a 1 micro-F capacitor to measure the integration of the voltage.

The samples were irradiated obtaining fluence in the range of 10^{13} to 10^{16} electrons/cm². Formula (24) was used to determine the exact fluence. Dark current measurements were performed just prior to irradiation and immediately after the irradiation. An attempt was made to measure dark current during

the irradiation by placing the beam in standby, however, this was fruitless due to the excitation of the samples.

After the samples have been removed from the vacuum chamber and monitored for residual radiation, they were sent to LANL for post-irradiation measurements. These measurements followed the exact procedure as for the pre-irradiation measurements and the two were compared to determine the effect of the electron bombardment. The results are displayed in Figures 9 through 25 and listed in Tables 3 and 4.

DARK CURRENT - INP:FE

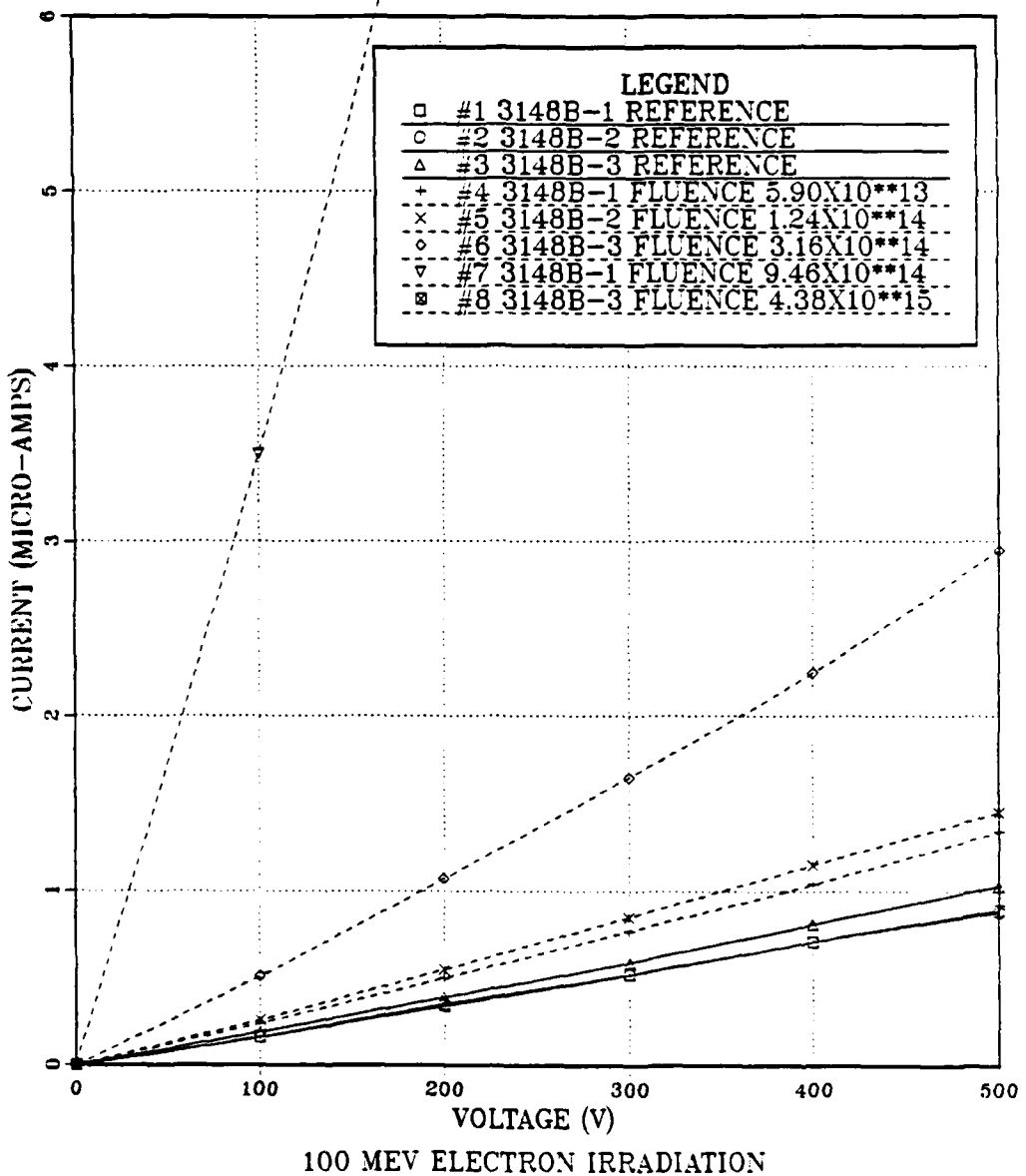


Figure 9. Dark Current--InP:Fe Ingot number: CCIPS-3148B
 Data for curve #8 was not obtained due
 to device breakdown at 5 volts

DARK CURRENT - INP:FE

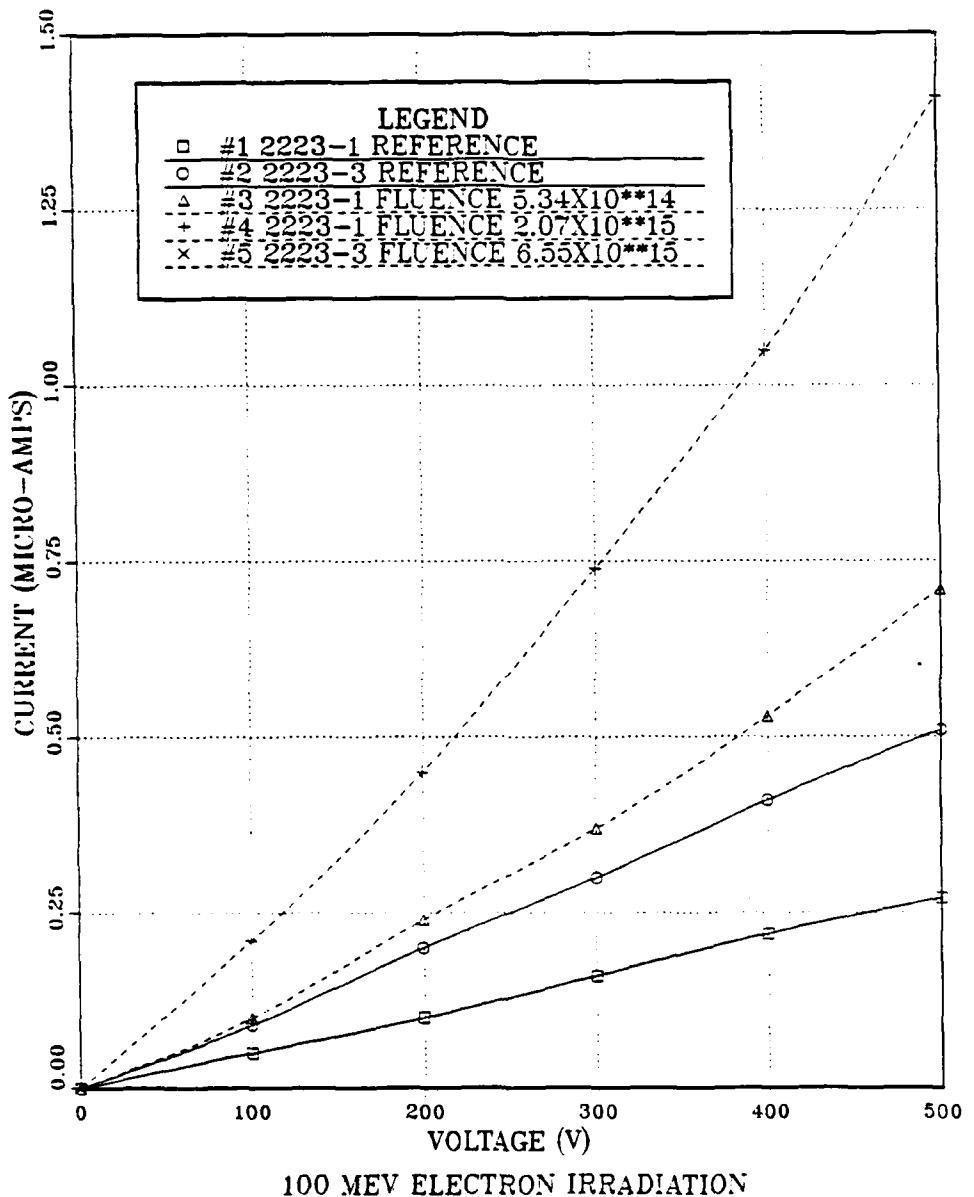


Figure 10. Dark Current--InP:Fe Ingot number: CCIPS-2223
 Data for curve #5 was not obtained due to
 device breakdown at 50 volts

DARK CURRENT - INP:FE

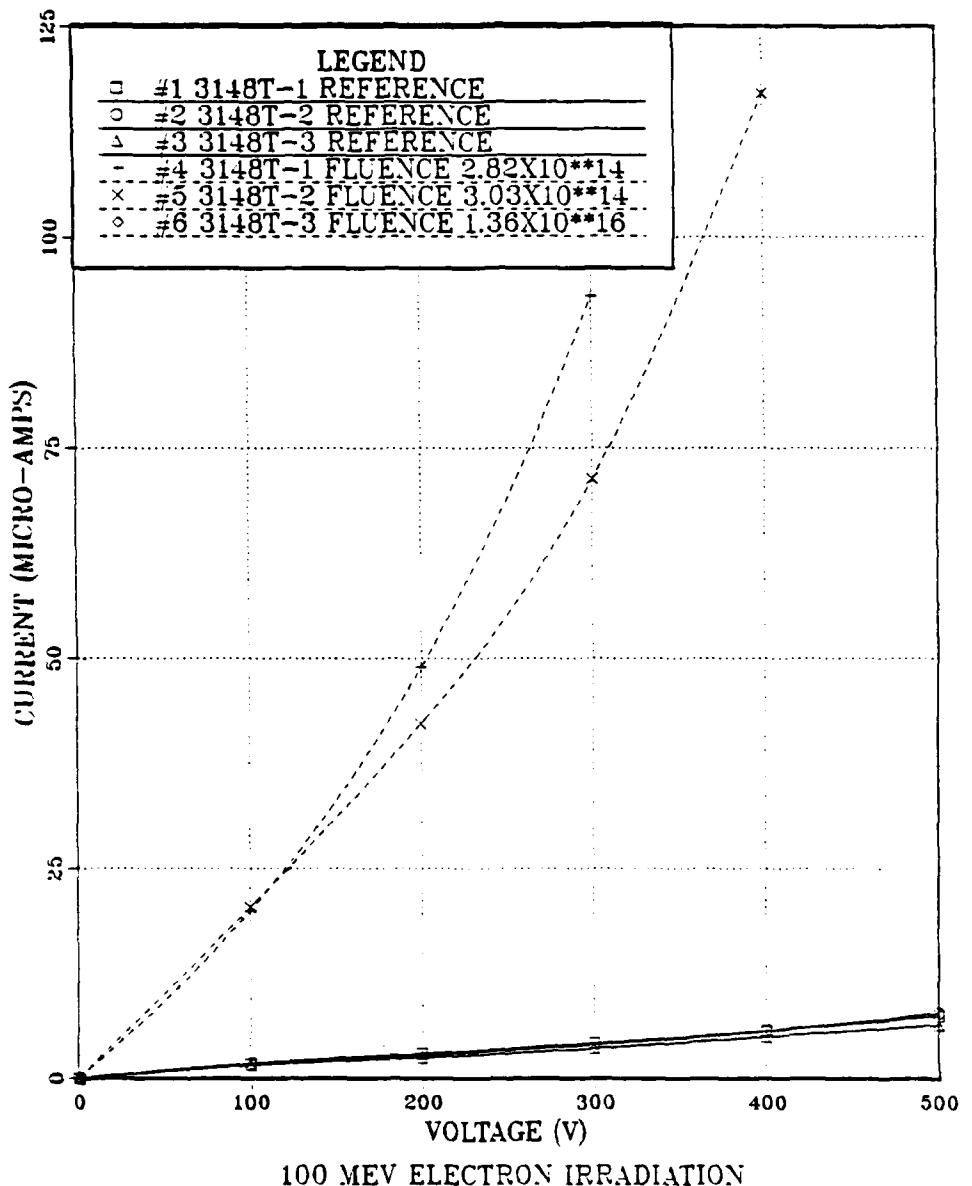


Figure 11. Dark Current--InP:Fe Ingot number: CCIPS-3149T
 Data for curve #6 was not obtained due to device breakdown at 39 volts

DARK CURRENT - GAAS:CR

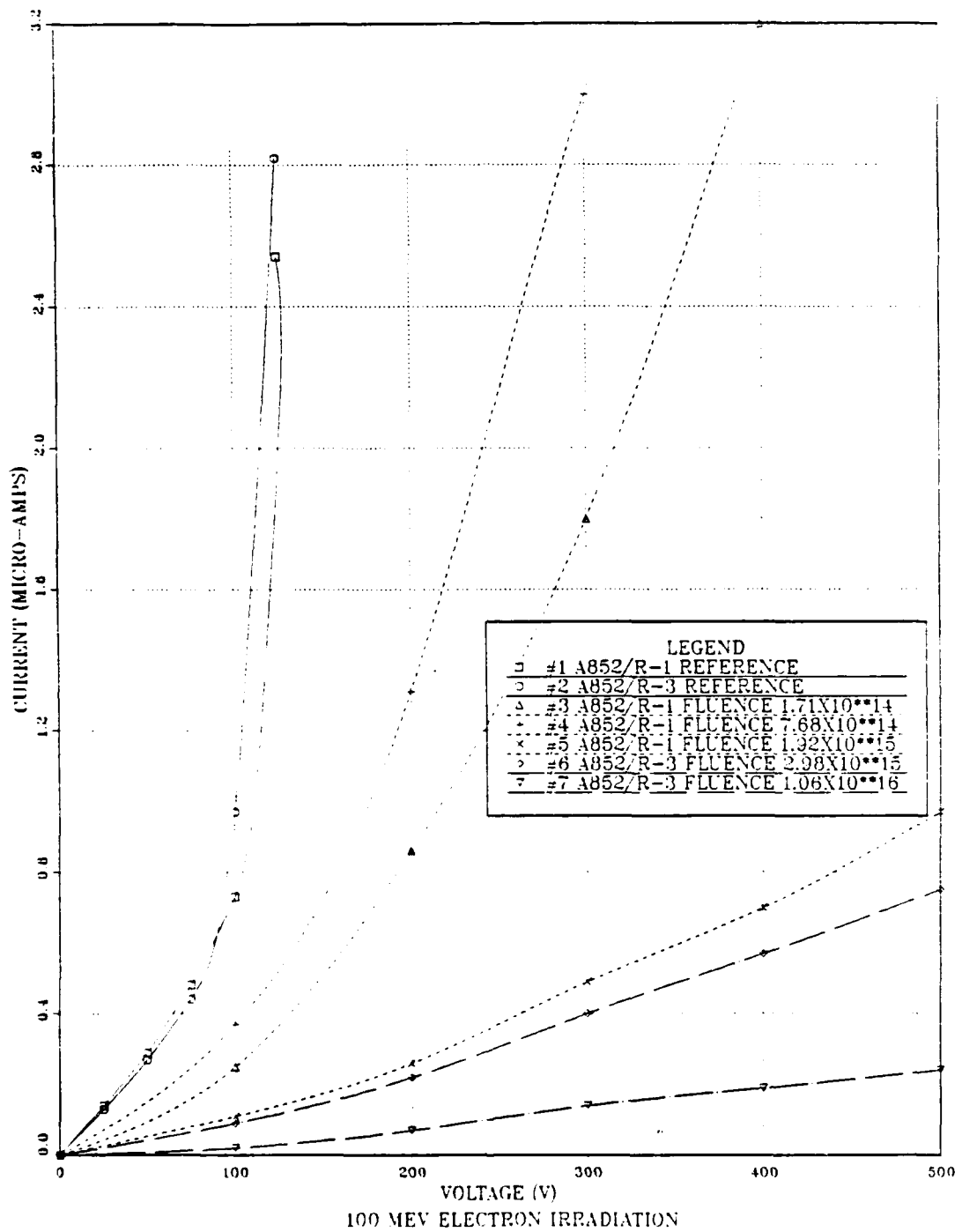


Figure 12. Dark Current--GaAs:Cr Ingot number: Cambridge--A852/R

DARK CURRENT - GAAS:CR

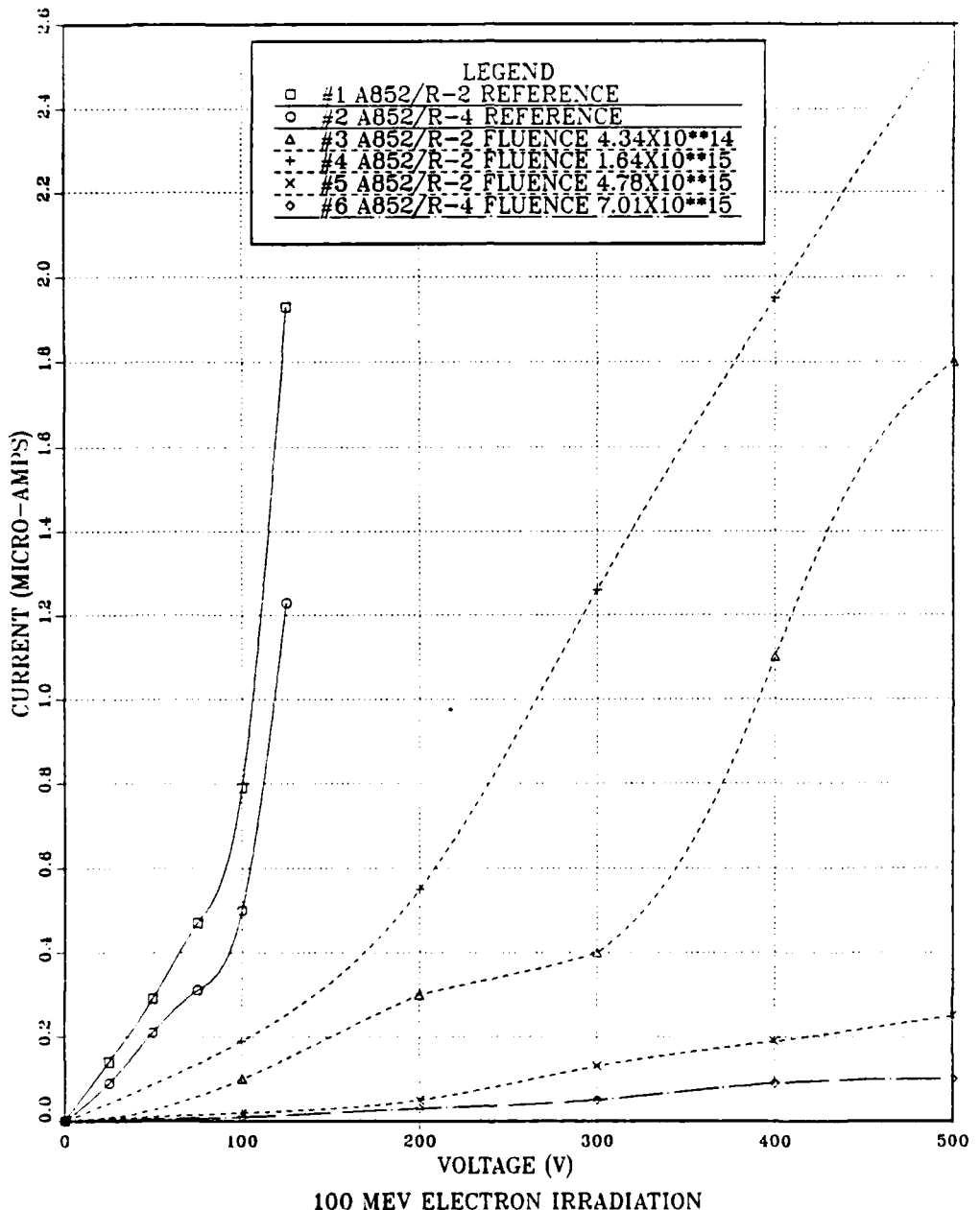


Figure 13. Dark Current--GaAs:Cr Ingot number:
Cambridge-A852/R

TABLE 3
IMPULSE RESPONSE MEASUREMENTS

Sample #	Fluence (e/cm ²)	Total Dose RADS	Dose InP:Fe	Amplitude (mV)		FWHM (ps)	Baseline (ns)
				Pre Irradiation	Post Irradiation		
1	3148B-1	5.9 × 10 ¹³	1.53 × 10 ⁶	390	575	260	280
2	3148B-2	1.24 × 10 ¹⁴	3.22 × 10 ⁶	330	500	220	220
3	3148T-1	2.81 × 10 ¹⁴	7.30 × 10 ⁶	335	450	600	260
4	3148T-2	3.03 × 10 ¹⁴	7.87 × 10 ⁶	230	480	520	240
5	3148B-3	3.16 × 10 ¹⁴	8.21 × 10 ⁶	385	380	260	240
6	2223-1	5.34 × 10 ¹⁴	1.39 × 10 ⁷	190	160	160	140
7	3148B-1	9.46 × 10 ¹⁴	2.46 × 10 ⁷	390	170	260	130
8	2223-1	2.07 × 10 ¹⁵	5.37 × 10 ⁷	190	088	160	135
9	3148B-3	4.38 × 10 ¹⁵	1.13 × 10 ⁸	385	---	260	---
10	2223-3	6.55 × 10 ¹⁵	1.70 × 10 ⁸	225	---	170	---
11	3148T-3	1.36 × 10 ¹⁶	3.53 × 10 ⁸	470	018	680	165

* Samples 1,2,5,7,9 Ingot: CCIPS # 3148-Bottom
3,4,11 Ingot: CCIPS # 3148-Top
6,8,10 Ingot: CCIPS # 2223

* --- Break down at applied voltages

TABLE 3 (CONTINUED)

Sample #	Fluence (e/cm ²)	Total Dose RADS	GaAs:Cr	GaAs:Cr		Baseline (ns)	
				Pre Irradiation	Post Irradiation	Pre Irradiation	Post Irradiation
1	1.71×10^{14}	4.48×10^6		260	400	260	260
2	4.34×10^{14}	1.14×10^7		285	280	255	210
3	7.68×10^{15}	2.01×10^7		260	440	260	230
4	1.64×10^{15}	4.30×10^7		285	340	255	220
5	1.92×10^{15}	5.04×10^7		260	200	260	140
6	2.98×10^{15}	7.81×10^7		285	144	240	180
7	4.78×10^{15}	1.25×10^8		285	058	255	160
8	7.01×10^{16}	1.83×10^8		275	025	250	140
9	1.06×10^{16}	2.79×10^8		285	040	240	160

* All Samples Ingot: Cambridge A852/R

IMPULSE RESPONSE MEASUREMENTS

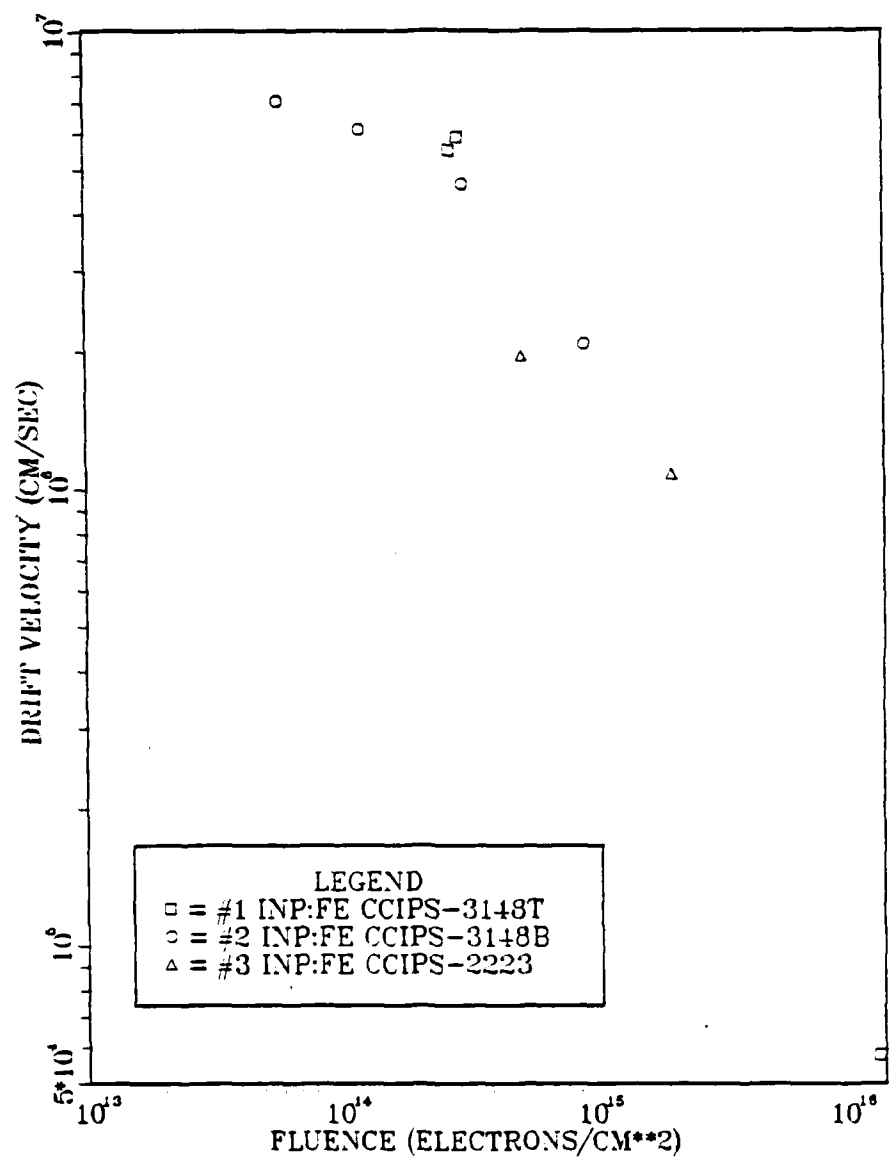


Figure 14. Impulse response measurement for InP:Fe
Drift velocity

IMPULSE RESPONSE MEASUREMENTS

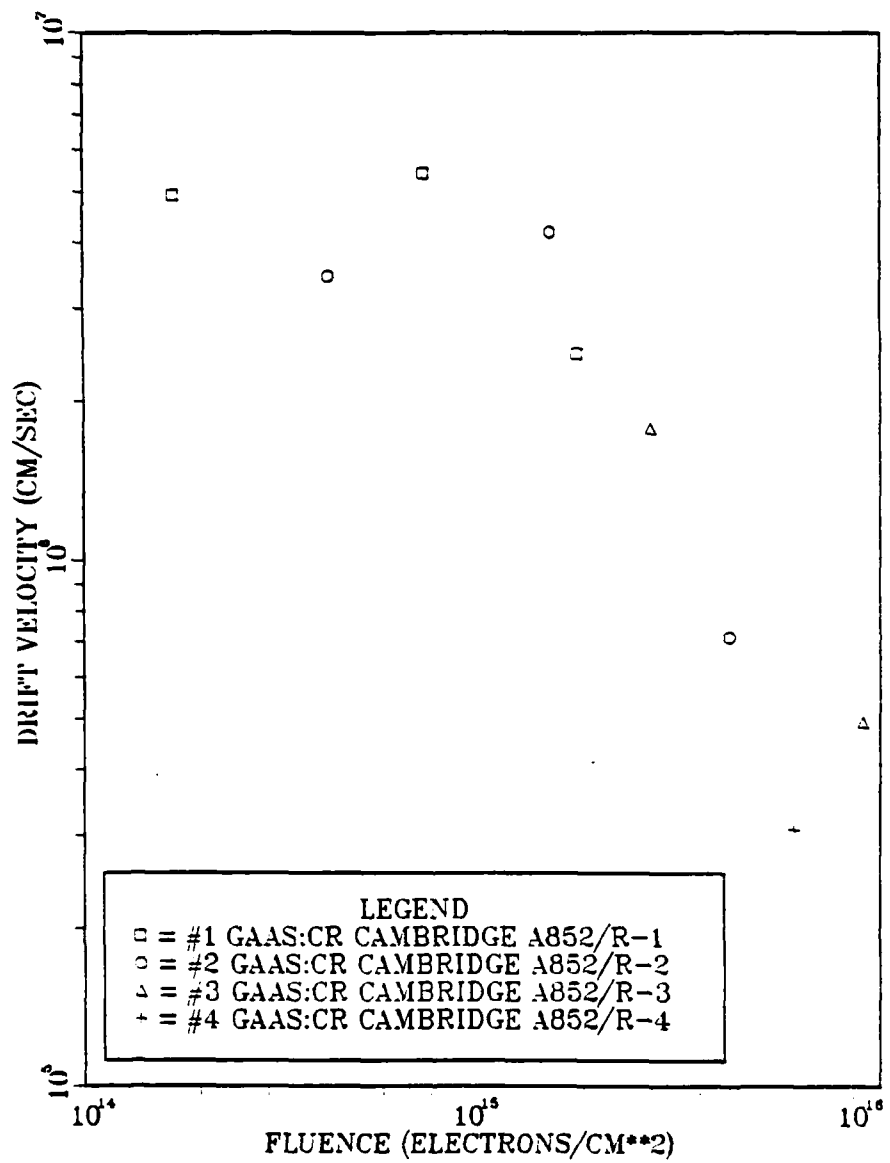


Figure 15. Impulse response measurement for GaAs:Cr
Drift velocity

IMPULSE RESPONSE MEASUREMENTS

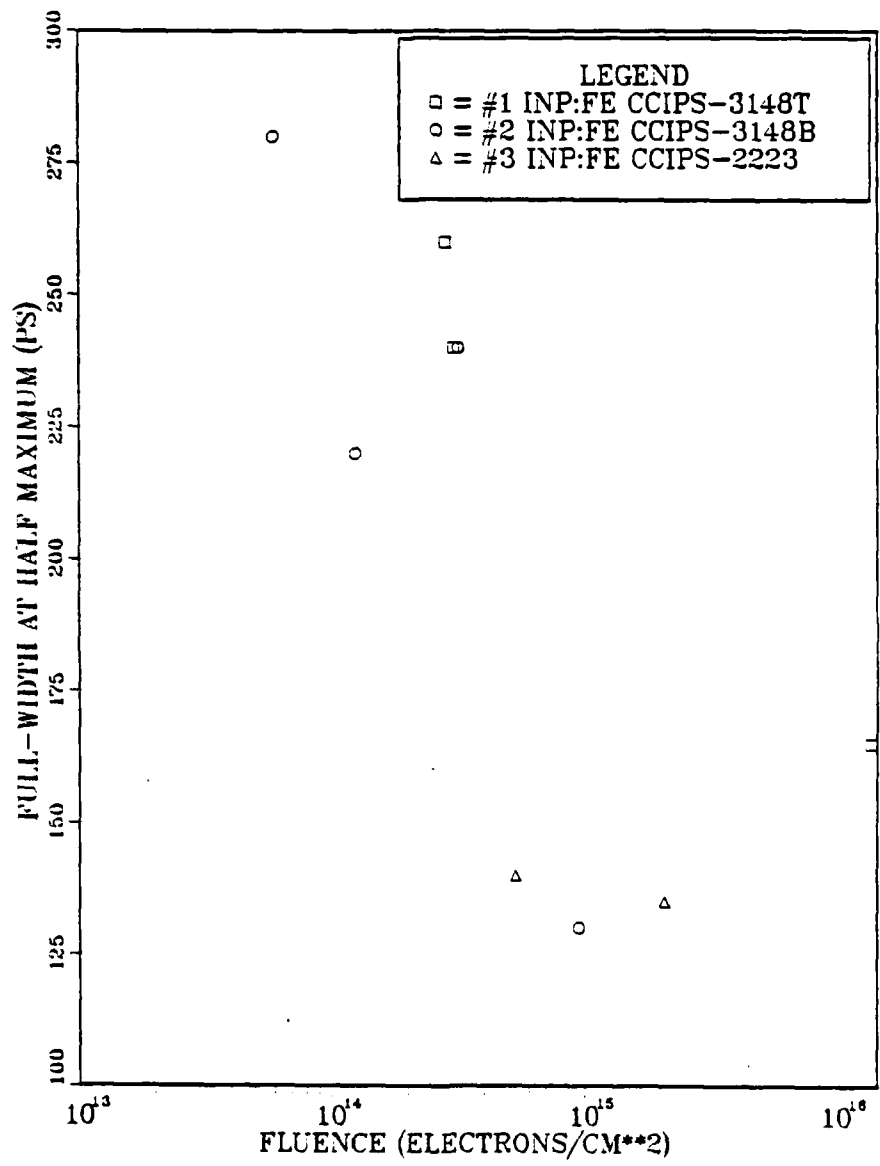


Figure 16. Impulse response measurement for InP:Fe
Full-width at half maximum (response speed)

IMPULSE RESPONSE MEASUREMENTS

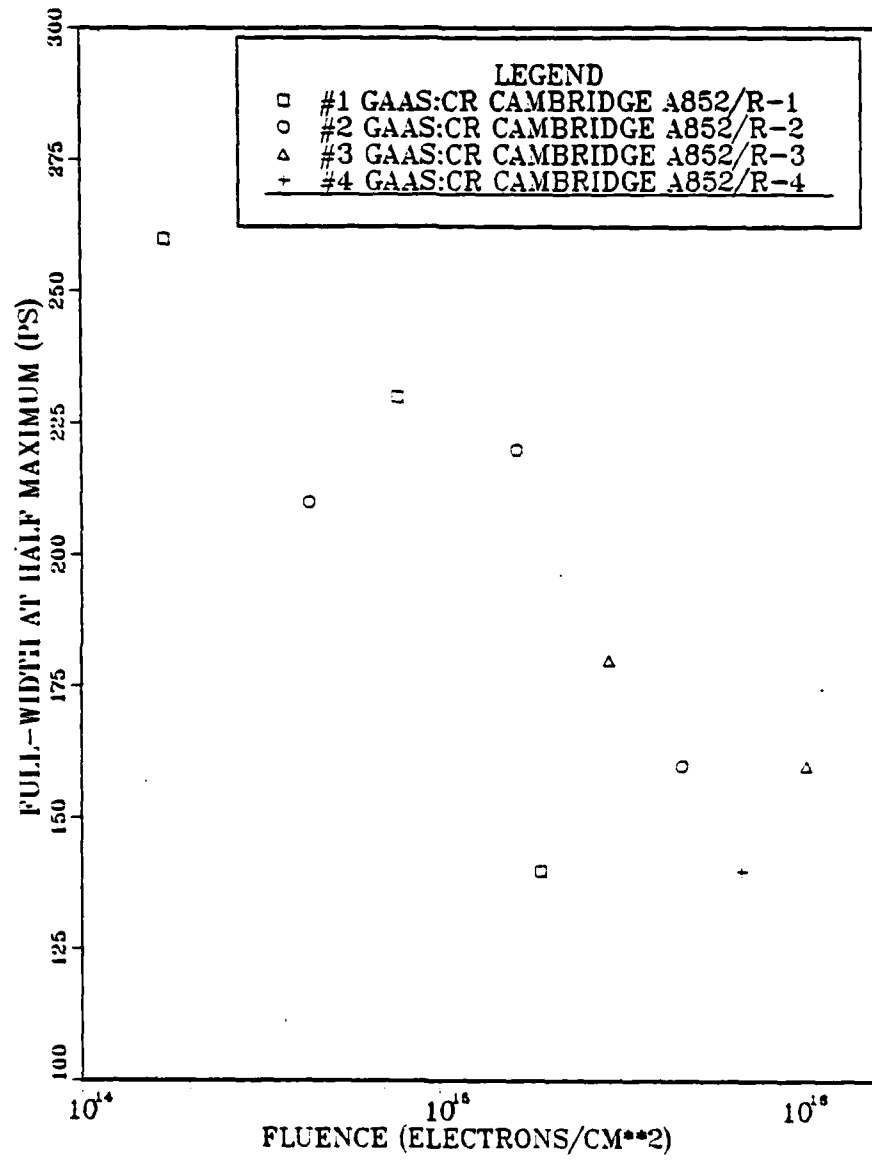
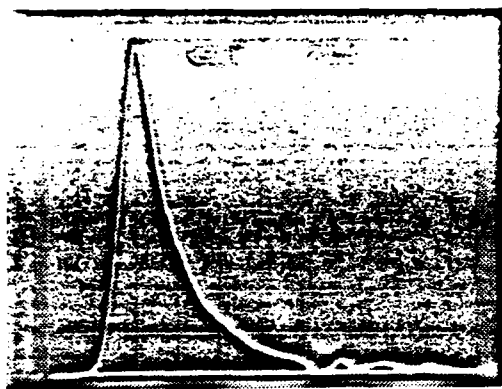
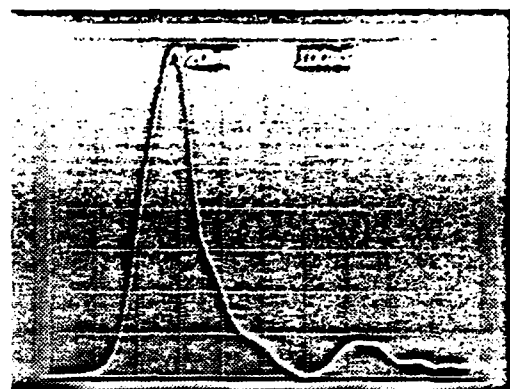


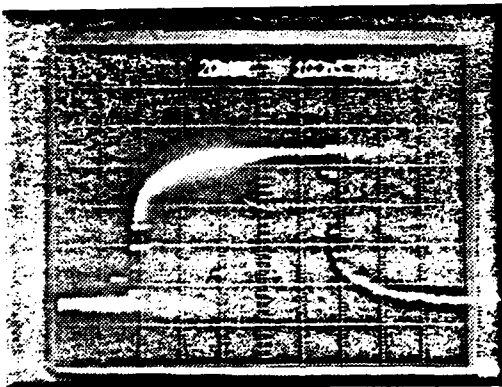
Figure 17. Impulse response measurement for GaAs:Cr
Full-width at half maximum (response speed)



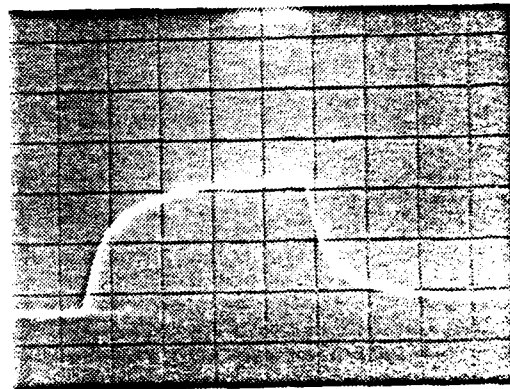
a) before irradiation impulse response FWHM 220-ps



b) after irradiation impulse response FWHM 140-ps

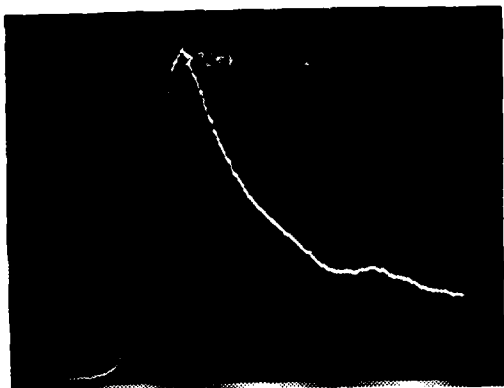


c) before irradiation square-pulse laser response

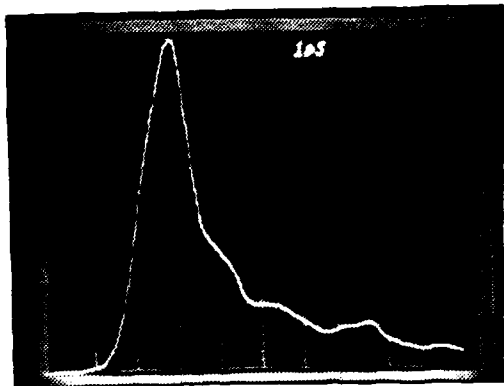


d) after irradiation square-pulse laser response

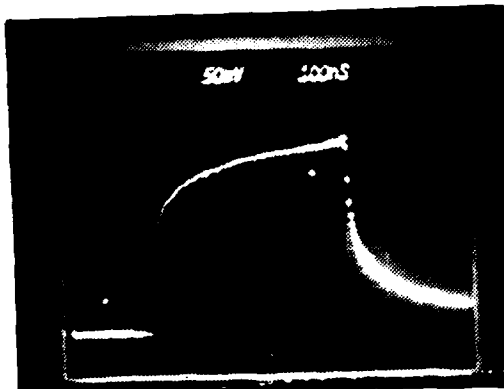
Figure 18. Comparison of InP:Fe impulse and square-pulse laser response before and after electron irradiation for a representative sample



a) before irradiation impulse response FWHM 260-ps



b) after irradiation impulse response FWHM 140-ps



c) before irradiation square-pulse laser response



d) after irradiation square-pulse laser response

Figure 19. Comparison of GaAs:Cr impulse and square-pulse laser response before and after electron irradiation for a representative sample

TABLE 4
SQUARE-PULSE RESPONSE MEASUREMENTS

Sample #	Fluence (e/cm^2)	Total Dose RADS	InP:Fe	InP:Fe		Risetime (10-90%) (ns)
				Pre Irradiation	Post Irradiation	
1	3148B-1	5.9 $\times 10^{13}$	1.53 $\times 10^6$	0.92	0.12	100 180
2	3148B-2	1.24 $\times 10^{14}$	3.22 $\times 10^6$	0.76	0.08	080 180
3	3148P-1	2.81 $\times 10^{14}$	7.30 $\times 10^6$	380	030	120 180
4	3148T-2	3.03 $\times 10^{14}$	7.87 $\times 10^6$	270	024	140 190
5	3148B-3	3.16 $\times 10^{14}$	8.21 $\times 10^6$	106	007	160 190
6	2223-1	5.34 $\times 10^{14}$	1.39 $\times 10^7$	034	026	180 200
7	3148B-1	9.46 $\times 10^{15}$	2.46 $\times 10^7$	092	028	100 210
8	2223-1	2.07 $\times 10^{15}$	5.37 $\times 10^8$	034	013	180 230
9	3148B-3	4.38 $\times 10^{15}$	1.13 $\times 10^8$	106	—	160 —
10	2223-3	6.55 $\times 10^{15}$	1.70 $\times 10^8$	046	—	140 —
11	3148T-3	1.36 $\times 10^{16}$	3.53 $\times 10^8$	540	—	080 —

* Samples 1,2,5,7,9 Ingot: CCIPS # 3148-Bottom
3,4,11 Ingot: CCIPS # 3148-Top
6,8,10 Ingot: CCIPS # 2223

* --- Break down at applied voltages

TABLE 4 (CONTINUED)

Sample #	Fluence (e/cm ²)	Total Dose RADS	Amplitude (mV)	Risetime (10-90%) (ns)	
				Pre Irradiation	Post Irradiation
1 A852/R-1	1.71×10^{14}	4.48×10^6	240	036	220
2 A852/R-2	4.34×10^{14}	1.14×10^7	250	120	240
3 A852/R-1	7.68×10^{15}	2.01×10^7	240	065	220
4 A852/R-2	1.64×10^{15}	4.30×10^7	250	028	240
5 A852/R-1	1.92×10^{15}	5.04×10^7	240	007	220
6 A852/R-3	2.98×10^{15}	7.81×10^8	170	034	120
7 A852/R-2	4.78×10^{15}	1.25×10^8	250	009	240
8 A852/R-4	7.01×10^{16}	1.83×10^8	200	020	220
9 A852/R-3	1.06×10^6	2.79×10^8	170	040	120

* All Samples Ingot: Cambridge A852/R

SQUARE-PULSE RESPONSE

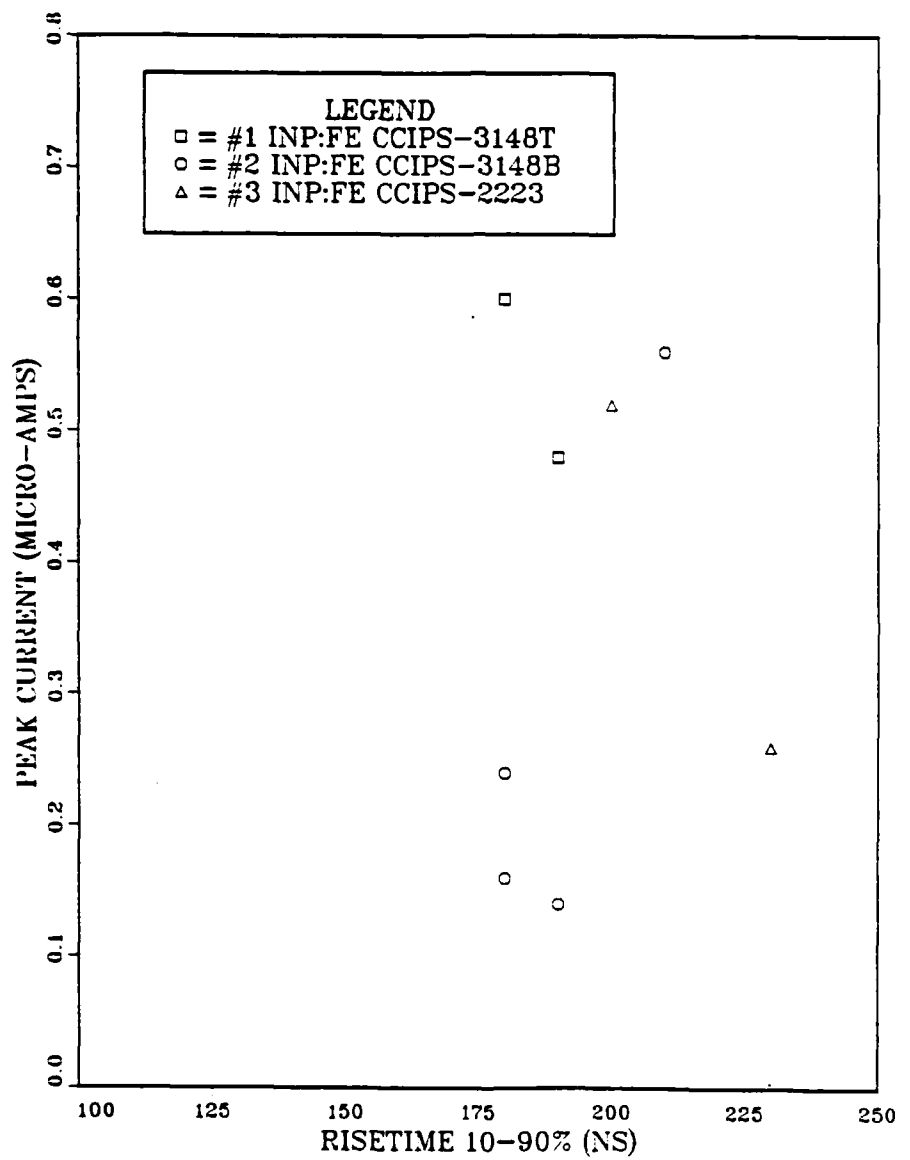


Figure 20. Square-pulse response measurement for InP:Fe
Peak current vs Risetime (10%-90%)

SQUARE-PULSE RESPONSE

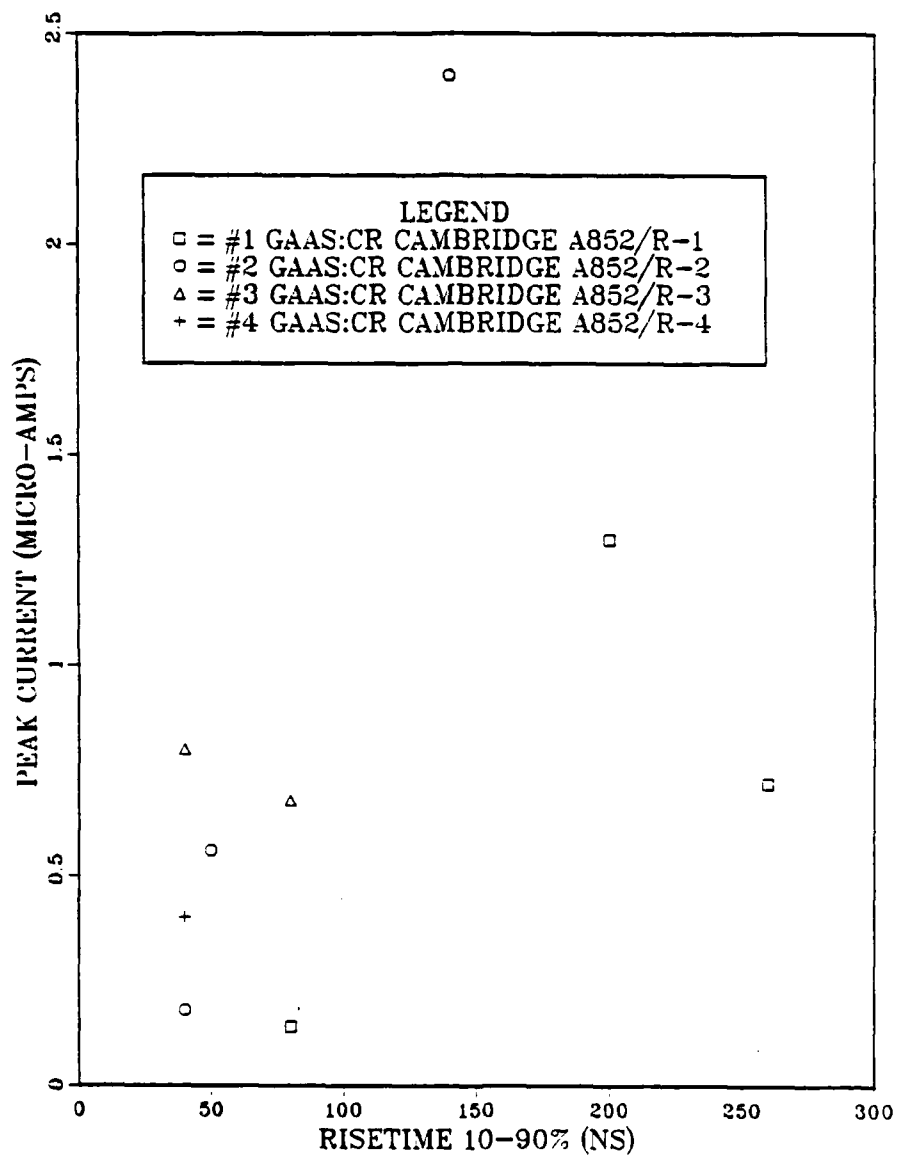


Figure 21. Square-pulse response measurement for GaAs:Cr
Peak Current vs Risetime (10%-90%)

SQUARE-PULSE RESPONSE

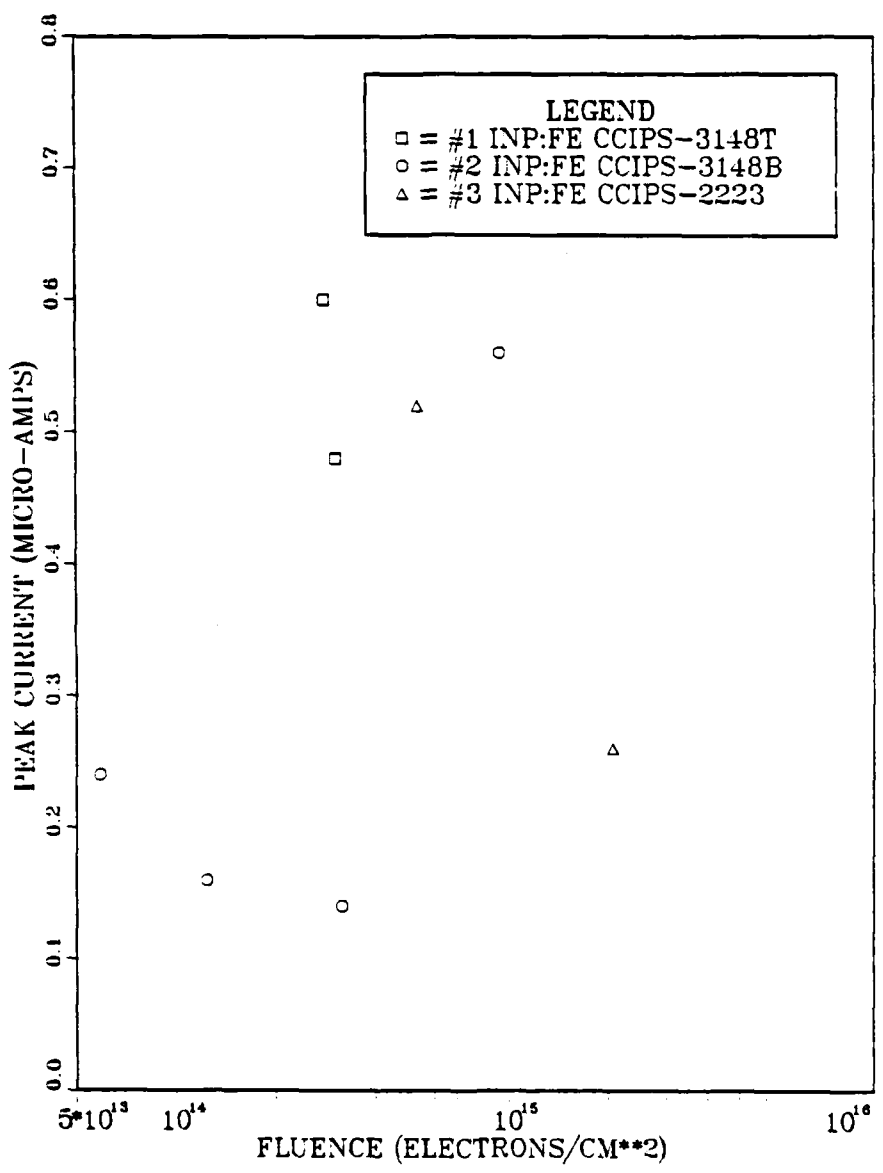


Figure 22. Square-pulse response measurement for InP:Fe
Peak current vs Fluence

SQUARE-PULSE RESPONSE

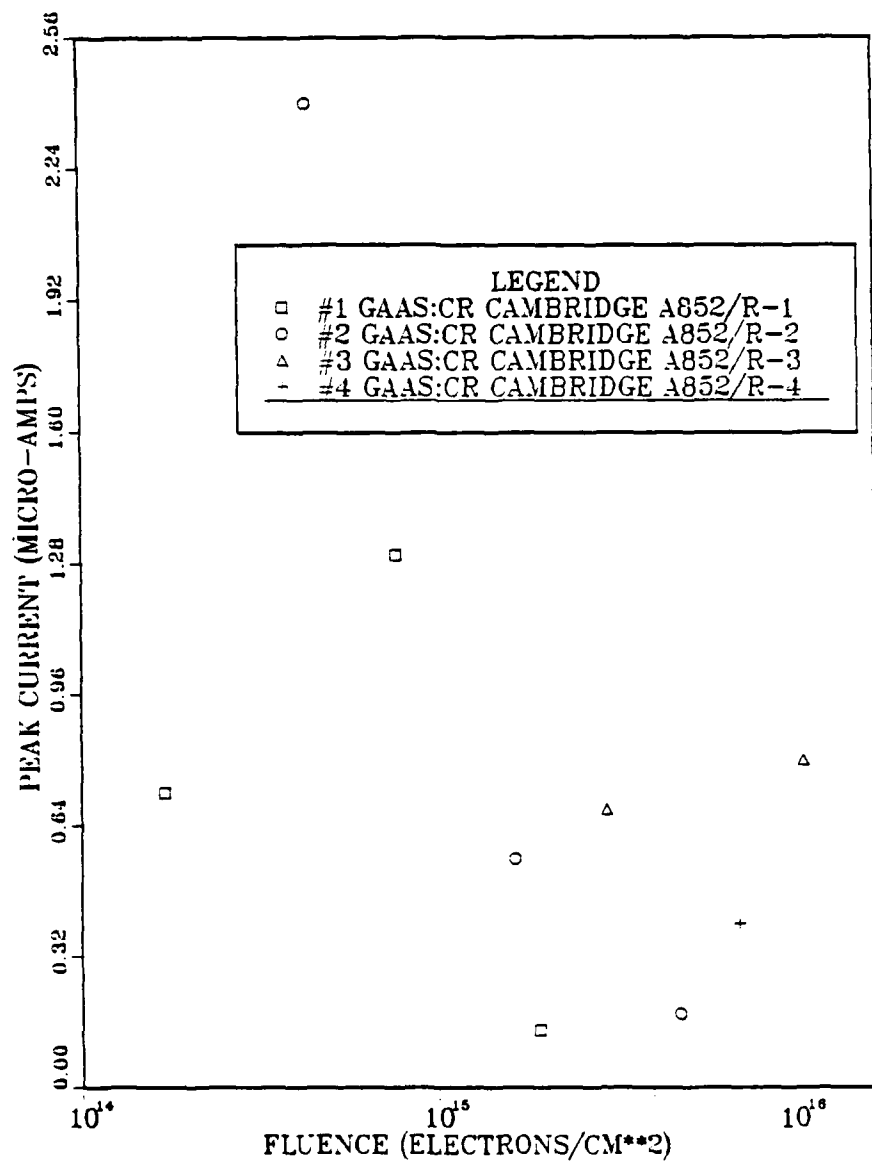


Figure 23. Square-pulse response measurement for GaAs:Cr
Peak current vs Fluence

SQUARE-PULSE RESPONSE

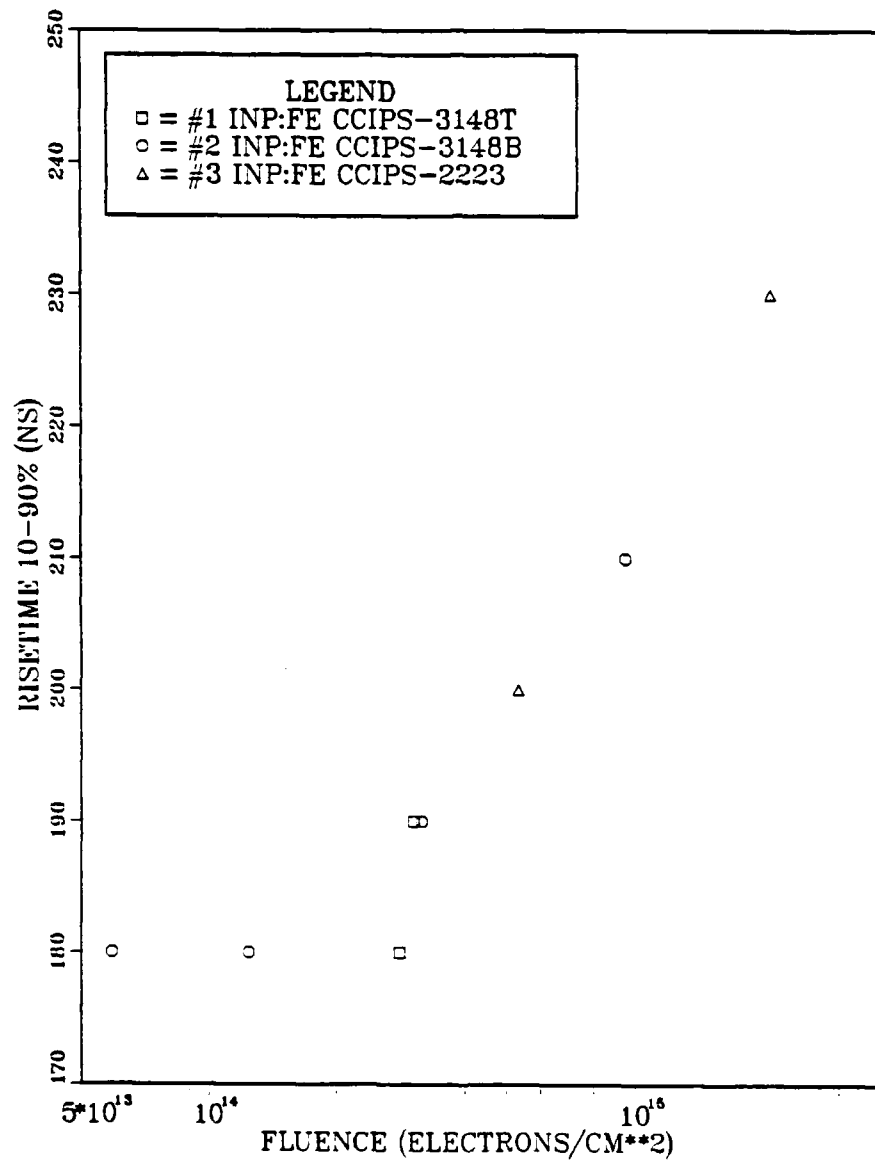


Figure 24. Square-pulse response measurement for InP:Fe
Risetime (10%-90%) vs Fluence

SQUARE-PULSE RESPONSE

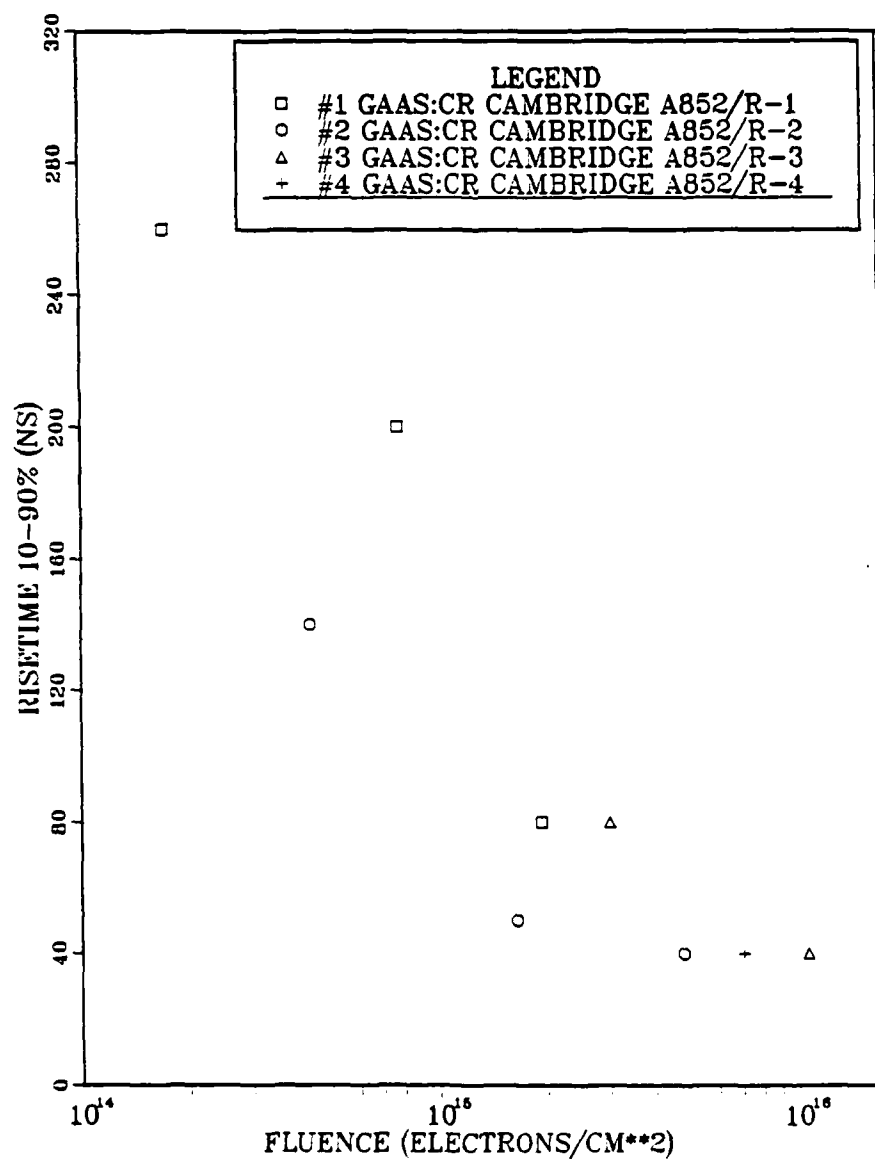


Figure 25. Square-pulse response measurement for GaAs:Cr
Risetime (10%-90%) vs Fluence

IV. EXPERIMENTAL RESULTS

A. DARK CURRENT

Dark current measurements taken before and after the 100 MeV electron irradiation were compared to determine the resulting change. Figures 9 through 13 display the results. The mode of preparation and impurity content of the material results in variation of the recombination lifetime [Ref. 16]. Since decay times are inversely proportional to the Fe dopant levels in InP:Fe [Ref. 25], samples were segregated depending on the source Ingot and whether the samples were prepared from the top or the bottom of a given Ingot. Higher dopant levels in the bottom of an Ingot are due to gravitational forces. Comparison of reference dark current measurements justify this segregation. All the GaAs:Cr samples were prepared from the same portion of the same Ingot.

Before irradiation, the InP:Fe samples were biased up to 500 volts in 100 volt increments and results indicate a linearity through 500 volts. The GaAs:Cr samples were biased up to 125 volts in 25 volt increments. They lose linearity at approximately 100 volts. Post-irradiation measurements indicate a noticeable change in the dark current. The InP:Fe sample results indicate an increase in dark current for the applied voltages. The amount of increase depends on the fluence with higher fluence yielding higher dark currents. The GaAs:Cr samples show a decrease in dark current with higher fluence.

B. IMPULSE RESPONSE

Impulse response measurements for pre and post 100 MeV electron irradiation are listed in Table 3. Included in these measurements are: 1) amplitude--from which I (peak current) can be determined thus allowing for the determination of electron mobility and electron drift velocity, 2) full-width at half maximum (FWHM)--from which carrier relaxation time (response speed) is resolved, and 3) baseline tail--which gives an indication of whether the detector returns to its reference point after having been excited by the photon source, and if so, within what time period.

Both the InP:Fe and GaAs:Cr samples are affected by the irradiations with the more pronounced effects resulting from the higher fluence. Figures 14 and 15 are graphs of the effective carrier drift velocity derived from Formulas 21 and 22. In these equations, electrons are assumed to be the carrier type due to the much higher drift velocities. The measured values of the peak current response are used along with the following experimental parameters: 1) reflectivity (R_r) is 30 percent, 2) the contact spacing (S) is equal to the .5 mm gap, 3) the energy necessary to create an electron-hole pair is assumed to be 5 eV, 4) the applied voltage (V_{appl}) is 200 Volts for InP:Fe and 100 Volts for GaAs:Cr, 5) q is the electronic charge and 6) the optical energy deposited into the detector by the incident photon source (E) is approximately 580 pJ. The effective drift velocity is then calculated by

$$V_d = \mu E_f \quad (25)$$

where $E_f = 4 \text{ kV/cm}$ for InP:Fe and 2 kV/cm for GaAs:Cr. Both figures show a decrease in the carrier drift velocity with increasing fluence. This suggests that electron mobility and electron drift velocity are inversely proportional to the incident electron fluence.

The response speed of the photoconductive detector is determined by the full-width at half maximum (FWHM) measurement of the impulse response. The trend of decreasing response time (decreasing FWHM) with increased fluence is summarized for both material types in Figures 16 and 17. These results are predictable due to the increased number of trapping and recombination centers created by the displacement damage. Figures 18 and 19 display a representative sample of the impulse response before and after irradiation for InP:Fe and GaAs:Cr respectively.

For the GaAs:Cr samples, all baseline tails were reduced. The InP:Fe sample results indicate that there was either no improvement or an increase in the baseline tails.

C. SQUARE-PULSE RESPONSE

Square-pulse response measurements for pre and post 100 MeV electron irradiation are listed in Table 4. Measurements include: 1) amplitude--from which I (peak current) is determined and 2) risetime (10%-90%) which gives an indication of the time involved for saturation of the neutral acceptor states by electrons and the simultaneous recombination of the negatively charged acceptor states by holes.

Figures 18 and 19 display a representative sample of the square-pulse measurement before and after irradiation for InP:Fe and GaAs:Cr respectively. Both material types show square-pulse nonlinearities for the pre-irradiated samples. After irradiation, the GaAs:Cr samples display significant improvement in accurately following the longer events. The quality of improvement is commensurate with higher fluence. This response is not found in the InP:Fe samples, but rather, an increase in nonlinearity for higher fluence. The dependency of peak current on risetime or fluence was not established for either material type as displayed in Figures 20 through 23. Risetime vs fluence is plotted in Figures 24 and 25. These graphs suggest a proportional relationship for fluence above 2.81×10^{14} (electrons/cm²) for the InP:Fe samples and an inversely proportional relationship for fluence below 4.78×10^{15} (electrons/cm²) for the GaAs:Cr samples.

D. COMPUTER SIMULATION

A computer simulation of a 100 MeV electron beam incident on a rectangular parallelepiped (RPP) semiconductor target was performed using the CRAY computer located at the Los Alamos National Laboratory. The ACCEPT code, one of the ITS: The Integrated TIGER Series of Coupled Electron/Photon Monte Carlo Transport Codes, was used. The ACCEPT input program along with the Cross Section Generations and the Monte Carlo executions for both the InP:Fe and GaAs:Cr samples is enclosed.

Quoting from the description of the code, "ITS is a Monte Carlo solution of linear time-integrated coupled electron photon radiation problems. The ETRAN model was used as the basis. It combines microscopic photon transport with a macroscopic random walk for electron transport. The ACCEPT code is a general three-dimensional transport code that uses a combinational geometry scheme" [Ref. 26].

The results in graphic form (normalized to one particle) for both electrons and photons are displayed in Figures 26 through 31. Both materials give similar results. It is obvious from the Angular Distribution graphs (Figures 26 and 27) that the overwhelming majority of both electrons and photons occur at an angle between 0 and 10 steradians. This would indicate that there is very little deflection of the incident electrons or the resulting photons. The Energy Spectra of the escaping electrons (Figure 28) indicate that most are leaving the target with energies between 90-100 MeV, therefore, only a small percentage of the total energy is actually deposited into the device. The actual energy deposition per electron is 1.762×10^{-2} MeV (1.476×10^{11} RADS-InP Coul) for InP:Fe and 1.993×10^{-2} MeV (1.500×10^{11} RADS-GaAs/Coul) for GaAs:Cr. The charge deposition is -2.059×10^{-3} for InP:Fe and -1.993×10^{-3} for GaAs:Cr. Most of the photons are in the low energy range (Figure 29). The Flux Distributions (Figures 30 and 31) substantiate these results with the highest flux for electrons in the high energy regions whereas the highest flux for photons is in the lower energy regions. The results are not surprising given the thickness of

ANGULAR DISTRIBUTION

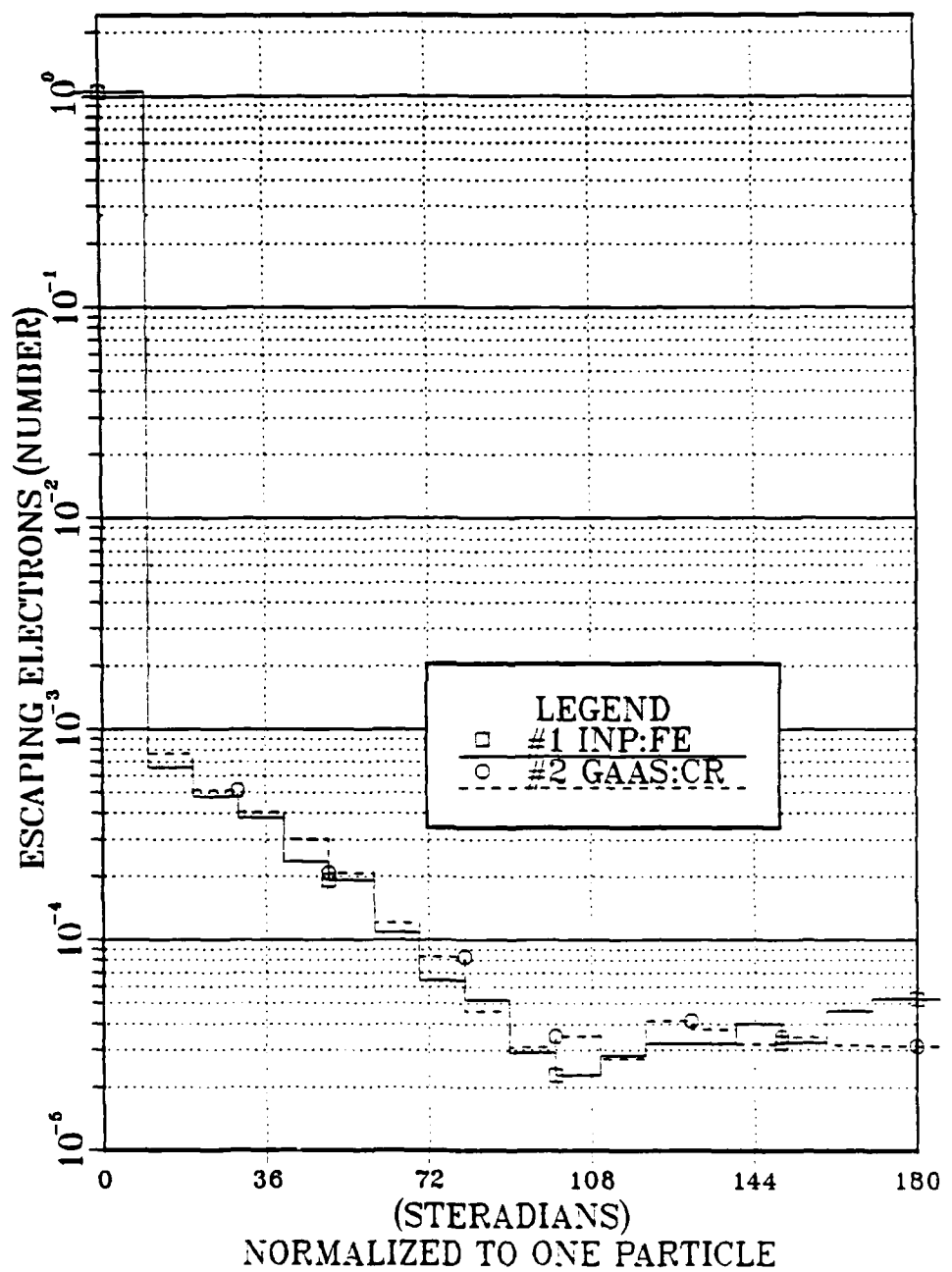


Figure 26. Angular Distribution (Electrons)

ANGULAR DISTRIBUTION

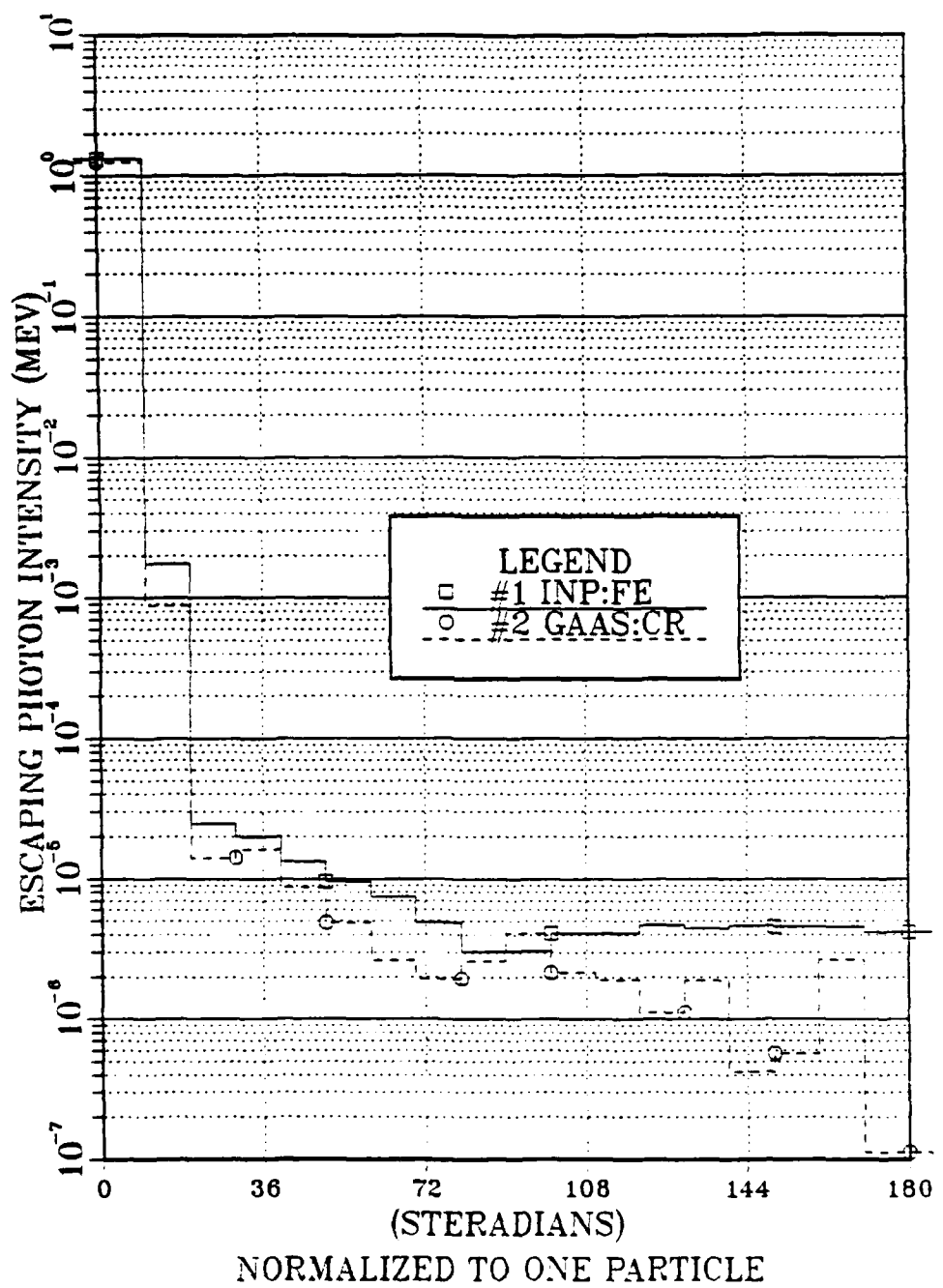


Figure 27. Angular Distribution (Photons)

ENERGY SPECTRA (ELECTRONS)

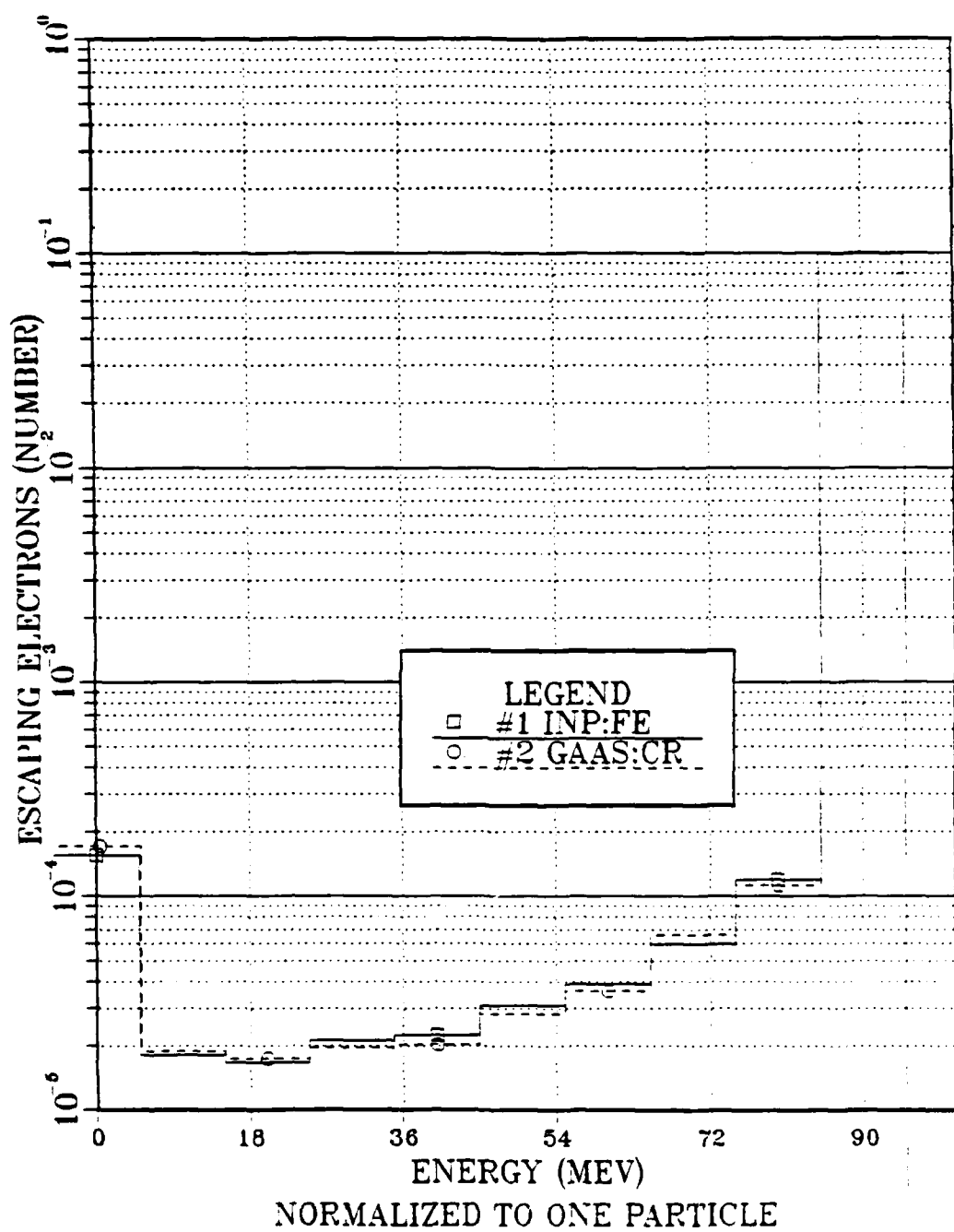


Figure 28. Energy Spectra (Electrons)

ENERGY SPECTRA (PHOTONS)

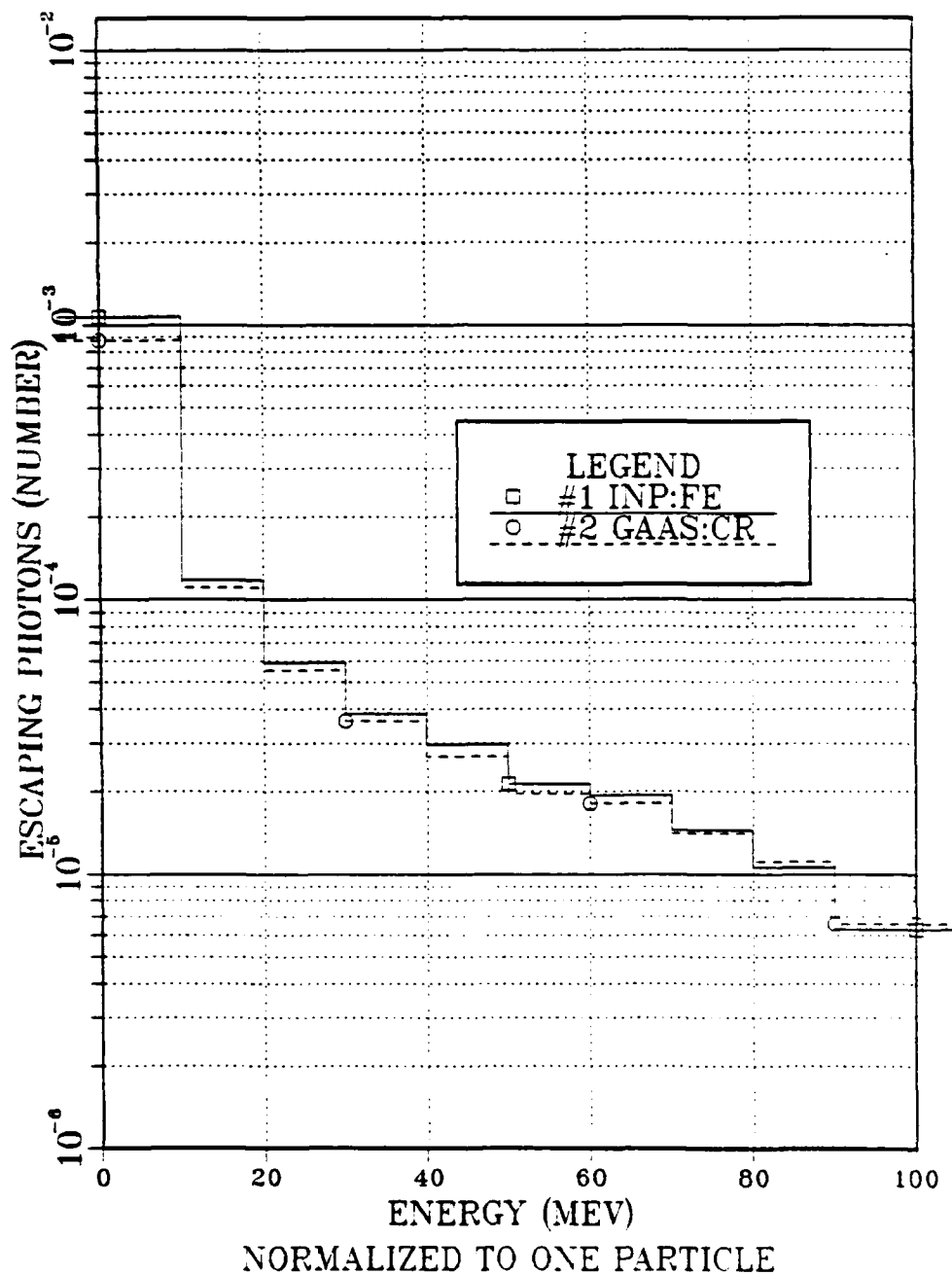


Figure 29. Energy Spectra (Photons)

ELECTRON FLUX DISTRIBUTION

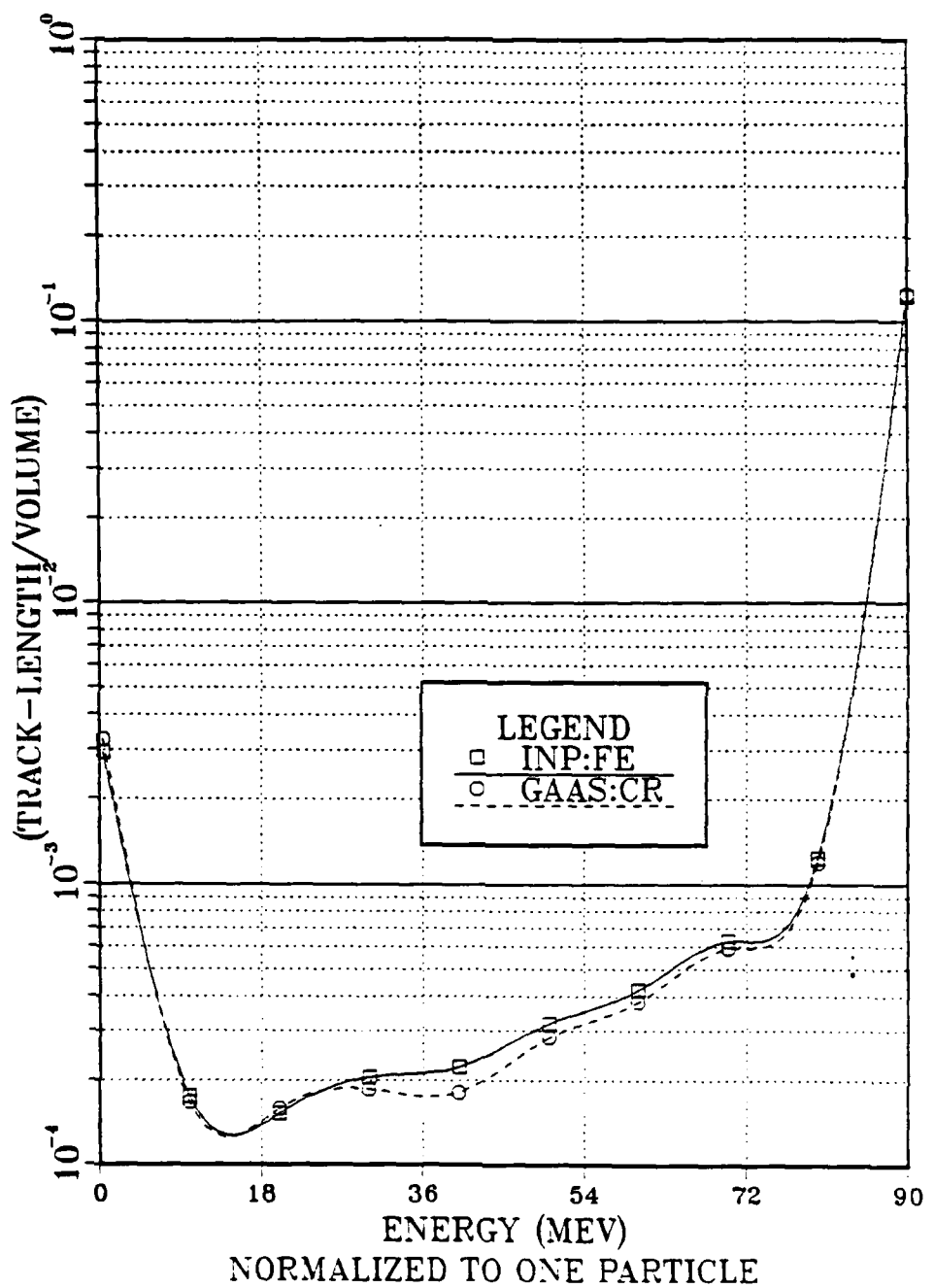


Figure 30. Electron Flux Distribution

PHOTON FLUX DISTRIBUTION

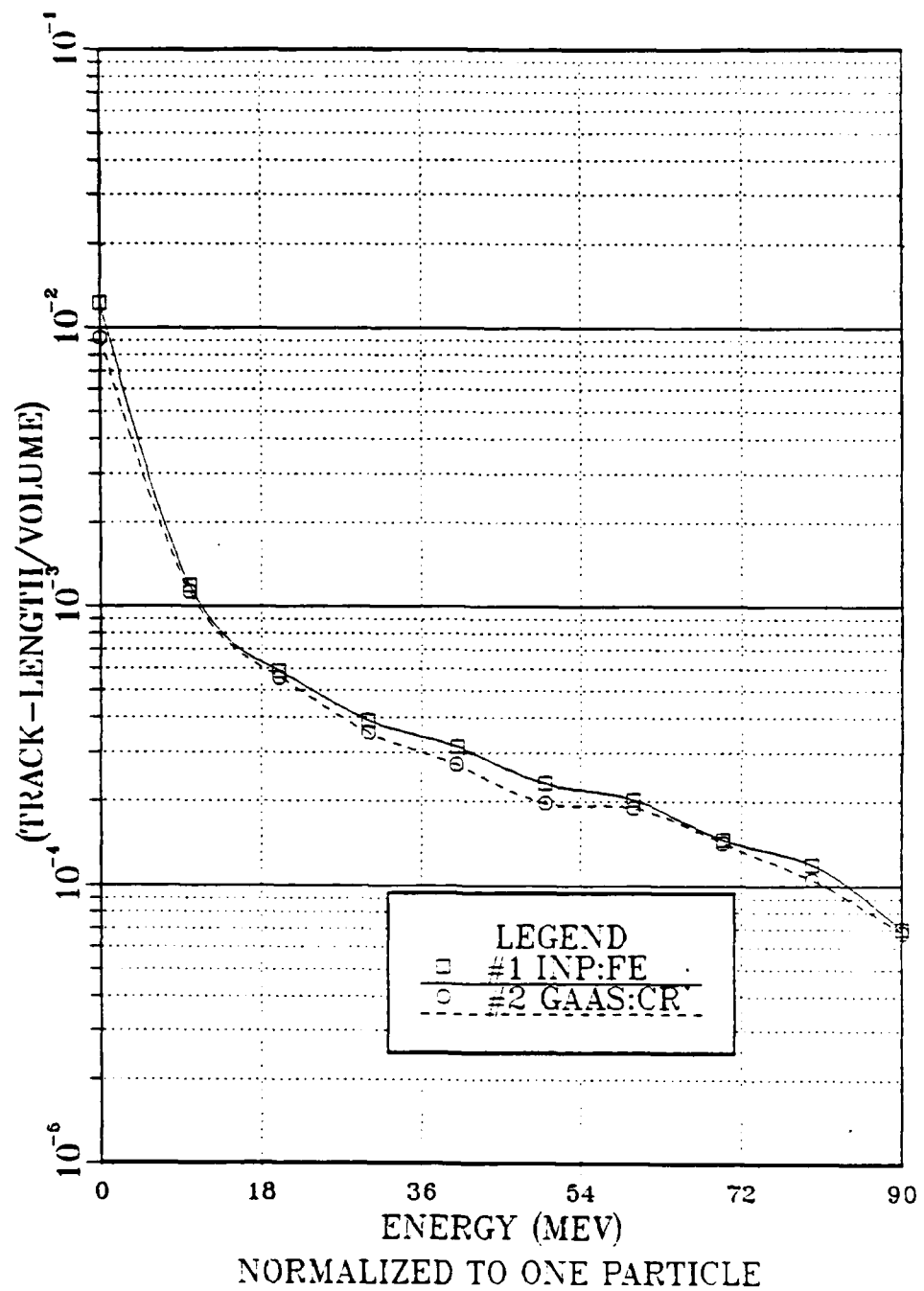


Figure 31. Photon Flux Distribution

the sample (thin sample) and the energy of the incident electrons thus legitimizing the use of thin sample approximations. Included in the Monte Carlo executions are listings of the physical options based on 10 batches of 100,000 histories each. Bremsstrahlung represents the highest number generated, more than all others combined.

E. DISPLACEMENTS

In determining the number of displacements from formulas 5-10, an equal probability of collision for the secondary atoms was assumed. Since these devices are compounds, a range of the displacement cross section and therefore a range of the number of displacements is accounted for through the Threshold Displacement Energies in Table 1. The Kinchin and Pease model was used in determining the average number of displacements per primary recoil of energy T_d . Table 5 is normalized to one particle.

F. COMPARISON WITH NEUTRON DAMAGED DEVICES

Results obtained from electron irradiation of InP:Fe and GaAs:Cr concur with those obtained by Wagner et al. [Ref. 1] for neutron irradiated samples. This substantiative agreement holds for dark current, impulse and square-pulse response measurements. Both material types have extremely fast impulse response with differences showing up in the dark current and square-pulse responses. The GaAs:Cr samples exhibit those desirable qualities at higher fluence which include lower dark current and better accuracy in following the longer event of the square-pulse.

TABLE 5
DISPLACEMENTS

<u>Material</u>	<u>In</u>	<u>P</u>	<u>Ga</u>	<u>As</u>
N_o #lattice atoms/(cm ³)	2.97×10^{22}	2.97×10^{22}	4.42×10^{22}	4.42×10^{22}
Minimum Displacement Cross Section (cm ²)		3.94×10^{-22}		1.95×10^{-22}
Maximum Displacement Cross Section (cm ²)	1.49×10^{-21}		1.07×10^{-21}	
Minimum number of Displacements (atoms/cm ³)		11.70		43.66
Maximum number of Displacements (atoms/cm ³)	44.25		47.29	
Minimum number of Displacements in the sample (atoms)		.029		.109
Maximum number of Displacements in the sample (atoms)	.111		.118	
Number of Replacements (atoms/cm ³)	24.47	25.03	23.99	23.61

V. CONCLUSIONS

A new class of compact, reliable, sensitive and extremely high speed radiation detectors are currently being developed at the Los Alamos National Laboratory Electronics Division. They utilized neutron irradiation to introduce trapping and recombination centers into the semiconductor to speed up hole trapping for better characterization of long-event pulses. In this work, we have demonstrated that electron irradiation at 100 MeV energies is capable of qualitatively and quantitatively producing the same desirable effects.

Dark current in the GaAs:Cr devices decreases for increasing fluence whereas dark current in the InP:Fe devices increases for the same range of fluence. Impulse response controlled by carrier relaxation has been improved by electron irradiation, with response speeds < 100-ps having been achieved by both material types. Electron mobility, drift velocity and response speed have been shown to decrease with increasing fluence for both material types. In contrast to InP:Fe, the electron damaged GaAs:Cr devices show significant improvement in accurately following the longer event square-pulses by exhibiting linearity. The GaAs:Cr devices fulfill the necessary requirements for detector utilization and are expected to replace InP:Fe as the bulk-semiconductor material for many applications.

Electron irradiation from the NPS LINAC has been shown to be an alternative source for the introduction of trapping and

recombination centers resulting from irradiation damage. The LINAC provides the advantage of a well focused beam, variable energies and controlled fluence.

ITS: The Integrated TIGER Series of Coupled Electron/Photon Monte Carlo Transport Codes provides a theoretical means for characterizing an electron beam incident on detectors of various geometric shapes and sizes.

APPENDIX A
IMPULSE RESPONSE MEASUREMENT EQUIPMENT LIST

EQUIPMENT

1. Hewlett-Packard 6515A DC Power Supply
2. Hewlett-Packard 3465A Digital Multimeter
3. Ortec Detector Control Unit Model 210
4. Hamamatsu C1308 Picosec Light Pulser--
 Maximum Peak Power 10 Watts
 Wavelength 820 nm
 Repetition Rate 10 KHz
5. Newport Research Corporation Magnetic Base Model 100,
 430, 360, 420
6. Tektronix 7704A Oscilloscope
7. Tektronix P7001 Processor
8. Tektronix A7704 Acquisition Unit with
 1) S-6 Sampling Head and
 2) S-53 Trigger Recognizer
9. Tektronix TDR/Sampler
10. Tektronix Amplifier
11. Tektronix Oscilloscope Camera C-27

APPENDIX B

SQUARE-PULSE RESPONSE MEASUREMENT EQUIPMENT LIST

EQUIPMENT

1. Exact Model 508A Log Sweep Function Generator

Ramp Mode - TRIG
Ramp Time - 100 msec
Mode - TRIG PULSE
Range - 100 Hz

2. Hewlett-Packard 1900A Pulse Generator

Output 50 Ohms
Volts into 50 Ohms
Amplitude 2-5
Offset 0-2
Width 100-1K nsec
Time Interval 10-100 micro-sec
Rate 2.5K-25K

3. Tektronix FG 503 Function Generator

Trigout 2.5V into 600 Ohms
Function - Square Pulse
Frequency - 200 Hz

4. Tektronix PG 501 Pulse Generator

Trigout > 1V into 50 Ohms

5. Hewlett-Packard 6515A DC Power Supply

6. Hewlett-Packard 3435A Digital Multimeter

7. Keithly 177 Microvolt DMM

8. Tektronix 7104 Oscilloscope

a) 7S11 Sampling Unit with Type S-4 Sampling
b) 7T11 Sampling Sweep Unit
c) 7B92A Dual Time Base
d) Oscilloscope Camera C-27

9. Princeton Applied Research (EG+G) Model 4202 Signal Averager

10. Hewlett-Packard 7044A X-Y Recorder

11. Intronics Regulated Power Supply Model EPM 200/15TD
12. Micro Controle Newport Research Corporation
Model B-1
Model AC-1

APPENDIX C

INPUT PROGRAM FOR ELECTRON/PHOTON TRANSPORT ACCEPT CODE

A. CROSS SECTION

```
1 MATERIAL IN .788 P .212 DENSITY 4.78 SUBSTEP 40
2 MATERIAL GA .482 AS .518 DENSITY 5.32 SUBSTEP 40
3 TITLE
4 100.0 MEV CROSS SECTIONS FOR PHOTOCOCONDUCTORS
5 ENERGY 100.0
```

B. MONTE CARLO

```
1 ECHO 1
2 TITLE
3 ... 100.0 MEV KEIPPER TEST PROGRAM
4 *****GEOMETRY*****
5 GEOMETRY 1 0
6 RPP 0.00 0.50 0.00 0.10 0.00 0.05
7 SPH 0.00 0.00 0.00 2.0
8 SPH 0.00 0.00 0.00 4.0
9 END
10 Z1 + 1
11 Z2 + 2 - 1
12 Z3 + 3 - 2
13 END
14 0.0025 33.5 267.9
15 *MAT ECUT PTCZ
16 1
17 0
18 0
19 *****SOURCE*****
20 ELECTRONS
21 ENERGY 100.0
22 POSITION 0.0 0.0 0.0
23 RADIUS 0.5
24 DIRECTION 0.0
25 CUTOFFS 0.05 .001
26 *****OUTPUT OPTIONS*****
27 ELECTRON-ESCAPE
28 NBINE 10
29 PHOTON-ESCAPE
30 NBINE 10
31 ELECTRON-FLUX 1 1
32 NBINE 10
33 PHOTON-FLUX 1 1
34 BNINE 10
35 *****OTHER OPTIONS*****
36 HISTORIES 100000
```

095200

XGENPJK

USER NUMBER	095200
WORKER MACHINE	V
DATE SENT	09 Oct 1985
TIME SENT	08:06:34
XEROX UNIT	A
PAGES DATE	9-08-1985
PAGES TIME	08:09:03 JUN 4/20/85 1

```

1000 0 NE. ESCAPEE EFIELD PROGRAM
*****GEOMETRY*****
GEOMETRY 1.0
RPF 0.00 0.50 0.00 0.10 0.00 0.05
S2= 0.00 0.00 0.00 2.0
SPH 0.00 0.00 0.00 4.0
END
Z1 +1
Z2 +2 -1
Z3 +3 -2
END
0.0025 33.5 267.9
-MAT ECUT PTC2
1
C
C
*****SOURCE*****
ELECTRONS
ENERGY 100.0
POSITION 0.0 0.0 0.0
RADIUS 0.5
DIRECTION 0.0
CUTOFFS 0.05 .001
*****OUTPUT OPTIONS*****
ELECTRON-ESCAPE
NBINE 10
PHOTON-ESCAPE
NBINE 10
ELECTRON-FLUX 1 1
NBINE 10
PHOTON-FLUX 1 1
NBINE 10
*****OTHER OPTIONS*****
HISTORIES 1000000

```

095200

CROSS

USER NUMBER	095200
WORKER MACHINE	V
DATE SENT	10 Oct 1985
TIME SENT	14:28:07
WORKER INIT	A
PAGES DATE	10 Oct 1985
TRACES TIME	14:32:29 10 Oct 1985

1 J98-322313 5 51210 0 20987 3 TOKYO 0 29714
 398-322313 5 51210 0 20987 3 TOKYO 0 29714
 1 EFFECTIVE Z/A = 0 43895 FF3895 ELECTRON RESULTS
 0 ENERGY STOPPING POWER IONIZATION POTENTIAL = 398.32 EV CRITICAL ENERGY = 19.398 MEV
 0 N COLLISION RADIATION TOTAL RADIATION DENSITY RAD/COL DENSITY DENSITY DIVISION
 MEV CM2/G MEV CM2/G MEV CM2/G G/CM2 G/CM2

N	MEV	MEV CM2/G	MEV CM2/G	MEV CM2/G	G/CM2	G/CM2
134	9.894e-04	3.708e-01	2.421e-01	0.371e+01	1.33e-05	0.000e+00
133	1.079e-03	3.678e-01	2.430e-02	3.860e-01	1.576e-05	5.435e-05
132	1.176e-03	3.628e-01	2.419e-02	3.610e-01	1.443e-05	4.088e-04
131	1.283e-03	3.561e-01	2.418e-02	3.563e-01	2.139e-05	1.519e-04
130	1.399e-03	3.480e-01	2.417e-02	3.481e-01	1.962e-04	1.962e-04
129	1.525e-03	3.389e-01	2.415e-02	3.391e-01	2.837e-05	2.383e-04
128	1.664e-03	3.288e-01	2.414e-02	3.291e-01	2.785e-04	2.785e-04
127	1.814e-03	3.182e-01	2.412e-02	3.184e-01	3.715e-05	3.172e-04
126	1.978e-03	3.010e-01	2.411e-02	3.073e-01	4.241e-05	5.549e-04
125	2.157e-03	2.066e-01	2.409e-02	2.958e-01	4.835e-05	9.198e-04
124	2.353e-03	2.329e-01	2.408e-02	2.442e-01	5.098e-05	1.962e-04
123	2.566e-03	2.722e-01	2.406e-02	2.725e-01	6.274e-05	4.645e-04
122	2.798e-03	2.652e-01	2.404e-02	2.667e-01	7.446e-05	5.098e-04
121	3.051e-03	2.489e-01	2.402e-02	2.591e-01	9.506e-05	1.874e-04
120	3.328e-03	2.314e-01	2.401e-02	2.377e-01	9.275e-05	5.749e-04
119	3.629e-03	2.262e-01	2.399e-02	2.264e-01	1.057e-04	6.131e-04
118	3.957e-03	2.152e-01	2.397e-02	2.154e-01	1.207e-04	6.522e-04
117	4.315e-03	2.045e-01	2.395e-02	2.078e-01	1.377e-04	6.929e-04
116	4.706e-03	1.941e-01	2.393e-02	1.944e-01	1.573e-04	7.350e-04
115	5.124e-03	1.841e-01	2.391e-02	1.843e-01	1.798e-04	7.789e-04
114	5.596e-03	1.741e-01	2.389e-02	1.747e-01	2.057e-04	8.248e-04
113	6.103e-03	1.651e-01	2.386e-02	1.654e-01	2.355e-04	8.748e-04
112	6.655e-03	1.562e-01	2.383e-02	1.564e-01	2.699e-04	9.277e-04
111	7.258e-03	1.476e-01	2.382e-02	1.479e-01	3.095e-04	9.771e-04
110	7.915e-03	1.395e-01	2.380e-02	1.397e-01	3.497e-04	1.021e-03
109	8.631e-03	1.317e-01	2.377e-02	1.319e-01	4.080e-04	1.093e-03
108	9.412e-03	1.242e-01	2.375e-02	1.245e-01	4.690e-04	1.175e-03
107	1.026e-02	1.171e-01	2.373e-02	1.174e-01	5.395e-04	1.224e-03
106	1.119e-02	1.104e-01	2.371e-02	1.107e-01	6.111e-04	1.271e-03
105	1.220e-02	1.041e-01	2.369e-02	1.043e-01	7.155e-04	1.371e-03
104	1.331e-02	9.801e-02	2.367e-02	9.824e-02	8.247e-04	1.451e-03
103	1.451e-02	9.259e-02	2.365e-02	9.526e-02	9.511e-04	1.531e-03
102	1.583e-02	8.668e-02	2.363e-02	8.712e-02	1.098e-04	1.628e-03
101	1.726e-02	8.177e-02	2.361e-02	8.178e-02	1.246e-04	1.772e-03
100	1.882e-02	7.695e-02	2.360e-02	7.719e-02	1.464e-04	1.828e-03
99	2.052e-02	7.241e-02	2.359e-02	7.265e-02	1.744e-04	1.875e-03
98	2.238e-02	6.813e-02	2.358e-02	6.837e-02	1.955e-04	1.938e-03
97	2.441e-02	6.411e-02	2.358e-02	6.434e-02	2.151e-04	2.036e-03
96	2.662e-02	6.032e-02	2.358e-02	6.056e-02	2.312e-04	2.142e-03
95	2.903e-02	5.677e-02	2.359e-02	5.700e-02	3.025e-04	2.520e-03
94	3.166e-02	5.343e-02	2.361e-02	5.366e-02	5.01e-04	3.454e-03
93	3.452e-02	5.030e-02	2.363e-02	5.051e-02	6.655e-04	4.651e-03
92	3.765e-02	4.736e-02	2.367e-02	4.769e-02	8.689e-04	5.375e-03
91	4.105e-02	4.462e-02	2.371e-02	4.485e-02	5.427e-04	5.179e-03
90	4.471e-02	4.205e-02	2.377e-02	4.228e-02	6.281e-04	5.312e-03
89	4.862e-02	3.964e-02	2.384e-02	3.988e-02	7.268e-04	5.519e-03
88	5.324e-02	3.740e-02	2.393e-02	3.764e-02	8.410e-04	5.739e-03
87	5.806e-02	3.433e-02	2.396e-02	3.554e-02	9.728e-04	5.973e-03
86	6.332e-02	3.155e-02	2.413e-02	3.176e-02	1.125e-04	6.228e-03
85	6.905e-02	2.952e-02	2.416e-02	3.171e-02	1.301e-04	6.486e-03
84	7.503e-02	2.743e-02	2.411e-02	3.011e-02	1.501e-04	6.769e-03
83	8.211e-02	2.835e-02	2.415e-02	3.048e-02	1.736e-04	7.077e-03
82	8.955e-02	2.678e-02	2.416e-02	2.703e-02	1.049e-04	7.266e-03
81	9.765e-02	2.512e-02	2.496e-02	2.567e-02	2.120e-04	7.952e-03
80	1.064e-01	2.415e-02	2.572e-02	2.441e-02	2.615e-04	8.152e-03
79	1.161e-01	2.248e-02	2.546e-02	2.174e-02	3.161e-04	8.802e-03

78	1.2664801	2.199e+00	2.575e+02	2.166e+00	3.534e+02	6.859e+03	3.578e+01	0.046e+00	1.176e+02	4.535e+03	1.187e+04
77	1.3811801	2.090e+00	2.680e+02	1.160e+00	4.064e+02	7.284e+03	1.803e+01	0.000e+00	1.248e+02	5.297e+03	1.373e+04
76	1.5611601	1.994e+00	2.646e+02	2.024e+00	4.664e+02	7.731e+03	4.035e+01	0.000e+00	1.325e+02	6.044e+03	1.588e+04
75	1.624e+01	1.931e+00	2.616e+02	1.930e+00	5.356e+02	8.210e+03	4.773e+01	0.000e+00	1.406e+02	6.844e+03	1.836e+04
74	1.7910801	1.831e+00	2.734e+02	1.861e+00	6.139e+02	8.713e+03	4.517e+01	0.000e+00	1.491e+02	7.828e+03	2.122e+04
73	1.9511501	1.762e+00	2.787e+02	1.790e+00	7.027e+02	9.246e+03	4.766e+01	0.000e+00	1.582e+02	8.885e+03	2.453e+04
72	2.1598e+01	1.697e+00	2.848e+02	1.256e+00	8.336e+02	9.810e+03	5.018e+01	0.000e+00	1.679e+02	1.105e+02	2.836e+04
71	2.3227e+01	1.637e+00	2.916e+02	1.604e+00	9.724e+02	1.041e+03	5.214e+01	0.000e+00	1.782e+02	1.038e+02	2.273e+04
70	2.5129e+01	1.582e+00	2.991e+02	1.126e+00	1.046e+01	1.101e+02	5.530e+01	0.000e+00	1.861e+02	1.284e+02	3.191e+04
69	2.7621e+01	1.532e+00	3.076e+02	1.563e+00	1.190e+01	1.116e+02	5.787e+01	0.000e+00	1.945e+02	1.445e+02	4.384e+04
68	3.0211e+01	1.481e+00	3.172e+02	1.519e+00	1.216e+01	1.135e+02	6.042e+01	0.000e+00	2.023e+02	1.623e+02	5.071e+04
67	3.2848e+01	1.441e+00	3.281e+02	1.480e+00	1.248e+01	1.172e+02	6.295e+01	0.000e+00	2.167e+02	1.819e+02	5.869e+04
66	3.5820e+01	1.411e+00	3.401e+02	1.445e+00	1.294e+01	1.212e+02	6.494e+01	0.000e+00	2.267e+02	1.919e+02	6.795e+04
65	3.9632e+01	1.379e+00	3.531e+02	1.414e+00	1.341e+01	1.241e+02	6.788e+01	0.000e+00	2.346e+02	2.105e+02	7.866e+04
64	4.2598e+01	1.350e+00	3.671e+02	1.387e+00	1.381e+01	1.271e+02	7.026e+01	0.000e+00	2.525e+02	2.323e+02	8.766e+04
63	4.6535e+01	1.324e+00	3.819e+02	1.364e+00	1.424e+01	1.319e+02	7.256e+01	0.000e+00	2.695e+02	2.604e+02	9.054e+04
62	5.0588e+01	1.304e+00	3.919e+02	1.319e+00	1.460e+01	1.373e+02	7.478e+01	0.000e+00	2.838e+02	2.701e+02	9.204e+04
61	5.5233e+01	1.285e+00	3.976e+02	1.291e+00	1.421e+01	1.352e+02	7.692e+01	0.000e+00	2.986e+02	2.834e+02	9.434e+04
60	6.0233e+01	1.269e+00	4.451e+02	1.314e+00	1.530e+01	1.421e+02	7.916e+01	0.000e+00	3.144e+02	3.066e+02	1.115e+04
59	6.5955e+01	1.256e+00	4.989e+02	1.303e+00	1.543e+01	1.534e+02	8.123e+01	0.000e+00	3.267e+02	3.178e+02	1.244e+04
58	7.1641e+01	1.245e+00	4.989e+02	1.296e+00	1.405e+01	1.494e+02	8.346e+01	0.000e+00	3.405e+02	3.316e+02	1.307e+04
57	7.8125e+01	1.237e+00	5.313e+02	1.241e+00	1.414e+01	1.506e+02	8.568e+01	0.000e+00	3.527e+02	3.416e+02	1.376e+04
56	8.5596e+01	1.231e+00	5.623e+02	1.287e+00	1.455e+01	1.551e+02	8.794e+01	0.000e+00	3.656e+02	3.568e+02	1.487e+04
55	9.2071e+01	1.221e+00	5.983e+02	1.286e+00	1.505e+01	1.614e+02	9.013e+01	0.000e+00	3.878e+02	3.893e+02	1.593e+04
54	1.0132e+00	1.2248e+00	6.271e+02	1.248e+00	1.570e+01	1.708e+02	9.288e+01	0.000e+00	4.120e+02	4.208e+02	1.636e+04
53	1.1049e+00	1.2231e+00	6.833e+02	1.2211e+00	1.719e+01	1.749e+02	9.500e+01	0.000e+00	4.423e+02	4.589e+02	1.712e+04
52	1.2019e+00	1.2236e+00	7.343e+02	1.2236e+00	1.722e+01	1.772e+02	9.719e+01	0.000e+00	4.744e+02	4.944e+02	1.791e+04
51	1.3139e+00	1.2256e+00	7.952e+02	1.3041e+00	1.730e+01	1.830e+02	1.018e+02	0.000e+00	5.056e+02	5.254e+02	2.166e+04
50	1.4318e+00	1.2284e+00	8.591e+02	1.3148e+00	1.724e+01	1.893e+02	1.048e+02	0.000e+00	5.376e+02	5.654e+02	2.579e+04
49	1.6275e+01	1.2376e+00	9.294e+02	1.281e+00	1.724e+01	1.978e+02	1.171e+02	0.000e+00	5.746e+02	6.164e+02	2.985e+04
48	1.7039e+01	1.2316e+00	9.621e+02	1.287e+00	1.724e+01	2.051e+02	1.214e+02	0.000e+00	6.026e+02	6.548e+02	3.295e+04
47	1.8811e+01	1.2416e+00	1.039e+03	1.313e+00	1.735e+01	2.136e+02	1.250e+02	0.000e+00	6.378e+02	6.933e+02	3.678e+04
46	2.0623e+01	1.2505e+00	1.1977e+01	1.5427e+00	1.741e+01	2.172e+02	1.313e+02	0.000e+00	6.788e+02	7.310e+02	4.036e+04
45	2.2097e+01	1.2570e+00	1.381e+01	1.570e+00	1.750e+01	2.225e+02	1.367e+02	0.000e+00	7.246e+02	7.826e+02	4.418e+04
44	2.4098e+01	1.2654e+00	1.4257e+01	1.608e+00	1.732e+01	2.262e+02	1.425e+02	0.000e+00	7.758e+02	8.216e+02	4.805e+04
43	2.6278e+01	1.2711e+00	1.4711e+01	1.646e+00	1.741e+01	2.327e+02	1.487e+02	0.000e+00	8.323e+02	8.895e+02	5.156e+04
42	2.8556e+01	1.2828e+00	1.5221e+01	1.687e+00	1.752e+01	2.387e+02	1.551e+02	0.000e+00	8.952e+02	9.559e+02	5.566e+04
41	3.1505e+01	1.2924e+00	1.5826e+01	1.7416e+00	1.781e+01	2.458e+02	1.614e+02	0.000e+00	9.556e+02	1.021e+03	6.000e+04
40	3.4078e+01	1.3024e+00	1.6316e+01	1.803e+00	1.810e+01	2.518e+02	1.674e+02	0.000e+00	1.076e+03	1.171e+03	6.492e+04
39	3.7163e+01	1.3111e+00	1.6916e+01	1.843e+00	1.851e+01	2.576e+02	1.735e+02	0.000e+00	1.136e+03	1.291e+03	6.992e+04
38	4.0225e+01	1.3216e+00	2.5432e+01	1.8716e+00	1.902e+01	2.637e+02	1.797e+02	0.000e+00	1.204e+03	1.353e+03	7.528e+04
37	4.4944e+01	1.3316e+00	2.8056e+01	1.9126e+00	1.961e+01	2.708e+02	1.861e+02	0.000e+00	1.274e+03	1.413e+03	8.118e+04
36	4.9894e+01	1.3420e+00	3.2053e+01	1.9594e+00	1.961e+01	2.790e+02	1.901e+02	0.000e+00	1.342e+03	1.481e+03	8.718e+04
35	5.2556e+01	1.3521e+00	3.1981e+01	1.9594e+00	1.961e+01	2.850e+02	1.959e+02	0.000e+00	1.412e+03	1.537e+03	9.318e+04
34	5.7333e+01	1.3613e+00	3.1640e+01	1.9594e+00	1.961e+01	2.818e+02	1.928e+02	0.000e+00	1.482e+03	1.597e+03	9.918e+04
33	6.2508e+01	1.3713e+00	3.1661e+01	1.9594e+00	1.961e+01	2.818e+02	1.928e+02	0.000e+00	1.552e+03	1.667e+03	1.051e+05
32	6.8157e+01	1.3814e+00	3.1697e+01	1.9594e+00	1.961e+01	2.818e+02	1.928e+02	0.000e+00	1.621e+03	1.734e+03	1.124e+05
31	7.4225e+01	1.3916e+00	3.1771e+01	1.9594e+00	1.961e+01	2.818e+02	1.928e+02	0.000e+00	1.691e+03	1.804e+03	1.194e+05
30	8.1052e+01	1.4016e+00	3.2161e+01	1.9594e+00	1.961e+01	2.818e+02	1.928e+02	0.000e+00	1.761e+03	1.874e+03	1.264e+05
29	8.8888e+01	1.4151e+00	3.2816e+01	1.9594e+00	1.961e+01	2.837e+02	1.947e+02	0.000e+00	1.831e+03	1.943e+03	1.334e+05
28	9.6388e+01	1.4254e+00	3.3616e+01	1.9594e+00	1.961e+01	2.847e+02	1.967e+02	0.000e+00	1.901e+03	2.013e+03	1.434e+05
27	1.0611e+01	1.4313e+00	3.4216e+01	1.9594e+00	1.961e+01	2.857e+02	1.987e+02	0.000e+00	1.971e+03	2.083e+03	1.535e+05
26	1.1633e+01	1.4343e+00	3.4761e+01	1.9594e+00	1.961e+01	2.867e+02	2.007e+02	0.000e+00	2.041e+03	2.153e+03	1.635e+05
25	1.2630e+01	1.4353e+00	3.5113e+01	1.9594e+00	1.961e+01	2.877e+02	2.027e+02	0.000e+00	2.111e+03	2.223e+03	1.734e+05
24	1.3631e+01	1.4364e+00	3.5176e+01	1.9594e+00	1.961e+01	2.887e+02	2.047e+02	0.000e+00	2.179e+03	2.294e+03	1.833e+05
23	1.4655e+01	1.4374e+00	3.5186e+01	1.9594e+00	1.961e+01	2.897e+02	2.067e+02	0.000e+00	2.248e+03	2.364e+03	1.933e+05
22	1.6310e+01	1.4416e+00	3.2126e+01	1.9594e+00	1.961e+01	2.907e+02	2.087e+02	0.000e+00	2.318e+03	2.434e+03	2.033e+05
21	1.7678e+01	1.4516e+00	3.1928e+01	1.9594e+00	1.961e+01	2.917e+02	2.107e+02	0.000e+00	2.388e+03	2.514e+03	2.133e+05
20	1.9218e+01	1.4616e+00	3.1821e+01	1.9594e+00	1.961e+01	2.927e+02	2.127e+02	0.000e+00	2.468e+03	2.684e+03	2.233e+05
19	2.1022e+01	1.4716e+00	3.1640e+01	1.9594e+00	1.961e+01	2.937e+02	2.147e+02	0.000e+00	2.548e+03	2.854e+03	2.333e+05
18	2.2625e+01	1.4816e+00	3.1413e+01	1.9594e+00	1.961e+01	2.947e+02	2.167e+02	0.000e+00	2.628e+03	2.924e+03	2.433e+05
17	2.5008e+01	1.4926e+00	3.1169e+01	1.9594e+00	1.961e+01	2.957e+02	2.187e+02	0.000e+00	2.708e+03	3.094e+03	2.533e+05
16	2.7637e+01	1.5036e+00	3.1016e+01	1.9594e+00	1.961e+01	2.967e+02	2.207e+02	0.000e+00	2.790e+03	3.164e+03	2.633e+05
15	2.9173e+01	1.5156e+00	3.0539e+01	1.9594e+00	1.961e+01	2.977e+02	2.227e+02	0.000e+00	2.870e+03	3.234e+03	2.733e+05

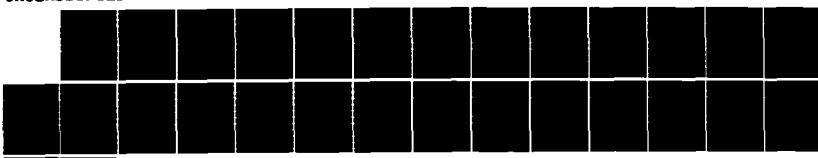
RD-A164 413

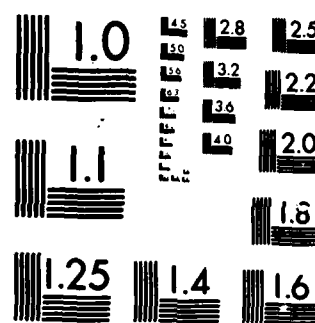
INP:FE AND GARS:CR PICOSECOND PHOTOCONDUCTIVE RADIATION 2/2
DETECTORS(U) NAVAL POSTGRADUATE SCHOOL MONTEREY CA
P J KEPPEL DEC 85

UNCLASSIFIED

F/G 18/4

NL





MICROCOPY RESOLUTION TEST CHART
NATIONAL BUREAU OF STANDARDS 1963 A

115	5	112.18	0.1	1	953e+003	1	B10e+02	1	961e+001	1	657e+04	5	716e+04	1	1979e+02	0	0.00e+00	9	678e+04	0	115e+02	0	0.00e+00	4	010e+01	0
114	5	59.30e	0.1	1	85.1e+001	1	85.1e+002	1	85.1e+001	1	901e+01	6	106e+04	2	155e+02	0	0.00e+00	1	0.22e+00	0	4.1e+02	0	5.16e+02	0	4.1e+02	0
113	6	107.5e	0.3	1	75.1e+001	1	B10e+02	1	75.1e+001	1	78.2e+04	6	435e+04	2	347e+02	0	0.00e+00	1	0.08e+00	0	3.2e+02	0	8.11e+02	0	5.322e+07	0
112	6	65.95e	0.3	1	654e+001	1	654e+002	1	654e+001	1	507e+04	6	823e+04	2	555e+02	0	0.00e+00	1	143e+01	0	3.24e+05	0	6.137e+07	0	1.43e+01	0
111	7	269.3e	0.3	1	56.1e+001	1	B10e+02	1	56.1e+001	1	56.1e+04	7	232e+04	2	782e+02	0	0.00e+00	1	210e+03	0	3.74e+05	0	7.022e+07	0	7.022e+07	0
110	7	915.1e	0.3	1	47.1e+001	1	B10e+02	1	47.1e+001	1	47.1e+04	7	665e+04	3	928e+02	0	0.00e+00	1	1283e+03	0	4.379e+05	0	8.177e+07	0	8.177e+07	0
109	8	6117.6e	0.1	1	38.1e+001	1	B10e+02	1	39.1e+001	1	38.1e+04	8	192e+04	3	395e+02	0	0.00e+00	1	504e+03	0	5.04e+05	0	1.417e+07	0	1.417e+07	0
108	9	412.9e	0.3	1	30.9e+001	1	B10e+02	1	31.1e+001	1	30.9e+04	8	606e+04	3	595e+02	0	0.00e+00	1	40.8e+03	0	4.08e+05	0	1.092e+06	0	1.092e+06	0
107	10	126.6e	0.2	1	23.1e+001	1	B10e+02	1	23.1e+001	1	23.1e+04	9	606e+04	4	424e+02	0	0.00e+00	1	52.9e+03	0	6.69e+05	0	1.261e+06	0	1.261e+06	0
106	11	119.4e	0.2	1	16.1e+001	1	B10e+02	1	16.1e+001	1	16.1e+04	9	637e+04	4	424e+02	0	0.00e+00	1	47.7e+03	0	7.750e+05	0	1.461e+06	0	1.461e+06	0
105	12	220.7e	0.2	1	19.1e+001	1	B10e+02	1	19.1e+001	1	19.1e+04	1	671e+04	4	612e+02	0	0.00e+00	1	72.1e+03	0	8.981e+05	0	1.691e+06	0	1.691e+06	0
104	13	312.2e	0.2	1	27.9e+001	1	B10e+02	1	27.9e+001	1	27.9e+04	1	691e+04	5	914e+02	0	0.00e+00	1	828e+03	0	1.041e+05	0	1.958e+06	0	1.958e+06	0
103	14	4517.6e	0.2	9	6.15e+000	1	B10e+02	1	6.15e+000	1	6.15e+04	1	153e+03	3	449e+02	0	0.00e+00	1	1.942e+03	0	2.00e+04	0	2.261e+06	0	2.261e+06	0
102	15	58.1e	0.2	9	10.4e+000	1	B10e+02	1	10.4e+000	1	10.4e+04	1	224e+03	2	532e+02	0	0.00e+00	1	3.08e+03	0	3.08e+04	0	6.235e+06	0	6.235e+06	0
101	16	72.6e	0.2	8	5.53e+000	1	B10e+02	1	5.53e+000	1	5.53e+04	1	209e+03	2	6429e+02	0	0.00e+00	1	5.12e+03	0	6.21e+04	0	3.434e+06	0	3.434e+06	0
100	17	88.1e	0.2	8	0.49e+000	1	B10e+02	1	8.0e+000	1	318e+03	3	318e+03	2	6.98e+02	0	0.00e+00	1	8.759e+03	0	5.256e+06	0	1.486e+06	0	1.486e+06	0
99	18	2.052e	0.2	7	5.68e+000	1	B10e+02	1	5.78e+000	1	606e+03	3	462e+03	7	576e+02	0	0.00e+00	1	4.777e+03	0	1.179e+04	0	4.086e+06	0	4.086e+06	0
98	19	2.2188e	0.2	7	1.16e+000	1	B10e+02	1	8.73e+000	1	853e+03	3	219e+03	3	8.73e+03	0	0.00e+00	1	6.332e+03	0	5.217e+04	0	4.735e+06	0	4.735e+06	0
97	20	4.414e	0.2	6	6.91e+000	1	B10e+02	1	6.70e+000	1	6.70e+04	2	182e+03	1	6.59e+03	0	0.00e+00	1	7.930e+03	0	9.231e+04	0	4.489e+06	0	4.489e+06	0
96	21	6.664e	0.2	6	2.91e+000	1	B10e+02	1	2.72e+000	1	316e+03	2	492e+03	3	6.76e+03	0	0.00e+00	1	2.793e+03	0	9.912e+04	0	3.362e+06	0	3.362e+06	0
95	22	9.923e	0.2	5	9.11e+000	1	B10e+02	1	9.12e+000	1	9.12e+04	1	959e+03	1	6.59e+02	0	0.00e+00	1	9.638e+03	0	1.65e+04	0	9.460e+06	0	9.460e+06	0
94	23	16.68e	0.2	5	5.51e+000	1	B10e+02	1	5.51e+000	1	5.51e+04	1	939e+03	1	1.04e+03	0	0.00e+00	1	3.168e+03	0	1.65e+04	0	5.753e+06	0	5.753e+06	0
93	24	4.527e	0.2	5	2.36e+000	1	B10e+02	1	2.553e+000	1	2.553e+04	1	3.02e+03	1	1.39e+03	0	0.00e+00	1	3.367e+03	0	1.567e+04	0	5.586e+06	0	5.586e+06	0
92	25	7.652e	0.2	4	9.21e+000	1	B10e+02	1	8.73e+000	1	4.94e+04	2	4.85e+03	2	229e+03	0	0.00e+00	1	3.25e+03	0	1.03e+04	0	3.275e+06	0	3.275e+06	0
91	26	105.9e	0.2	4	6.49e+000	1	B10e+02	1	6.74e+000	1	6.58e+04	2	1.95e+03	3	3.68e+03	0	0.00e+00	1	6.432e+03	0	1.639e+04	0	3.213e+06	0	3.213e+06	0
90	27	4.710.3e	0.2	4	3.70e+000	1	B10e+02	1	3.87e+000	1	2.94e+04	2	1.96e+03	3	5.46e+03	0	0.00e+00	1	2.930e+03	0	2.251e+04	0	1.542e+05	0	1.542e+05	0
89	28	4.8928e	0.2	4	1.18e+000	1	B10e+02	1	1.18e+000	1	1.18e+04	2	1.371e+03	6	9.61e+03	2	0.00e+00	1	6.68e+03	0	9.517e+04	0	1.781e+05	0	1.781e+05	0
88	29	5.1247e	0.2	3	6.68e+000	1	B10e+02	1	6.68e+000	1	6.68e+04	2	2.22e+03	2	7.61e+03	0	0.00e+00	1	7.61e+03	0	5.91e+04	0	9.735e+05	0	9.735e+05	0
87	30	8.8674e	0.2	3	6.61e+000	1	B10e+02	1	6.61e+000	1	6.61e+04	2	2.20e+03	2	7.61e+03	0	0.00e+00	1	7.61e+03	0	5.91e+04	0	9.735e+05	0	9.735e+05	0
86	31	3.322e	0.2	3	4.55e+000	1	B10e+02	1	4.55e+000	1	4.55e+04	2	2.05e+03	2	6.24e+03	0	0.00e+00	1	6.24e+03	0	5.601e+04	0	9.901e+05	0	9.901e+05	0
85	32	6.9053e	0.2	3	2.61e+000	1	B10e+02	1	2.84e+000	1	2.84e+04	2	1.51e+03	3	3.26e+03	0	0.00e+00	1	3.26e+03	0	4.653e+04	0	9.213e+05	0	9.213e+05	0
84	33	7.510.3e	0.2	3	1.61e+000	1	B10e+02	1	1.61e+000	1	1.61e+04	2	1.51e+03	3	3.26e+03	0	0.00e+00	1	3.26e+03	0	4.653e+04	0	9.213e+05	0	9.213e+05	0
83	34	8.2119e	0.2	3	2.92e+000	1	B10e+02	1	2.92e+000	1	2.92e+04	2	6.01e+03	3	5.78e+03	0	0.00e+00	1	5.78e+03	0	9.513e+04	0	2.510e+05	0	2.510e+05	0
82	35	1.501e	0.2	2	1.771e+001	1	B10e+02	1	1.771e+001	1	1.771e+04	2	9.24e+03	2	7.577e+03	0	0.00e+00	1	7.577e+03	0	1.791e+04	0	4.291e+06	0	4.291e+06	0
81	36	2.915.6e	0.2	2	6.11e+000	1	B10e+02	1	6.11e+000	1	6.11e+04	2	1.01e+03	3	8.71e+03	0	0.00e+00	1	8.71e+03	0	1.844e+04	0	4.184e+06	0	4.184e+06	0
80	37	6.649e	0.1	2	4.49e+000	1	B10e+02	1	4.49e+000	1	4.49e+04	2	6.50e+03	3	1.01e+03	0	0.00e+00	1	1.01e+03	0	2.772e+04	0	3.370e+05	0	3.370e+05	0
79	38	1.613.6e	0.1	2	1.77e+000	1	B10e+02	1	1.77e+000	1	1.77e+04	2	4.52e+03	3	1.52e+03	0	0.00e+00	1	1.52e+03	0	4.224e+04	0	6.360e+05	0	6.360e+05	0
78	39	266.4e	0.1	2	2.61e+000	1	B10e+02	1	2.61e+000	1	2.61e+04	2	4.52e+03	3	1.52e+03	0	0.00e+00	1	1.52e+03	0	4.224e+04	0	6.360e+05	0	6.360e+05	0
77	40	3.321e	0.1	2	6.16e+000	1	B10e+02	1	6.16e+000	1	6.16e+04	2	4.52e+03	3	1.52e+03	0	0.00e+00	1	1.52e+03	0	4.224e+04	0	6.360e+05	0	6.360e+05	0
76	41	3.811e	0.1	2	1.61e+000	1	B10e+02	1	1.61e+000	1	1.61e+04	2	4.52e+03	3	1.52e+03	0	0.00e+00	1	1.52e+03	0	4.224e+04	0	6.360e+05	0	6.360e+05	0
75	42	5.1216e	0.1	2	5.31e+000	1	B10e+02	1	5.31e+000	1	5.31e+04	2	3.31e+03	3	3.31e+03	0	0.00e+00	1	3.31e+03	0	6.281e+04	0	1.368e+05	0	1.368e+05	0
74	43	7.911e	0.1	2	1.89e+000	1	B10e+02	1	1.89e+000	1	1.89e+04	2	4.52e+03	3	1.89e+03	0	0.00e+00	1	1.89e+03	0	4.237e+04	0	6.360e+05	0	6.360e+05	0
73	44	2.112e	0.1	2	7.51e+000	1	B10e+02	1	7.51e+000	1	7.51e+04	2	4.52e+03	3	1.89e+03	0	0.00e+00	1</								

51	1	1139e+000	249e+000	6	227e+000	02	310e+000	8	89e+000	01	2	655e+002	02	9	216e+001	01	1	114e+002	02	4	993e+001	
50	43	4128e+000	250e+000	6	751e+000	1	311e+000	9	795e+001	01	2	844e+002	02	9	309e+001	01	1	822e+002	02	5	873e+001	
49	49	5625e+000	253e+000	7	316e+002	02	326e+000	0	078e+000	3	050e+002	02	3	393e+002	02	0	096e+002	02	5	909e+001		
48	48	7039e+000	251e+000	7	987e+002	02	337e+000	0	184e+000	3	274e+002	02	9	468e+001	01	2	632e+001	01	8	133e+001		
47	47	1158e+000	263e+000	8	710e+002	02	358e+000	0	299e+000	3	518e+002	02	9	853e+001	01	2	616e+002	02	1	148e+001		
46	46	2162e+000	263e+000	9	521e+002	02	364e+000	0	423e+000	3	784e+002	02	9	594e+001	01	2	505e+002	02	1	936e+001		
45	45	21097e+000	215e+000	2	521e+000	01	388e+000	0	556e+000	4	423e+000	02	9	317e+002	02	8	176e+002	02	1	133e+002		
44	44	4097e+000	281e+000	1	144e+001	01	397e+000	1	701e+000	4	388e+002	02	9	694e+001	01	3	635e+002	02	4	41e+001		
43	43	6278e+000	291e+000	2	507e+000	01	606e+000	1	416e+000	0	655e+000	4	733e+002	02	9	755e+001	01	4	055e+002			
42	42	8656e+000	299e+000	1	525e+001	01	417e+000	2	022e+000	5	108e+002	02	9	771e+001	01	4	456e+001	01	6	667e+001		
41	41	1250e+000	308e+000	0	525e+000	01	160e+000	1	201e+000	5	517e+002	02	9	803e+001	01	4	819e+001	01	1	166e+001		
40	40	34078e+000	317e+000	0	631e+001	01	485e+000	0	392e+000	5	963e+002	02	9	830e+001	01	5	321e+001	01	2	603e+001		
39	39	3163e+000	326e+000	0	851e+001	01	512e+000	0	449e+000	5	449e+002	02	9	854e+001	01	2	227e+001	01	3	890e+001		
38	38	40526e+000	316e+000	2	205e+000	01	534e+000	0	154e+000	4	819e+000	6	919e+002	02	9	875e+001	01	6	212e+002			
37	37	4194e+000	316e+000	2	261e+000	01	572e+000	0	490e+000	7	549e+002	02	9	893e+001	01	6	236e+002	02	5	089e+001		
36	36	4194e+000	316e+000	3	507e+000	01	606e+000	1	307e+000	8	169e+002	02	9	908e+001	01	7	328e+002	02	1	849e+001		
35	35	52556e+000	305e+000	2	771e+001	01	642e+000	0	575e+000	8	839e+002	02	9	921e+001	01	7	451e+002	02	1	849e+001		
34	34	81123e+000	315e+000	0	963e+001	01	682e+000	0	3861e+000	9	561e+002	02	9	931e+001	01	8	462e+002	02	2	227e+001		
33	33	62800e+000	315e+000	0	316e+001	01	724e+000	0	466e+000	1	034e+001	0	943e+002	02	9	962e+001	01	3	046e+001			
32	32	61574e+000	315e+000	0	770e+001	01	770e+000	0	490e+000	1	117e+001	0	951e+001	01	6	682e+001	01	2	238e+001			
31	31	74325e+000	315e+000	0	405e+000	4	197e+001	0	819e+000	4	834e+000	1	207e+001	0	953e+001	01	1	154e+001				
30	30	81052e+000	315e+000	0	451e+000	4	572e+001	0	915e+000	1	230e+000	0	953e+001	01	2	944e+001	01	3	438e+001			
29	29	83886e+000	316e+000	0	458e+000	5	582e+001	0	130e+000	0	584e+000	1	404e+001	0	963e+001	01	1	158e+001				
28	28	93886e+000	316e+000	0	450e+000	5	582e+001	0	130e+000	0	584e+000	1	404e+001	0	963e+001	01	1	158e+001				
27	27	10511e+000	415e+000	6	167e+001	01	616e+000	2	061e+000	6	422e+000	1	627e+001	01	919e+001	01	3	11e+001	01	4	327e+001	
26	26	1463e+000	454e+000	6	811e+001	01	135e+000	2	135e+000	0	875e+000	1	749e+001	01	992e+001	01	4	634e+001	01	9	919e+001	
25	25	1463e+000	454e+000	6	521e+001	01	216e+000	2	216e+000	0	352e+000	1	872e+001	01	995e+001	01	4	616e+001	01	9	919e+001	
24	24	13650e+000	454e+000	6	304e+000	2	404e+000	0	853e+000	1	404e+000	01	912e+001	01	998e+001	01	4	637e+001	01	3	966e+001	
23	23	4865e+000	761e+000	7	101e+000	01	199e+000	2	199e+000	0	378e+000	1	989e+000	1	202e+001	01	998e+001	01	4	532e+001		
22	22	6210e+000	1421e+000	0	161e+001	01	250e+000	2	197e+000	0	510e+000	1	404e+001	0	917e+001	01	1	154e+001	01	4	532e+001	
21	21	7768e+000	501e+000	0	155e+000	01	616e+000	2	616e+000	0	455e+001	0	915e+001	01	176e+001	01	1	167e+001	01	2	168e+001	
20	20	19278e+000	509e+000	0	210e+000	01	739e+000	2	739e+000	0	108e+000	1	614e+001	0	913e+001	01	3	210e+001	01	4	304e+001	
19	19	21022e+000	518e+000	0	518e+000	01	872e+000	0	724e+000	1	724e+000	01	912e+001	01	912e+001	01	6	149e+001	01	5	976e+001	
18	18	22925e+000	517e+000	0	517e+000	01	821e+000	0	321e+000	2	137e+001	01	950e+001	01	2	048e+001	01	6	457e+001			
17	17	25000e+000	515e+000	0	615e+000	01	182e+000	1	203e+000	2	125e+001	01	996e+001	01	2	117e+001	01	1	105e+000			
16	16	27261e+000	513e+000	0	613e+000	01	183e+000	1	183e+000	0	373e+000	1	997e+001	01	2	126e+001	01	1	157e+001			
15	15	29730e+000	512e+000	0	161e+001	01	250e+000	0	817e+000	2	301e+001	01	998e+001	01	1	154e+001	01	1	151e+001			
14	14	3241e+000	512e+000	0	161e+001	01	250e+000	0	817e+000	2	301e+001	01	998e+001	01	1	154e+001	01	1	151e+001			
13	13	32552e+000	508e+000	0	417e+000	2	375e+000	0	418e+000	3	865e+001	01	998e+001	01	2	514e+001	01	1	149e+001			
12	12	32552e+000	508e+000	0	417e+000	2	375e+000	0	418e+000	3	865e+001	01	998e+001	01	2	514e+001	01	1	149e+001			
11	11	42045e+000	508e+000	0	581e+000	2	923e+000	4	506e+000	1	651e+001	01	950e+001	01	2	710e+001	01	1	987e+001			
10	10	45850e+000	508e+000	0	581e+000	2	213e+000	4	804e+000	1	733e+001	01	444e+001	0	999e+001	01	2	178e+001	01	1	157e+001	
9	9	50000e+000	508e+000	0	581e+000	2	513e+000	5	129e+000	1	817e+000	01	629e+001	01	999e+001	01	2	126e+001	01	1	157e+001	
8	8	54525e+000	613e+000	0	819e+000	3	548e+000	0	134e+000	0	3488e+001	01	998e+001	01	3	046e+001	01	2	416e+001	01	1	159e+001
7	7	54640e+000	613e+000	0	819e+000	3	548e+000	0	134e+000	0	3488e+001	01	998e+001	01	3	046e+001	01	2	416e+001	01	1	159e+001
6	6	64840e+000	620e+000	0	617e+000	4	260e+000	0	836e+000	2	078e+000	5	219e+001	01	998e+001	01	3	223e+001	01	1	156e+001	
5	5	70111e+000	627e+000	0	617e+000	4	260e+000	0	836e+000	2	078e+000	5	219e+001	01	998e+001	01	3	223e+001	01	1	156e+001	
4	4	77111e+000	634e+000	0	617e+000	4	260e+000	0	836e+000	2	078e+000	5	219e+001	01	998e+001	01	3	223e+001	01	1	156e+001	
3	3	8490e+000	634e+000	0	617e+000	4	260e+000	0	836e+000	2	078e+000	5	219e+001	01	998e+001	01	3	223e+001	01	1	156e+001	
2	2	91700e+000	634e+000	0	617e+000	4	260e+000	0	836e+000	2	078e+000	5	219e+001	01	998e+001	01	3	223e+001	01	1	156e+001	
1	1	10000e+000	634e+000	0	617e+000	4	260e+000	0	836e+000	2	078e+000	5	219e+001	01	998e+001	01	3	223e+001	01	1	156e+001	

END OF
PROGRAM X16N
END OF

095200

INP

USER NUMBER	095200
WORKER MACHINE	Y
DATE SENT	10-Oct-1985
TIME SENT	15:17:31
XEROX UNIT	A
PAGE 5 DATE	10-Oct-1985
PAGE 5 TIME	15:18:29
JUN 1985 INP 1	

SPH 0 00 0 00 2 0 SPH 0 00 2 0
 REAL DATA FOR BODY 2 IS STORED IN PCD ARRAY LOCATIONS 10 THROUGH 14
 SPH 0 00 0 00 4 0 SPH 0 00 4 0
 REAL DATA FOR BODY 3 IS STORED IN PCD ARRAY LOCATIONS 15 THROUGH 20
 PCD
 NUMBER OF BODIES J

INPUT ZONE DATA

21 0 1
 22 0 2 -1
 23 0 3 -2
 END
 0 COMPARISON OF GEOMETRY REQUIREMENTS VS ALLOCATIONS
 LENGTH OF ARRAY CONTAINING REAL BODY DATA / INPUT 4 20 / 1000
 NUMBER OF INPUT ZONES / INPUT 3 / 100
 NUMBER OF CODE ZONES / INPUT 3 / 100
 LENGTH OF GEOMETRY ARRAY CONTAINING INTEGER DATA / INPUT 65 / 1000
 LENGTH OF ARRAY CONTAINING CODE ZONE BODY DATA / INPUT 2 / 50

CODE ZONE INPUT ZONE ZONE DATA LOC HD OF BODIES

1	1	16	1
2	2	20	2
3	3	28	2

OPTION 1 WAS USED IN CALCULATING VOLUMES FOR 3 INPUT ZONES

INPUT MEANING
 0 - ALL VOLUMES SET TO 1.0
 1 - READ INPUT VOLUMES
 2 - USER LOGIC TO COMPUTE VOLUMES

VOLUME (CM³)

ZONE	0	2	3
VOLUME	2.50e-03	3.350e-01	2.619e+02
MAX ECU1 PIC2			

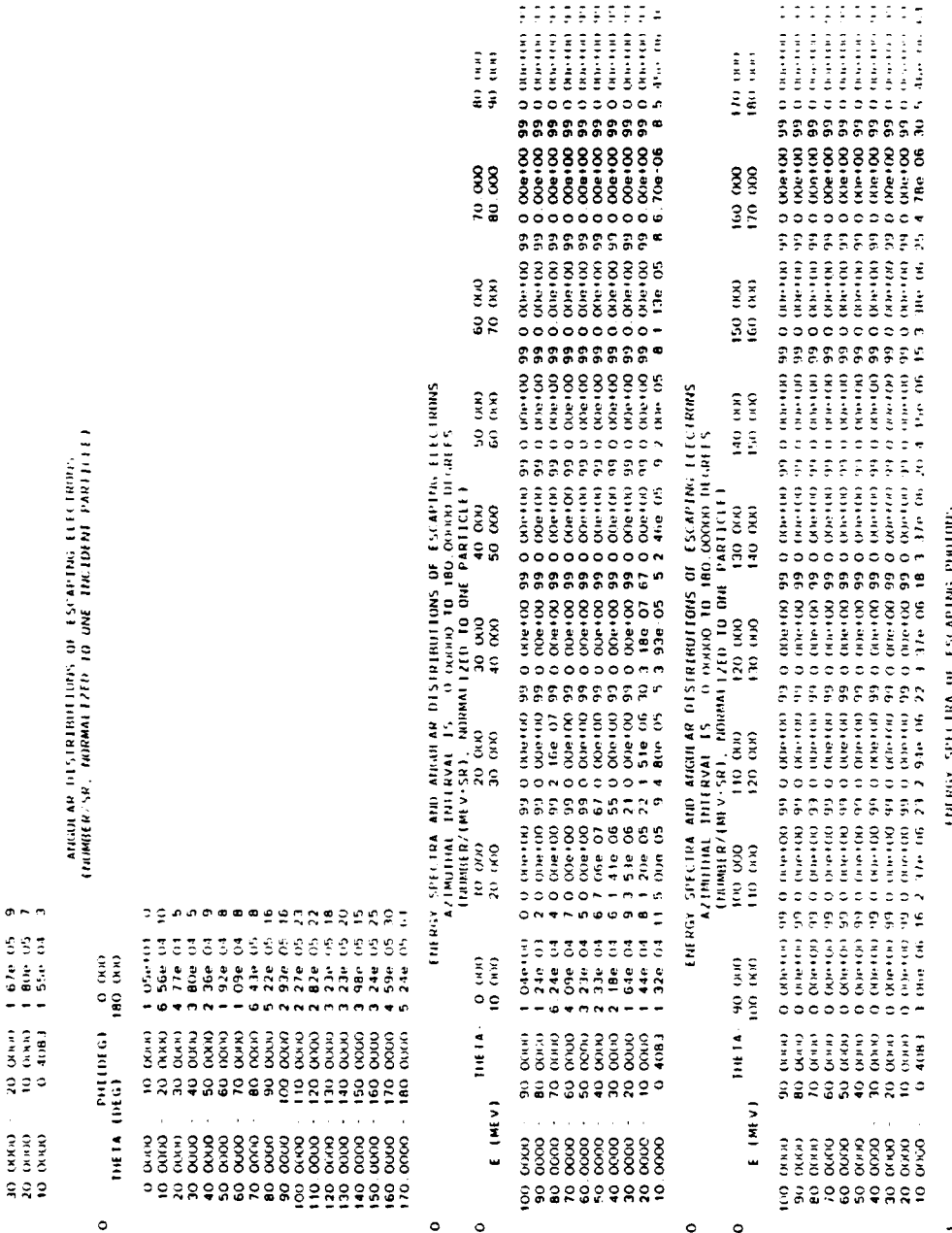
0 ***** SOURCE *****

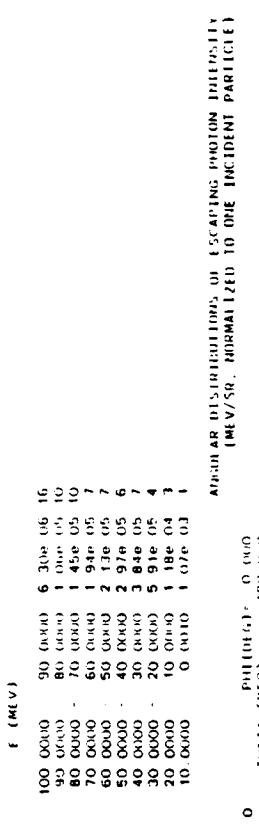
ELECTRONS
 ENERGY 100.0
 POSITION 0.0 0.0 0.0
 RADIUS 0.5
 DIRECTION 0.0
 CUTOFFS 0.05 0.201
 ***** OUTPUT OPTIONS *****
 ELECTRON ESCAPE
 PRIME 10
 PHOTON ESCAPE
 PRIME 10
 ELECTRON FLUX 1 1
 PHOTON FLUX 1 1
 NPHOT 10

HISTORY RECORDS
 0 OF 5 BIGN PRODUCTIVE INPUT

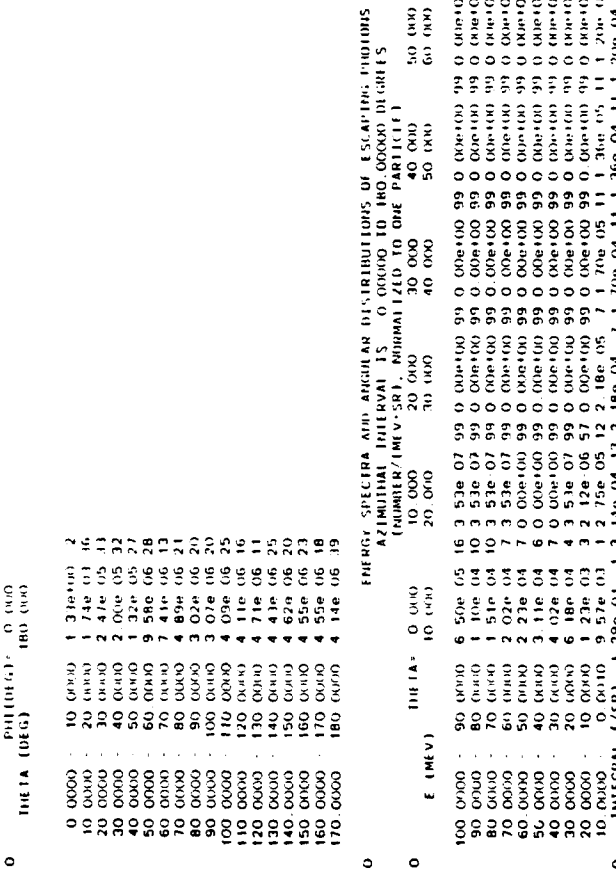
 ***** COMPARISON OF STORAGE REQUIREMENTS VS ALLOCATIONS *****

 NUMBER OF MATERIALS IN CROSS SECTION FILE / INPUT 2 / 5

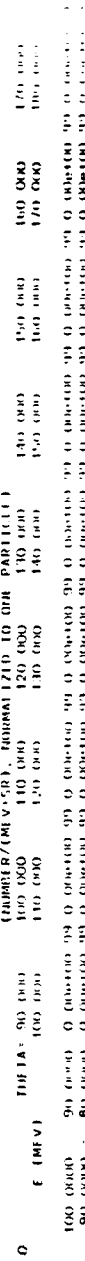




ABSORBING PHOTON INTENSITY
(MEV/SR) NORMALIZED TO ONE INCIDENT PARTICLE



ENERGY SPECTRA AND SPATIAL DISTRIBUTIONS OF ESCAPEE PHOTONS AT PHOTON INTERVALS OF ONE TO TWO CYCLES IN ENERGY



卷之三

THE NUMBER OF DATA FOR WHICH STATISTICAL ESTIMATES HAVE BEEN PROVIDED IS

095200

GAAS

USER NUMBER	095200
WORKER MACHINE	Y
DATE SHIFT	10-Oct-1985 11.03.57
FILED BY UNIT	A
PAGE 5, DATE	10-Oct-1985
PAGE 5 TIME	13.06.14.00: 45.440 Pages: 1

PROGRAM IIS, DECEMBER 16, 1984
 VERSION 1.0
 ACCEPT
 CHAMFER OF MATERIALS
 2
 GAMMA RAY CROSS SECTION DATA FOR MATERIAL CHAMFER 1
 CHAMFER MIND MAX
 25 6 39
 ENERGIES (MEV)
 1000 0.00000 800 0.00000 600 0.00000 500 0.00000 400 0.00000 300 0.00000
 2000 0.00000 1500 0.00000 1000 0.00000 800 0.00000 600 0.00000 500 0.00000
 40 0.00000 30 0.00000 20 0.00000 15 0.00000 10 0.00000 8 0.00000
 6 0.00000 5 0.00000 4 0.00000 3 0.00000 2 0.00000 1 0.00000
 1 0.00000 0.8 0.00000 0.6 0.00000 0.5 0.00000 0.4 0.00000 0.3 0.00000
 0.2 0.00000 0.15 0.00000 0.1 0.00000 0.05 0.00000 0.025 0.00000 0.0125 0.00000
 0.027940 0.029400 0.030930 0.032438 0.033938 0.035438 0.036938
 0.038438 0.040000 0.041500 0.043000 0.044500 0.046000 0.047500
 0.049044 0.050500 0.051950 0.053400 0.054850 0.056300 0.057750
 0.059243 0.060698 0.062153 0.063608 0.065063 0.066518 0.067973
 0.061989 0.063443 0.064897 0.066351 0.067805 0.069259 0.070713
 0.062615 0.064169 0.065723 0.067277 0.068831 0.070385 0.071939
 0.064265 0.065820 0.067374 0.068928 0.070482 0.072036 0.073590
 0.058324 0.059876 0.061428 0.062980 0.064532 0.066084 0.067636
 0.052681 0.054233 0.055785 0.057337 0.058889 0.060441 0.061993
 14 58.593 31 16.4482 37 392754 1 231901 2.22180 4 849174 7 973909
 6 269423 16 0.19371 35 5.96110 10.8 5.62363 199 314251 430 4 12449
 1051 3.167174 926 19275 1076 23960 1120 238467
 848 4.1036 400 50743 709 21948 1613 524968
 1127 93030 1332 818662 326525 6389 511380
 ORALIN OF SCATTERING, PLUS PAIR PRODUCTION, 10 10 10 ALIENATION COEFFICIENTS
 0.999991 0.949988 0.99994 0.999980 0.999775 0.99966
 0.999961 0.949926 0.999826 0.999865 0.999771 0.999726
 0.999937 0.949947 0.999847 0.999884 0.999774 0.999704
 0.999702 0.949957 0.999857 0.999894 0.999777 0.999750
 0.95687 0.948869 0.998869 0.999830 0.999754 0.999724
 0.418614 0.255855 0.105715 0.049250 0.019442 0.006464
 0.010481 0.016655 0.016514 0.016514 0.016514 0.016514
 0.024873 0.016155 0.016155 0.016155 0.016155 0.016155
 0.000165 0.000165 0.000165 0.000165 0.000165 0.000165
 0.000187 0.000187 0.000187 0.000187 0.000187 0.000187
 0.000204 0.000204 0.000204 0.000204 0.000204 0.000204
 0.000243 0.000243 0.000243 0.000243 0.000243 0.000243
 0.000155 0.000155 0.000155 0.000155 0.000155 0.000155
 ORALIN OF SCATTERING, PLUS PAIR PRODUCTION, 10 10 ALIENATION COEFFICIENTS
 0.002932 0.001679 0.001679 0.001679 0.001679 0.001679
 0.158189 0.021568 0.013314 0.013314 0.013314 0.013314
 0.015181 0.127583 0.196442 0.196442 0.196442 0.196442
 0.567301 0.631889 0.162447 0.162447 0.162447 0.162447

OK 0.00050 0.00026
0.00049 0.00014
0.000127 0.000099
OKAY 0.00127 0.00099
OKAY OF SCATTERING TO SCATTERING PLUS PAIR PRODUCTION ATTENUATION COEFFICIENTS
0.003562 0.00484 0.00642 0.007307 0.009231 0.012506
0.019266 0.02635 0.04730 0.06235 0.07847 0.081451
0.11160 0.151439 0.23419 0.30586 0.30269 0.428713 0.51524
0.627310 0.701006 0.785222 0.875673 0.939669 0.909810
1.000000
OK SHELL IONIZATION DATA
OK BINDING ENERGY (MEV) PHOTODEFICIENCY AND FLUOROSCENI EFFICIENCY
0.011867 0.416827 0.520756
OK X-RAY ENERGIES (MEV)
0.010690 0.010550 0.010490 0.010690
OKAY ACCUMULATED RELATIVE INTENSITIES
1.00000 1.00000 1.00000 1.00000
OKAY ELECTRIN ENERGIES (MEV)
0.010690 0.010550 0.010490 0.010690
OKAY ELECTRON ACCUMULATED RELATIVE INTENSITIES
1.00000 1.00000 1.00000

ELECTRON CROSS SECTION DATA FROM PROGRAM DAIPAC

CHAMBER OF SETS ON DAIPAC TAPE 2

100.0 MEV CROSS SECTIONS FOR PHOTOSCENIORS

MATERIAL	DENSITY	DEFLUX	DEFLUX
1	0.47800e+01	0.73100e+00	W
2	0.53200e+01	0.195100e+00	W
3	0.31000e+02	0.30974e+02	0.21200e+00
4	0.49000e+02	0.1148e+03	0.78000e+00
5	0.33000e+02	0.74922e+02	0.51800e+00
6	0.31000e+02	0.1516e+03	0.78000e+00
NSET	11111	12111	15111
1	1	1	1
2	5	1	1
3	0	40	1
4	0	1	1
5	1	1	1
DATAFILE	DATAFILE	DATAFILE	DATAFILE
1	64	64	64
2	33	40	33
3	40	40	40
4	121	121	121
5	2	2	2

OK COLLISION / TOTAL DEFLX RADIUS FOR DAIPAC SET 2
OK CUMULATIVE BREMS STRAHLUNG CROSS SECTIONS FOR DAIPAC SET 2
OK LANGMUIR. EQUIPROBABLE ENPOINT DISTRIBUTIONS FOR DAIPAC SET 1
OK X-RAY PRODUCTION FOR DAIPAC SET 2
OK PHOTODEFICIENCY AND FLUOROSCENI EFFICIENCIES FOR DAIPAC SET 1
OK PAIR ELECTRIN ENERGY DISTRIBUTION DISTRIBUTION (LAD)

BEGIN READING INPUT

100.0 MEV KLEPPER TEST PROGRAM

GEOMETRY 10

```

SPH 0 00 0 00 0 00 2 0
REAL DATA FOR BODY 2 IS STORED IN FPD ARRAY LOCATIONS 11 THROUGH 14
SPH 0 00 0 00 0 00 4
REAL DATA FOR BODY 3 IS STORED IN FPD ARRAY LOCATIONS 17 THROUGH 20
END
NUMBER OF BODIES 3

```

INPUT ZONE DATA

```

21 +1
22 +2 -1
23 +3 -2
END
O COMPARISON OF GEOMETRY REQUIREMENTS VS ALLOCATIONS
LENGTH OF ARRAY CONTAINING REAL BODY DATA / LENGTH / 20 / 1000
NUMBER OF INPUT ZONES / LENGTH / 3 / 100
NUMBER OF CODE ZONES / LENGTH / 3 / 100
LENGTH OF GEOMETRY ARRAY CONTAINING INTEGER DATA / LENGTH / 65 / 10000
LENGTH OF ARRAY CONTAINING CODE ZONE BODY DATA / LENGTH / 2 / 50

```

CODE ZONE	INPUT ZONE	ZONE DATA LOC	NO OF BODIES
1	1	16	1
2	2	20	2
3	3	28	2

```

OPTION 1 WAS USED IN CALCULATING VOLUMES FOR 3 INPUT ZONE'S
IVOP1 MEANING
0 ALL VOLUMES SET TO 1.0
1 READ INPUT VOLUMES
2 USER LOGIC TO COMPUTE VOLUMES

```

VOLUMES (CM³)

ZONE 1	2	3
VOLUME 2	500e-03	3.35e+01
SMAT ECU1 PIC2		2.679e+02

2

.....SOURCE.....

ELECTRONS

ENERGY 100.0
POSITION 0.0 0.0 0.0
RADIUS 0.5
DIRECTION 0.0
CUTOFFS 0.05 0.001

.....INPUT OPTIONS.....

ELECTRON-ESCAPE

PHOTON-ESCAPE

NAME 10 ELECTRON-FIUX 11
NAME 10 ELECTRON-FIUX 11
NAME 10 PHOTON-FIUX 11
NAME 10 PHOTON-FIUX 11

.....OTHER OPTIONS.....

HISTORIES (NUMBER)

O EOP ON UNIT 5 (HIGH PROCESSING) IAHU

.....COMPARISON OF STORAGE REQUIREMENTS VS ALLOCATIONS.....

.....NUMBER OF MATERIALS OR CRYSTALS SECTION FILE.....

UNSCATTERED PRIMARY PHOTONS ARE INCLUDED FROM ALL SUR-FACED PHOTON ESCAPE FRACTIONS
NUMBER ESCAPE FRACTIONS = KNOCK ON AND PINKIN GEM RATIO ELECTRONS, ANNIHILATION RADIATION, K X RAYS (MATERIAL NO. 1)

0 KNOCK TOTAL ESCAPE K X RAY(1) K X RAY(2) K X RAY(3)

1 6.3e-03 2 5.5e-05 1.2 6.0e-06 5.1 0.1e-00 9.3 1.67e-04 7

NUMBER AND ENERGY ESCAPE FRACTIONS

		TOTAL ESCAPE		PHOTON		PHOTON	
		ELCTRON	PHOTON	NUMBER	EN.HEV	NUMBER	EN.HEV
1	1.0e+00	0.9 9.9e-01	0.00168	1.18e-02	1.12e-01	2	11782

1 ENERGY AND CHARGE DEPOSITION

(NORMALIZED TO ONE INCIDENT PARTICLE)

ZONE NO.	PRIM	INITIAL ENERGY (MEV)	INITIAL KINICK	PRIM	INITIAL ENERGY (MEV)	INITIAL KINICK	CHARGE (ELECTRONS)	INITIAL			
		G SEC			G SEC		G SEC				
1	2	4.54e-02	1	4.632e-03	4	1.81e-05	0.2	1.916e-03	2	7.700e-05	16
2	0	0.000e+00	0	0.000e+00	99	0.000e+00	99	0.000e+00	99	0.000e+00	99
3	0	0.000e+00	0	0.000e+00	99	0.000e+00	99	0.000e+00	99	0.000e+00	99
0 TOTAL	2.454e-02	1	4.632e-03	4	1.81e-05	0.2	1.916e-03	2	7.700e-05	16	

0 THE ENERGY CONSERVATION FRACTION IS 0.999999000751100. 0

IF LUX CALCULATION - ELECTRONS LEFT AT FLUX CUTOFF ENERGY (NUMBER, NORMALIZED TO ONE INCIDENT PARTICLE)

1 1.22e-03 2

1 ELECTRON FLUX DISTRIBUTION

(TRACK LENGTH/VOLUME MEV. NORMALIZED TO ONE INCIDENT PARTICLE)

OE (MEV)	ZONE NO.								
90.0000	1	2.40e-01	1	9.0e-03	2	1.90e-03	4	1.90e-03	1
80.0000	1	1.90e-03	1	9.0e-03	2	1.90e-03	4	1.90e-03	1
70.0000	5	9.0e-04	4	9.0e-04	5	9.0e-04	6	9.0e-04	5
60.0000	3	8.0e-04	6	8.0e-04	5	8.0e-04	5	8.0e-04	5
50.0000	2	8.0e-04	5	8.0e-04	5	8.0e-04	5	8.0e-04	5
40.0000	1	8.0e-04	6	8.0e-04	5	8.0e-04	5	8.0e-04	5
30.0000	1	6.6e-04	10	6.6e-04	10	6.6e-04	10	6.6e-04	10
20.0000	1	5.8e-04	6	5.8e-04	7	5.8e-04	7	5.8e-04	7
10.0000	1	6.7e-04	7	6.7e-04	7	6.7e-04	7	6.7e-04	7
0.0010	0	3.26e-03	2	3.26e-03	2	3.26e-03	2	3.26e-03	2

1 ELECTRON FLUX DISTRIBUTION

(TRACK LENGTH/VOLUME MEV. NORMALIZED TO ONE INCIDENT PARTICLE)

OE (MEV)	ZONE NO.								
90.0000	6	7.8e-05	16	7.8e-05	16	7.8e-05	16	7.8e-05	16
80.0000	1	0.5e-04	10	0.5e-04	10	0.5e-04	10	0.5e-04	10
70.0000	1	1.2e-04	7	1.2e-04	7	1.2e-04	7	1.2e-04	7
60.0000	1	9.0e-04	8	9.0e-04	8	9.0e-04	8	9.0e-04	8
50.0000	2	7.0e-04	7	7.0e-04	7	7.0e-04	7	7.0e-04	7
40.0000	3	5.3e-04	8	5.3e-04	8	5.3e-04	8	5.3e-04	8
30.0000	5	5.9e-04	5	5.9e-04	5	5.9e-04	5	5.9e-04	5
20.0000	1	1.1e-03	3	1.1e-03	3	1.1e-03	3	1.1e-03	3
10.0000	1	9.2e-03	1	9.2e-03	1	9.2e-03	1	9.2e-03	1

1 ENERGY SPECTRA OF ESCAPING ELECTRONS

(NUMBER/MEV. NORMALIZED TO ONE INCIDENT PARTICLE)

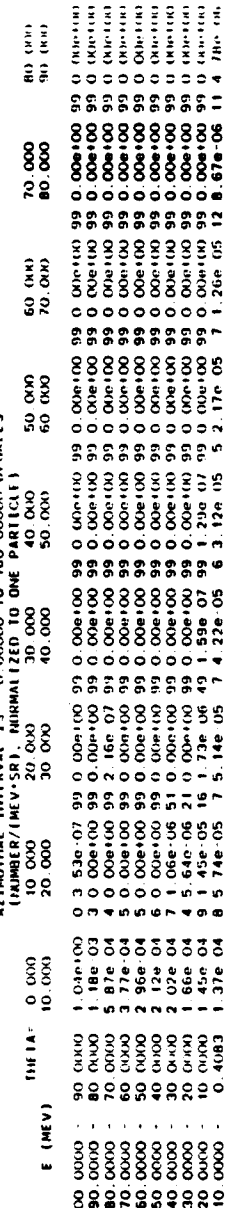
E (MEV)									
100.0000	90.0000	9.97e-02	0	9.97e-02	0	9.97e-02	0	9.97e-02	0
90.0000	80.0000	1.13e-02	3	1.13e-02	3	1.13e-02	3	1.13e-02	3
80.0000	70.0000	5.6e-03	4	5.6e-03	4	5.6e-03	4	5.6e-03	4
70.0000	60.0000	3.6e-03	5	3.6e-03	5	3.6e-03	5	3.6e-03	5
60.0000	50.0000	2.8e-03	5	2.8e-03	5	2.8e-03	5	2.8e-03	5
50.0000	40.0000	2.0e-03	6	2.0e-03	6	2.0e-03	6	2.0e-03	6
40.0000	30.0000	1.9e-03	7	1.9e-03	7	1.9e-03	7	1.9e-03	7

JO 0000 20 0000 1 74e 05 3
20 0000 10 0000 1 89e 05 6
10 0000 0 4083 1 72e 04 2

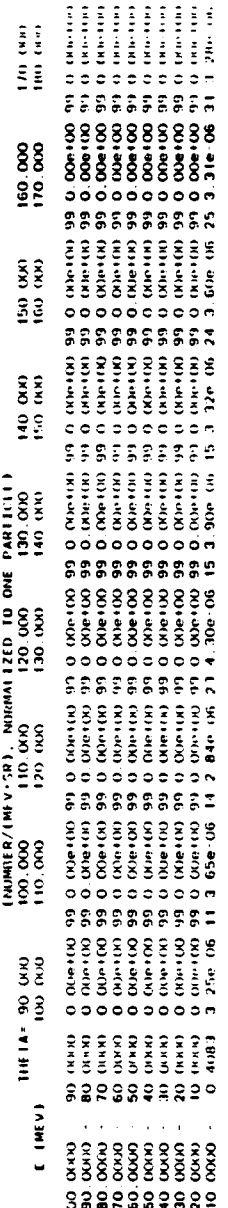
APPROXIMATE DISTRIBUTIONS OF ESCAPING ELECTRONS
(NUMBER/F.S.R. NORMALIZED TO ONE INCIDENT PARTICLE)



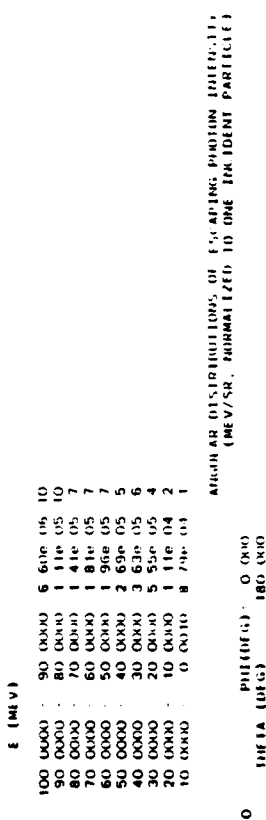
ENERGY SPECTRA AND ANGULAR DISTRIBUTIONS OF ESCAPING ELECTRONS
ANGULAR INTERVAL IS 0.00000 TO 180.00000 DEGREES



ENERGY SPECTRA AND ANGULAR DISTRIBUTIONS OF ESCAPING ELECTRONS
ANGULAR INTERVAL IS 0.00000 TO 180.00000 DEGREES

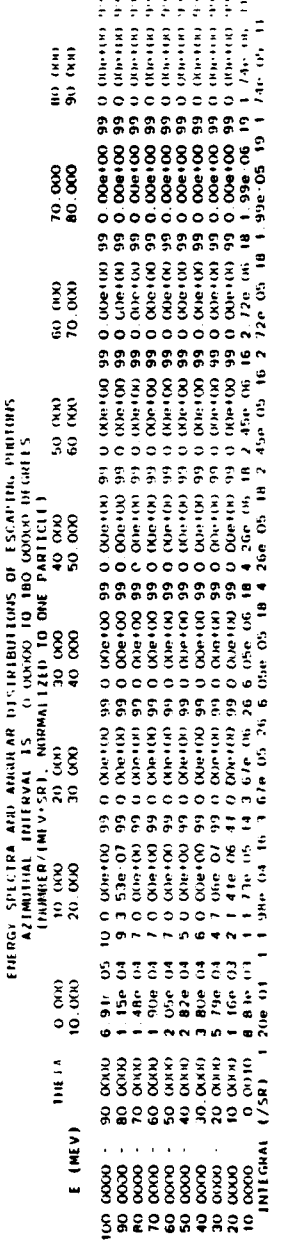


ENERGY SPECTRA AND ANGULAR DISTRIBUTIONS OF ESCAPING ELECTRONS
(NUMBER/F.S.R. NORMALIZED TO ONE PARTICLE)



APPENDIX B: DISTRIBUTION OF EXPANDING POSITION IDENTITIES (MEV/SR, NORMALIZED TO ONE IDENT PARTICLE)

ALUMNI ARE INVITED TO JOIN THE 1995 MEV/SR. MUNICIPAL LEAD TO ONE IN ONE PARTICIPATION TEAM.



ESCAPING THE CONDITIONS OF EXILE

AZIMUTHAL INTEGRAL 15. 0.00000 10.180 (OPENED IN CAFE 5)									
LUMINOSITY (fb ⁻¹)		PHYSICAL STATE		PARTICLE		PARTICLE		PARTICLE	
THE 1. - 90 (GeV)	THE 2. - 90 (GeV)	THE 1. - 100 (GeV)	THE 2. - 100 (GeV)	THE 1. - 120 (GeV)	THE 2. - 120 (GeV)	THE 1. - 130 (GeV)	THE 2. - 130 (GeV)	THE 1. - 140 (GeV)	THE 2. - 140 (GeV)
100.00000	90.00000	0.000000000	0.000000000	90.00000	90.00000	0.000000000	0.000000000	0.000000000	0.000000000
90.00000	80.00000	0.000000000	0.000000000	80.00000	80.00000	0.000000000	0.000000000	0.000000000	0.000000000

THE NUMBER OF DATA FOR WHICH STATISTICAL ESTIMATES HAVE BEEN PROVIDED IS 5000

LIST OF REFERENCES

1. Los Alamos Electronics Division Research and Development Technical Report, Picosecond Photoconductors as Radiation Detectors, by R.S. Wagner, J.M. Bradley and R.B. Hammond, November 1985 (unpublished).
2. Berger, M.J. and Seltzer, S.M., Stopping Powers and Ranges of Electrons and Positrons, U.S. Department of Commerce, Washington D.C. 20234, 1982.
3. Rohrlich, Carlson, R.C., Physics Review 93, 39, 1954.
4. Rudie, N.J., Principles and Techniques of Radiation Hardening, 2nd ed., v. 2, pp. 14-38, 1980.
5. Corbett, J.W., Electron Radiation Damage in Semiconductors and Metals, 1st ed., Academic Press, New York, p. 3, 1966.
6. Vavilov, V.S., Effects of Radiation on Semiconductors, Chapter V, Consultants Bureau, New York, p. 196, 1965.
7. Seitz, F. and Koehler, J.S., Solid State Phys. 2, 307, 1956.
8. McKinley, W.A., Jr., and Feshbach, H., Physics Review 74.1759, 1948.
9. Willardson, R.K. and Beer, A.C., Semiconductors and Semimetals, vol. 4 Physics of III-V Compounds, Chapter 6, Academic Press, New York, 1968.
10. Dienes, G.J. and Vineyard, G.H., Radiation Effects in Solids, Interscience Publishers, New York, 1957.
11. Kinchin, G.H., and Pease, R.S., Rept. Progr. Phys. 13, 1, 1955.
12. Snyder, W.S. and Neufeld, J., Phys. Review 97, 1637, 1955.
13. Chaffin, R.J., Microwave Semiconductor Devices: Fundamentals and Radiation Effects, John Wiley and Sons, Inc., New York, 1957.
14. James, H.M. and Lark-Horovitz, K., Z Physik. Chem. 193, 107, 1951.

15. Blount, E.I., Phys. Rev. 113, 995, 1959.
16. Madelung, O., Physics of III-V Compounds, John Wiley and Sons, Inc., New York, 1964.
17. Los Alamos Electronics Division Research and Development Progress Report, FY 82, #LA-9726-PR, Photon-Controlled Circuit Elements, by R.B. Hammond, pp. 3-24.
18. Hammond, R.B., Paultre, N.G., Iverson, A.E. and Smith, R.C., Sub-100ps Bulk Recombination-Limited InP:Fe Photoconductive Detector, Technical Digest of the International Electron Devices Meeting, Washington, 1981, pp. 157-160.
19. Bube, R.H., Photoconductivity of Solids, John Wiley and Sons, Inc., New York, 1960, pp. 56-74, 303-318.
20. Rose, A., Performance of Photoconductors, RCA Laboratories, Princeton, Photoc inductivity Conference, John Wiley and Sons, Inc., New York, 1954, p. 3-33.
21. Hammond, R.B., Wagner, R.S., and Paultre, N.G., "InP:Fe Picosecond Photoconductors," Proceedings of the Conference on Picosecond Optoelectronics, San Diego, 1983, SPIE Vol. 439, pp. 192-196.
22. Hammond, R.B., Paultre, N.G., Wagner, R.S., Springer, T.S., and MacRoberts, M.D.J., "InP:Fe Photoconductors as Photodetectors," IEEE Transactions on Electron Devices, Vol. ED-30, pp. 412-415, 1983.
23. Berard, R.W., Traverso, T.J., Neutron Form Factors from Elastic Electron-Dueteron Scattering Ratio Experiments at Very Low Momentum Transfers, Master's Thesis, Naval Postgraduate School, Monterey, California, June 1973.
24. Barnett, M.T., Jr., Cunneen, W.J., Design and Performance of the Electron Linear Accelerator at the Naval Post-graduate School, Master's Thesis, Naval Postgraduate School, Monterey, California, May 1966.
25. Hammond, R.B., Paultre, N.G., Wagner, R.S., and Springer, T.E., "Excitation and Fe Concentration Dependencies in the Impulse Photoconductance of InP:Fe," Appl. Phys. Lett. 44 (6), 15 March 1984, pp. 620-622.
26. Sandia Report SAND84-0513, ITS: The Integrated Tiger Series of Coupled Electrons/Photons Monte Carlo Transport Codes, by J.A. Halbleib and T.A. Mehlhom, Albuquerque, New Mexico, 1984.

INITIAL DISTRIBUTION LIST

	No. Copies
1. Defense Technical Information Center Cameron Station Alexandria, Virginia 22304-6145	2
2. Library, Code 0142 Naval Postgraduate School Monterey, California 93943-5100	2
3. Dr. Robert B. Hammond Principal Investigator Los Alamos National Laboratory Electronics Research P.O. Box 1663 Los Alamos, New Mexico 87545	2
4. Dr. Edith G. Leighty Pathology, Pharmacology and Toxicology Battelle Columbus Laboratories 505 King Avenue Columbus, Ohio 43201	1
5. Prof. F.R. Buskirk, Code 61Bs Department of Physics Naval Postgraduate School Monterey, California 93943-5100	3
6. Prof. J.R. Neighbours, Code 61Nb Department of Physics Naval Postgraduate School Monterey, California 93943-5100	1
7. Don Synder, Code 61Ds Department of Physics Naval Postgraduate School Monterey, California 93943-5100	1
8. Lt. Phillip J. Keipper, USN 1653 Fourth St. Portsmouth, Ohio 45662	3

END

FILMED

3-86

DTIC